

**AN INJECTABLE HYDROPHOBIC DELIVERY
FORMULATION BASED ON POLY(TRIMETHYLENE
CARBONATE) FOR THERAPEUTIC ANGIOGENESIS**

by

Sara Mohajeri

A thesis submitted to the Department of Chemical Engineering

In conformity with the requirements for

the degree of Doctor of Philosophy

Queen's University

Kingston, Ontario, Canada

(April 2018)

Copyright ©Sara Mohajeri, 2018

Abstract

The aim of this thesis was to determine the feasibility of an injectable delivery formulation based on low molecular weight poly(trimethylene carbonate) (PTMC) for localized delivery of vascular endothelial growth factor (VEGF). Formulations based on modified conjugated PTMC, ester or anhydride-linked PTMC, and poly(trimethylene carbonate-co-5-hydroxy trimethylene carbonate) (P(TMC-co-HTMC)), were synthesized. Polymers/copolymers were amorphous and injectable viscous liquids at 37 °C. *In vitro* degradation study of the conjugated PTMCs showed that the anhydride bond cleaved within 24 hours, generating acidic products that lowered the pH of the buffered degradation medium. In contrast, hydrolysis of the ester bond did not result in an acidic pH; however, it degraded too slowly for the intended application. Preparing P(TMC-co-HTMC) using different catalysts revealed that HCl-Et₂O is able to provide a random comonomer distribution and low toxicity burden. *In vitro* degradation of the resulting random copolymers was tailored by adjusting the initial HTMC content, initial molecular weight and the choice of initiator. During *in vitro* degradation, the pH of the medium surrounding the copolymer always remained near neutral. *In vivo* degradation study of P(TMC-co-HTMC)s at the molecular weight range of 1000-2000 Da with 30 mol% initial HTMC content revealed rapid degradation of the HTMC units followed by gradual elimination of the short chains produced via HTMC degradation. The inflammatory response to the injected copolymers subsided by time but was still ongoing after 22 weeks. The observed tissue response was comparable with the tissue response of a commercial MONOCRYL suture indicating that the copolymer can be considered biocompatible. *In vitro* protein release from the same copolymers was characterized by using lysozyme, bovine serum albumin and VEGF. This study revealed that the rate of protein release was controlled by the solubility of the lyophilized protein in the aqueous environment within the copolymer, the concentration of the salt included in the lyophilized powder, and the flexibility of the copolymer chains to form superhydrated regions. The released VEGF showed greater than 80% bioactivity throughout the release period. This delivery formulation can be used to deliver acid sensitive proteins for short or long-term delivery approaches depending on the protein physical properties.

Co-Authorship

Chapter 5 and sections of Chapter 7 have been filed in the United States Patent and Trademark Office (USPTO) in November 2017 with the following co-authors: Sara Mohajeri, Fei Chen, Brian G. Amsden.

Ms. Deborah Harrington performed the subcutaneous injection of poly(trimethylene carbonate-co-5-hydroxy trimethylene carbonate) in rats for *in vivo* experiments presented in Chapter 6 at the Animal Care Services of Queen's University. The bioactivity assay presented in Chapter 7 was performed in collaboration with Mr. Jonah Burke-Kleinman of Dr. Donald H. Maurice lab at Biomedical and Molecular Sciences Department of Queen's University.

Acknowledgements

In the first place, I would like to express sincere gratitude to my PhD supervisor, Dr. Brian Amsden for his guidance and constant encouragement during the whole period of my research. His knowledge, motivation, patience and friendship helped me to learn scientific concepts and pass this journey safe and sound.

I would like to thank my committee members, Dr. Donald H. Maurice from the Faculty of Biomedical and Molecular Sciences and Dr. Michael Cunningham from the Faculty of Chemical Engineering for their knowledge, support and suggestions to keep my project in the right direction.

I would also like to express special thanks to Dr. Fei Chen for his kind help, support and friendship over the past few years.

I am grateful to my research group: Shadi Taghavi, Dimitra Louka, Dr. Roshni Rainbow, Dr. Julian Chesterman, Dr. Moira Vyner, Dr. Stuart Young, Hossein Riahinezhad, Amanda Brissenden, Fiona Serack, and Dr. Gad Sabbatier. It has been a great and memorable experience working with such a group of scientists and friends. Also, I would like to thank Deborah Harrington and Jonah Burke-Kleinman during my collaboration at the Animal Care Services and Biomedical and Molecular Sciences Department.

I would like to express my special thanks to my husband Behnam Naderizand, my mother Fathiyeh Ehteshami and my father Firooz Mohajeri for their love, patience and support, without them I would never exist and be who I am. I would like to express my special thanks and love to my little son Aubteen Naderizand for his patience living with a busy mother and understanding her situation.

I would like to appreciate my beautiful lovely country IRAN for everything it has offered me to make my life and future. I hope one day I come back home and compensate all its unsparing generosity.

Table of Contents

Abstract.....	ii
Co-Authorship	iii
Acknowledgements.....	iv
List of Figures.....	ix
List of Tables	xiv
List of Abbreviations	xv
Chapter 1 Introduction	1
1.1 Clinical Significance	1
Chapter 2 Literature Review	4
2.1 Natural capillary formation and arteriogenesis.....	4
2.2 Therapeutic Angiogenesis	7
2.2.1 Cell therapy	7
2.2.2 Gene therapy	8
2.2.3 Protein therapeutics	9
2.3 Angiogenic Growth Factors	11
2.3.1 Vascular Endothelial Growth Factor (VEGF)	11
2.4 Angiogenic Growth Factor Delivery	12
2.5 Protein bioactivity	13
2.6 Growth Factor Delivery Approaches.....	15
2.6.1 Microspheres.....	17
2.6.2 Hydrogels.....	19
2.6.3 Osmotic Delivery Strategies.....	22
2.6.3.1 Solid Osmotic Delivery Formulations	23
2.6.3.2 Viscous Liquid Osmotic Delivery Formulations	24
2.7 Injectable Drug Delivery Vehicle Based on aliphatic polycarbonates	28
2.8 Polymerization Catalysts.....	30
2.9 Tissue response	35
2.10 Summary.....	39
Chapter 3 Proposed Approach and Objectives	41
3.1 Proposal	41
3.2 Objective.....	42
3.3 Specific Aims.....	42

Chapter 4 Hydrolysable, Conjugated, Low Molecular Weight Poly(trimethylene carbonate) (PTMC): Synthesis, Characterization and <i>In Vitro</i> Degradation	44
4.1 Abstract.....	44
4.2 Introduction.....	45
4.3 Materials	47
4.4 Methods	47
4.4.1 Synthesis of poly(trimethylene carbonate) (PTMC).....	47
4.4.2 Synthesis of carboxylic acid terminated PTMC (PTMC-COOH).....	48
4.4.3 Ester and anhydride conjugation	48
4.4.4 Polymer Characterization.....	49
4.4.5 <i>In vitro</i> Polymer Degradation.....	50
4.4.6 Statistics	51
4.5 Results and Discussion.....	51
4.5.1 Polymer Synthesis.....	51
4.5.2 PTMC Conjugation	54
4.5.3 <i>In vitro</i> Mass Loss of Conjugated PTMC.....	57
4.6 Conclusion	64
Chapter 5 Hydrolysable injectable delivery vehicle based on low molecular weight poly(trimethylene carbonate-co-5-hydroxy trimethylene carbonate): Synthesis, characterization and <i>in vitro</i> degradation...	66
5.1 Abstract.....	66
5.2 Introduction.....	67
5.3 Materials	70
5.4 Methods	71
5.4.1 Synthesis of P(TMC-co-BTMC) via different polymerization methods.....	71
5.4.1.1 Melt polymerization using Sn(Oct) ₂	71
5.4.1.2 Solution polymerization using HCl·Et ₂ O and DBU.....	72
5.4.2 Debenzylation of P(TMC-co-BTMC)	73
5.4.3 Polymer Characterization	74
5.4.4 <i>In vitro</i> degradation	77
5.4.5 Viscosity measurement	78
5.4.6 Statistical analysis	78
5.5 Results and Discussion.....	78
5.5.1 Influence of catalyst on copolymer conformation	78
5.5.2 Preparation and characterization of P(TMC-co-HTMC)s.....	90

5.5.3	<i>In vitro</i> degradation	92
5.5.4	Copolymer Viscosity	99
5.6	Conclusion	100
Chapter 6 <i>In vivo</i> degradation and tissue response to low molecular weight poly(trimethylene carbonate-co-5-hydroxyl trimethylene carbonate) (P(TMC-co-HTMC))		
6.1	Abstract	101
6.2	Introduction	102
6.3	Materials	103
6.4	Methods	104
6.4.1	Synthesis and characterization of P(TMC-co-HTMC)	104
6.4.2	<i>In vivo</i> biocompatibility and biodegradation	104
6.4.3	Histological and immunohistochemistry analysis	106
6.4.4	Statistics	108
6.5	Results and Discussion	108
6.5.1	Copolymer properties	108
6.5.2	Visual observation and <i>in vivo</i> biodegradation	109
6.5.3	Histological and immunohistochemistry analysis	113
6.6	Conclusion	122
Chapter 7 Protein release from low molecular weight poly(trimethylen carbonate-co-5- hydroxy trimethylene carbonate) (P(TMC-co-HTMC)): the effect of copolymer composition, degradation rate and the protein particle composition		
7.1	Abstract	123
7.2	Introduction	124
7.3	Materials	127
7.4	Method	128
7.4.1	Synthesis and characterization of P(TMC-co-HTMC)	128
7.4.2	Preparation of solid protein particles	128
7.4.2.1	Lysozyme and BSA particles	128
7.4.2.2	VEGF particles	129
7.4.3	<i>In vitro</i> release study	130
7.4.4	Cell culture	131
7.4.5	Bioactivity assay	131
7.4.6	Statistics	133
7.5	Results and Discussion	133

7.5.1	Release of model proteins	133
7.5.2	<i>In vitro</i> VEGF release	141
7.5.3	Bioactivity assay	146
7.6	Conclusion	147
Chapter 8 Conclusion and Recommendations.....		149
8.1	Conclusion	149
8.2	Recommendations.....	150
References		152
Appendix A.....		171
Appendix B.....		173
Appendix C.....		175

List of Figures

Figure 2.1. Schematic of the angiogenesis process and the growth factors utilized in each step. The schematic was adapted from Papetti and Herman and is used with permission.....	6
Figure 2.2. Pictorial representation of the osmotic release mechanism that involves the formation of zones of excess hydration wherein solute transport occurs.....	26
Figure 2.3. Chemical structure of BTMC and PHTMC, “I” in PHTMC structure represents the initiator.....	29
Figure 2.4. Mechanism of polymerization of ϵ -caprolactone in the presence of $\text{Sn}(\text{Oct})_2$ as a catalyst, including (A,B) formation of stannous alkoxide initiator, (C) catalyst deactivation by water, (D) propagation step via coordination/insertion of monomer into the stannous alkoxide bond, (E) deactivation of polymerizing center via reaction with water or alcoholic initiator as well as transesterification.....	32
Figure 2.5. Mechanism of polymerization of TMC in the presence of $\text{HCl}\cdot\text{Et}_2\text{O}$ as a catalyst, including (A) activation of monomer, (B) polymer initiation step via nucleophilic attack of the hydroxyl group on the alcoholic initiator, (C) propagation step via nucleophilic attack of the hydroxyl group on the growing chain end.....	33
Figure 2.6. Mechanism of polymerization of TMC in the presence of DBU as a catalyst, including (A) activation of the initiating/propagating hydroxyl group, (B) formation of alkoxide anion initiator and propagation step via the attack of anion to the carbonyl bond of TMC.	34
Figure 4.1. General chemical structure of low molecular weight PTMC blocks conjugated with a hydrolysable linkage (R).....	45
Figure 4.2. Chemical structure of A) initiator molecules, B) conjugation molecules used.....	46
Figure 4.3. ^1H NMR spectrum of PTMC initiated with 1-octanol obtained in DMSO-d_6 . $M/I=5$, $M_n=640$ Da. Peak “M” corresponds to the methylene groups linked to the carbonate bond of TMC monomer.....	52
Figure 4.4. ^1H NMR spectrum obtained in DMSO-d_6 of PTMC-COOH initiated with 1-octanol, $M/I=5$, $M_n=724$ Da. T’2 and T’3 are the peaks corresponding to the methylene groups of the remaining end unit of PTMC, and e’ is the unreacted succinic acid.....	53
Figure 4.5. ^1H NMR spectrum of ester-linked PTMC (OCT-CE-SC) obtained in DMSO-d_6	55
Figure 4.6. ^1H NMR spectrum of anhydride-linked PTMC (OCT-CA-SC) obtained in DMSO-d_6 . Peak “H” at 2.17 ppm represents the unreacted end methylene group of SC.....	56
Figure 4.7. pH of PBS during the <i>in vitro</i> degradation of anhydride-linked PTMC and dissolution of PTMC-COOH at 37 °C. The initial pH of the medium, replaced at each time point, was 7.4.....	58
Figure 4.8. Mass loss (%) of anhydride-linked PTMC and unlinked PTMC-COOH in 37 °C PBS at the initial pH of 7.4.....	59

Figure 4.9. ¹ H NMR spectrum obtained in DMSO-d ₆ of the OCT-CA-SC remaining at 24 h in 37 °C PBS at an initial pH of 7.4.....	60
Figure 4.10. ¹ H NMR spectrum of dissolved fraction of OCT-CA-SC at 24 h under <i>in vitro</i> degradation condition obtained in DMSO-d ₆ . In this figure abbreviations are as “SE”: sebacic acid, “SU”: succinic acid, “P”: polymer, “D”: 1,3-propanediol, i: initiator.....	61
Figure 4.11. Mass loss (%) of ester-linked PTMC and unlinked PTMC in 37 °C pH 7.4 PBS.....	62
Figure 4.12. ¹ H NMR spectrum obtained in DMSO-d ₆ of OCT-CE-SC remaining at 12 weeks under <i>in vitro</i> degradation conditions.....	63
Figure 4.13. Mass loss (%) of ester-linked PEG-initiated PTMC-OH in 37°C pH 7.4 PBS.....	64
Figure 5.1. Copolymer chemical structure; n and m refer to the number of repeating units of TMC and BTMC or HTMC along the copolymer backbone, k refers to the number of methylene (CH ₂) groups within the initiator (<i>e.g.</i> k = 3 is 1-butanol, k = 7 is 1-octanol).....	67
Figure 5.2. Chemical structure of monomers and catalysts.....	69
Figure 5.3. ¹ H NMR spectrum of OCT-P18-50B-HCl obtained in CDCl ₃ , M/I=18, M _n = 1440, Da, BTMC: 46%. Protons labelled with a prime correspond to the copolymer end group.....	80
Figure 5.4. Stacked ¹ H NMR spectra obtained in CDCl ₃ of TMC and BTMC conversion versus time during copolymerization. The initiator was 1-octanol, and the catalyst was HCl·Et ₂ O.....	81
Figure 5.5. Monomer conversion versus time for the copolymerization of TMC and BTMC using different catalysts: (A) Sn(Oct) ₂ , 130-135°C; (B) HCl·Et ₂ O, room temperature and (C) DBU, room temperature.....	82
Figure 5.6. Mechanism of polymerization of cyclic carbonate monomer in the presence of (A) Sn (Oct) ₂ , (B) HCl·Et ₂ O, (C) DBU as a catalyst.....	84
Figure 5.7. Possible sequences of carbonate bonds in the copolymer structure.....	86
Figure 5.8. ¹³ C NMR spectra of A) OCT-P18-50B-HCl (M _n = 1440 Da), B) PBTMC (M _n = 5100 Da), C) PTMC (M _n = 12600 Da), NMR solvent: CDCl ₃	87
Figure 5.9. ¹ H NMR spectrum of copolymer OCT-P18-30H obtained in DMSO-d ₆ . M/I=18, M _n = 1600 Da, HTMC: 30%. Labels with a prime correspond to the copolymer end group and the label (OH)TMC corresponds to the hydroxyl group of TMC end unit.....	91
Figure 5.10. Mass loss of the samples in PBS (pH 7.4) at 37 °C under horizontal agitation of 300 rpm. The PBS was replaced every second day. Statistical difference between copolymers containing 50 mol% initial HTMC over time (*), statistical difference of the copolymers containing 50 mol% initial HTMC with copolymers containing 30 mol% initial HTMC (**), p < 0.05, one-way ANOVA, n=3.....	93
Figure 5.11. HTMC percentage of the samples in PBS (pH 7.4) at 37 °C under horizontal agitation of 300 rpm. The PBS was changed every other day. A: 50% HTMC, B: 30% HTMC. Statistical difference with	

day 1 (*), Statistical difference of BU-P6-50H with other copolymers in week 1 (Ω), $p < 0.05$, One-way ANOVA, $n=3$94

Figure 5.12. Change in M_n of the samples in PBS (pH 7.4) at 37 °C under horizontal agitation of 300 rpm. The PBS was changed every other day. A: 50% HTMC, B: 30% HTMC. Statistical difference of OCT-P10-30H with OCT-P18-30H and BU-P18-30H overtime (*), $p < 0.05$, one-way ANOVA, $n=3$95

Figure 5.13. pH of degradation medium during *in vitro* degradation in PBS.....98

Figure 6.1. Representative photographs of copolymer samples in the subcutaneous tissue before explantation at time points of 1 to 22 weeks. A: BU-P18-3H, B: OCT-P18-30H, C: OCT-P10-30H.....110

Figure 6.2. Evolution of A: HTMC mole% and B: M_n (Da) during *in vivo* degradation. Each data point represents the average, and the error bars are the standard deviation about the average. Statistical difference between week 22 with previous time points (*), statistical difference between OCT-P18-30H with B-P18-30H at the same time point (**), $p < 0.05$, One-way ANOVA, $n=2$111

Figure 6.3. *In vivo* versus *in vitro* degradation changes of BU-P18-30H in : A) HTMC mole% and) M_n (Da). Each data point represents the average, and the error bars are the standard deviation about the average.....112

Figure 6.4. Representative photomicrographs of tissue sections (muscle side) of copolymer samples stained with Masson's trichrome at time points of 1, 2 and 4 weeks. A: BU-P18-3H, B: OCT-P18-30H, C: OCT-P10-30H, S: Suture, copolymer (P), suture (S), fibrous capsule (FC), copolymer particle (*). Scale bar: 50 μm , 20X. The dashed line represents the inflammatory zone.....114

Figure 6.5. Representative photomicrographs of tissue sections (muscle side) of copolymer samples stained with Masson's trichrome at time points of 12 and 22 weeks. A: BU-P18-3H, B: OCT-P18-30H, copolymer (P), suture (S), fibrous capsule (FC). Scale bar: 50 μm , 20X. The dashed line represents the inflammatory zone.....115

Figure 6.6. Thickness of the fibrous capsule formed around the implants after 2, 4, 12, and 22 weeks of subcutaneous injection in Wistar rats. Tissue sections were chosen randomly, and the error bars indicate the standard deviation of 5 images of each sample ($N=5$) on two different rats ($n=2$). Statistical difference with the previous time point for OCT-P18-30H (**), and BU-P18-30H (***), $p < 0.01$. Statistical difference between OCT-P10-30H with other copolymers at the same time point (θ'), $p < 0.05$. Two-way ANOVA with Bonferroni post-hoc test.....116

Figure 6.7. Number of cells at the copolymer-tissue interface and the surrounding fibrous capsule per $10^4 \mu\text{m}^2$ after 1 to 22 weeks of subcutaneous injection in Wistar rats. Tissue sections were chosen randomly, and the error bars indicate the standard deviation of 5 images of each sample ($N=5$) on two different rats ($n=2$). Statistical difference with the previous time point for OCT-P10-30H (*), OCT-P18-30H (**), BU-P18-30H (***) and suture (Δ), statistical difference between OCT-P10-30H with other copolymers at the same time point (θ), statistical difference between suture with copolymers at the same time point (Ω), $p < 0.01$, Two-way ANOVA with Bonferroni post-hoc test.....117

Figure 6.8. Representative photomicrographs of CD68+ cells in tissue (muscle side) surrounding BU-P18-30H and the suture control stained with the pan-macrophage marker CD68 at time points of 1, 4 and 22 weeks. Copolymer (P), suture (S), green color: CD68, blue color: DAPI. Scale bar: 50 μm , 40X.....118

Figure 6.9. Number of CD68+ cells at the copolymer-tissue interface and the surrounding fibrous capsule per $10^4 \mu\text{m}^2$ after 1 to 22 weeks of subcutaneous injection in Wistar rats. Tissue sections were chosen randomly, and the error bars indicate the standard deviation of 8 images of each sample (N=8) on two different rats (n=2). Statistical difference with the previous time point for OCT-P10-30H (*), OCT-P18-30H (**), BU-P18-30H (***) and suture (Δ), statistical difference between OCT-P10-30H with other copolymers at the same time point (θ), statistical difference between suture with copolymers at the same time point (Ω), $p < 0.01$, Two-way ANOVA with Bonferroni post-hoc test.....	119
Figure 7.1. Influence of P(TMC-co-HTMC) initiator and molecular weight on lysozyme release. The particle loading for each case was 1 wt%. Statistical difference of OCT-P18-30H with BU-P18-30H at each time point (*), statistical difference of OCT-P10-30H with OCT-P18-30H and BU-P18-30H at each time point (**), $p < 0.01$, n=3.....	136
Figure 7.2. Influence of particle loading on lysozyme release incorporated in L98/T2 particles from BU-P18-30H. Statistical difference of 1 wt% loading with 2 wt% loading at each time point (*), $p < 0.01$	137
Figure 7.3. <i>In vitro</i> release profiles of BSA incorporated in BSA98/T2 particles from BU-P18-30H copolymer. A) influence of particle loading on release of BSA incorporated into the particles prepared in PBS buffer (BSA98/T2 particles), and B) influence of salt content on BSA release incorporated into the BSA98/T2 particles prepared in PBS (BSA98/T2) or PB buffer (BSA98/T2-PB), n = 3.....	138
Figure 7.4. <i>In vitro</i> release profiles of BSA and lysozyme incorporated in protein particles containing the same concentration of salt and protein from BU-P18-30H copolymer showing the influence of protein physical properties. The particle loading for each case was 1 wt%, n = 3.....	139
Figure 7.5. Release of VEGF from BU-P18-30. The VEGF was incorporated into VEGF/BSA/T particles prepared in PBS. Statistical difference of 1 wt% loading with 2 wt% loading at each time point (*), $p < 0.01$, n = 3.....	143
Figure 7.6. Influence of the physical properties of the protein on the release rate from BU-P18-30H. The particle loading for each case was 1 wt%, n = 3.....	144
Figure 7.7. Influence of the particle salt content on VEGF release rate from BU-P18-30H. The particle loading for each case was 1 wt%. Statistical difference of Formulation A with Formulation B at each time point (*), $p < 0.01$, n = 3.....	145
Figure 7.8. Fraction of bioactive VEGF in the release media relative to the same concentration of as-received growth factors. Each point represents the average of the released protein from three samples with 3 replicates per sample.....	146
Figure A.1. ^1H NMR spectrum of PTMC initiated with P350 obtained in DMSO- d_6 , M/I= 6, Mn=950 Da.....	171
Figure A.2. ^1H NMR spectrum of ester-linked PTMC (OCT-CE-DGC) obtained in DMSO- d_6	171
Figure A.3. ^1H NMR spectrum of ester-linked PTMC (P350-CE-SC) obtained in DMSO- d_6 , EG/TMC: 1.3.....	172
Figure B.1. ^1H NMR spectrum of OCT-P18-50B-DBU obtained in CDCl_3 , M/I=40, Mn=3200 Da, BTMC: 32.8 %. Labels with prime are corresponding to the copolymer end group.....	173

Figure B.2. ^1H NMR spectrum of OCT-P18-50B-Sn obtained in CDCl_3 , $M/I=40$, $M_n=3920$ Da, BTMC:50 % . Labels with prime are corresponding to the copolymer end group.....	173
Figure B.3. ^{13}C NMR spectra of A) OCT-P18-50B-DBU obtained in CDCl_3 , $M_n=3200$ Da, BTMC: 32.8 %.....	174
Figure B.4. ^{13}C NMR spectra of A) OCT-P18-50B-Sn obtained in CDCl_3 , $M_n=3920$ Da, BTMC: 50 %.....	174
Figure B.5. The glass transition temperature of P(TMC-co-BTMC) from DSC heating thermograph:(A) $\text{Sn}(\text{Oct})_2$, (B) DBU, and (C) $\text{HCl}\cdot\text{Et}_2\text{O}$	174
Figure C.1. <i>In vivo</i> versus <i>in vitro</i> degradation changes of OCT-P18-30H in : A) HTMC mole% and) M_n (Da). Each data point represents the average, and the error bars are the standard deviation about the average.....	175
Figure C.2. <i>In vivo</i> versus <i>in vitro</i> degradation changes of OCT-P10-30H in : A) HTMC mole% and) M_n (Da). Each data point represents the average, and the error bars are the standard deviation about the average.....	176
Figure C.3. Photomicrographs of tissue sections (muscle side) of copolymers and suture extracted and stained for CD68. (P): copolymer, (S): suture, green color: FITC, blue color: DAPI, Scale bar: 50 μm , 40X.....	177

List of Tables

Table 4.1 Physical-chemical properties of conjugated PTMCs.....	57
Table 5.1. Characterization of the pure copolymers prepared with different catalysts.....	88
Table 5.2. Characterization of the pure copolymers prepared using HCl·Et ₂ O as catalyst.....	92
Table 5.3. viscosity measurements at 25 °C and 37 °C.....	99
Table 6.1. Physical-chemical properties of P(TMC-co-HTMC) copolymers.....	109
Table 7.1. Composition of protein particles prepared in PBS or PB buffer.....	129
Table 7.2. Composition of VEGF particles prepared in PBS or PB buffer.....	130
Table 7.3. Physical-chemical properties of P(TMC-co-HTMC).....	134

List of Abbreviations

Ang -1	Angiopoietins-1
AAV	Adeno-associated virus
ABI	Ankle brachial index
ASC	Adipose tissue derived stromal cell
BCA	Bicinchoninic acid
BSC	biosafety cabinet BSC
BM-MNC	Bone marrow mononuclear cell
BSA	Bovine serum albumin
BTMC	5-benzyloxy trimethylene carbonate
CCL-2	C-C chemokine ligand
CD	Cluster of differentiation
CD68⁺ cells	CD68 positive cells
CDCl₃	Deuterated chloroform
CLI	Critical limb ischemia
CR3	Complement receptor
DAPI	4',6-diamino-2-phenylindole
DBU	1,8-diazabicyclo-7-undecene
DCM	Dichloromethane
DGC	Diglycolyl chloride
DMSO-d₆	Deuterated dimethyl sulfoxide
EC	Endothelial cell

ECM	Extracellular matrix
EGM-2	Basal endothelial cell growth medium
EG/TMC	Ethylene glycol to TMC ratio
EPC	Endothelial progenitor cell
EGF	Epithelial growth factor
EtOAc	Ethyl acetate
Factor XIII	Fibrin stabilizing factor
FBS	Fetal bovine serum
FBGCs	Foreign body giant cells
FGF	Fibroblast growth factor
GA-1000	gentamicin amphotericin B
G-CSF	Granulocyte-colony stimulating factor
GF	Growth factor
GM-CSF	Granulocyte macrophage-colony stimulating factor
GPC	Gel permeation chromatography system
H₂	Hydrogen
HCl	Hydrogen chloride
HCl·Et₂O	Hydrogen chloride solution in diethyl ether
HFG	Hepatocyte growth factor
HIF-1α	Hypoxia-inducible factor
HIF-β	Hypoxia-inducible factor subunit β
IHC	Immunohistochemistry

IL-1	Interleukin-1
IL-6	Interleukin 6
IL-13	Interleukin-13
K₂CO₃	Anhydrous potassium carbonate
kDa	kg/mol
KH₂PO₄	Potassium phosphate monobasic
LCST	Lower critical solution temperatures
MCP-1	Monocyte chemoattractant protein-1
MeOH	Methanol
MMPs	Matrix metalloproteinases
Mn	Number average molecular weight
M/C	Monomer to catalyst mole ratio
M/I	Monomer to initiator mole ratio
OH	Hydroxyl
OCT-CA-SC	Octanol initiated PTMCs linked via anhydride bond using diglycolyl chloride
OC-CE-DGC	Octanol initiated PTMCs linked via ester bond using diglycolyl chloride
OCT-CE-SC	Octanol initiated PTMCs linked via ester bond using sebacoyl chloride
P350	Poly(ethylene glycol) methyl ether at 350 Da
PAD	Peripheral arterial disease
PB	Phosphate buffer without saline
PB-MNC	Peripheral blood mononuclear cell
PBS	Phosphate buffer saline

Pd/C	Palladium on carbon
Pd(OH)₂/C	palladium hydroxide on carbon
PDGF	Platelet derived growth factor
PEG	Poly(ethylene glycol)
PEG-HBP	Heparin-binding peptides
PEG-LMWH	Heparinized star PEG
PEKCDLLA	Poly(5-ethylene ketal ε-caprolactone-co-D,L-lactide)
PEO-PPO-PEO	Poly(ethyleneoxide)-poly(propyleneoxide)-Poly(ethylene oxide)
PF4	Platelet factor
PHBV	Poly(3-hydroxybutyrate-co-3-hydroxyvalerate)
PHTMC	Poly(2-hydroxyltrimethylene carbonate)
PLGA	Poly(lactide-co-glycolide)
PIGF	Placental growth factor
PMN	Polymorphonuclear leukocyte
PTMC	Poly(trimethylene carbonate)
PTA	Percutaneous transluminal angioplasty
PTMC-COOH	Carboxylic acid terminated PTMC
P(TMC-co-HTMC)	poly(trimethylene carbonate-co-5-hydroxy trimethylene carbonate)
ROP	Ring-opening polymerization
SC	Sebacoyl chloride
SDF-1	Stem cell-derived factor-1
SMC	Smooth muscle cells

Sn(Oct)₂	Tin(II) 2-ethylhexanoate
TBS	Tris hydrochloride
TEA	Triethylamine
TeloHAEC	Telomerase-immortalized human aortic endothelial cells
T_g	Glass transition temperature
TGF-β	Transforming growth factor
THF	Tetrahydrofuran
Tie2	Receptor tyrosine kinase expressed on angiopoietins
TMC	1,3-trimethylene carbonate
TNF-α	Tumor necrosis factor-α
UPA	Urokinase-plasminogen activator
VEGF	Vascular endothelial growth factor
VEGFR-1 (Flt-1)	Vascular endothelial growth factor receptor 1
VEGFR-2 (KDR/Flk-1)	Vascular endothelial growth factor receptor 2
WST	Water-soluble tetrazolium salts
wt%	Weight percentage
w/v	Weight/volume

Chapter 1

Introduction

1.1 Clinical Significance

Peripheral arterial disease (PAD) is a chronic condition caused by the formation and hardening of fatty plaque (atherosclerosis) within arteries and arterioles, resulting in narrowing or blocking of the vessels carrying blood to the limbs. Gradually, the flow of blood becomes restricted even at rest and deprives the tissue of oxygen and nutrients leading to critical limb ischemia (CLI) in the tissues fed by the diseased artery. In severe cases ulceration, gangrene or tissue loss result.¹⁻³ This condition affects 8.5 million Americans aged over 40, and the number of patients is expected to dramatically increase as the population age and the number of individuals with prolonged exposure to obesity, diabetes, smoking and hypertension increase.⁴⁻⁷ Moreover, PAD is asymptomatic and generally diagnosed at the late stages as the classic symptoms such as ischemic rest pain or ischemic ulcers are observed in just 10 % of the patients.^{8,9}

Current treatments include pharmacological therapy and controlling the risk factors,² percutaneous transluminal angioplasty (PTA)^{10,11} and bypass surgery.¹² These treatments have decreased the mortality rates; however, 10-40 % of patients with PAD still require amputation. Amputation itself causes 5-10% mortality for below-the-knee amputations and 15-20% for above-the-knee amputations after bypass surgery. Additionally, 30% of amputee survivors will die within 2 years, and the other 30% will require a second

amputation. Finally, full restoration of mobility with no amputation is achieved in less than 50% of patients.^{2,3}

The discovery of angiogenic growth factors and the natural mechanism of forming blood vessels represented a potential treatment approach, named therapeutic angiogenesis. In this approach new blood vessels (capillaries) are induced to grow from the pre-existing blood vessels around the arterial blockage to carry blood to the deprived tissue, bypassing the site of occlusion. The body is intrinsically able to produce endogenous angiogenic growth factors and subsequently induce new blood vessels at the site of ischemia. But this response occurs very slowly, and it cannot compensate for the lost blood flow completely.¹³ Therefore, the exogenous administration of angiogenic growth factors is required to facilitate the treatment. In this approach, angiogenic growth factors are administered directly to the ischemic site via a minimally invasive, biocompatible, and biodegradable delivery vehicle. Ideally, the delivery vehicle provides a sustained release of the growth factors at the effective local dose with a minimal initial burst effect while the bioactivity of the growth factor is preserved.¹⁴⁻¹⁶

To achieve this kind of delivery, in this work, a hydrolysable, viscous liquid formulation based on modified low molecular weight conjugated poly(trimethylene carbonate) (PTMC), ester or anhydride-linked PTMC, and low molecular weight poly(trimethylene carbonate-co-5-hydroxy trimethylene carbonate) (P(TMC-co-HTMC)), were studied. The synthesis, characterization and *in vitro* degradation of the conjugated PTMC and the copolymer were determined. Moreover, the *in vivo* degradation behavior and tissue response to, and the factors influencing the release rate of model proteins from the selected

P(TMC-co-HTMC)s were examined. Finally, as a demonstration of feasibility, the ability of the chosen formulation to release bioactive vascular endothelial growth factor (VEGF) was assessed.

Chapter 2

Literature Review

2.1 Natural capillary formation and arteriogenesis

Capillaries consist of a single layer of endothelial cells (EC) that are flattened and possess tight gap junctions. The ECs are enclosed by a basement membrane and are partially covered by pericytes/smooth muscle cells (SMC) on the abluminal site. Pericytes/SMCs envelop the vessel wall and regulate the barrier properties of the capillaries.^{16,17} To appreciate the issues surrounding therapeutic angiogenesis requires an understanding of the natural process of capillary formation *in vivo*.

Vascularisation occurs naturally in adults during the menstrual cycle, inflammation, and in such physiological repair processes as wound healing. Vascularisation includes two steps: angiogenesis and arteriogenesis.¹⁷⁻¹⁹ Angiogenesis refers to the process of new capillaries sprouting and developing from pre-existing blood vessels to form a new capillary network.^{19,20} Increasing the density of capillaries via angiogenesis leads to a decrease in the interspace between neighboring blood vessels, which subsequently increases blood perfusion and restores local oxygen and nutrients supply.^{20,21} Each step of angiogenesis is initiated and regulated by a variety of growth factors (GF) which are secreted in a tightly regulated spatial and temporal order. In general, during angiogenesis the existing branched network of vessels formed during vascularization (primary vascular plexus) is used as a scaffold and is remodelled through several circumstances as described below.

Normally stable endothelial cells become activated by locally introduced hypoxia in the surrounding tissue.²²⁻²⁴ Oxygen tension plays a key role in the secretion of proteinases, such as urokinase-plasminogen activator (UPA) and matrix metalloproteinases (MMPs) by ECs, which cause rapid degradation of the nearby extracellular matrix (ECM). While ECM is degrading and in response to hypoxia, intracellular stabilization of hypoxia-inducible factor subunit α (HIF-1 α) in the cytoplasm and the formation of the heterodimer of HIF- α with hypoxia-inducible factor subunit β (HIF- β) in the cell nuclei stimulates transcription of the potent angiogenic stimulator vascular endothelial growth factor (VEGF) in the nucleus.¹⁷ Subsequently, VEGF leads to the proliferation of ECs as well as endothelial permeabilization, which allows for extravasation of proteases and ECM components from the blood.²⁵ Several other growth factors including angiopoietins (Ang), transforming growth factor (TGF- β), fibroblast growth factor (FGF), epithelial growth factor (EGE), hepatocyte growth factor (HGF), platelet derived growth factor (PDGF), tumor necrosis factor- α (TNF- α) and receptor tyrosine kinase expressed on angiopoietins (Tie2) are involved in the different steps of angiogenesis which trigger capillary tube formation (Figure 2.1).^{19,24,26-28} The new ECM synthesized by pericytes and SMCs contains the soluble growth factors and provides a suitable condition for migration and proliferation of ECs into the ECM in response to the soluble and matrix-bound chemical signals which leads to the formation of a migrational column. Also, pericytes migrate towards the migrational column, deposit matrix and interact with ECs enveloping the vessel wall to stabilize the new vessels. After a sufficient number of divisions, ECs stop proliferating and form a new luminal vessel that fuses into the pre-existing mature vasculature, and blood flow is initiated.²⁵⁻²⁷

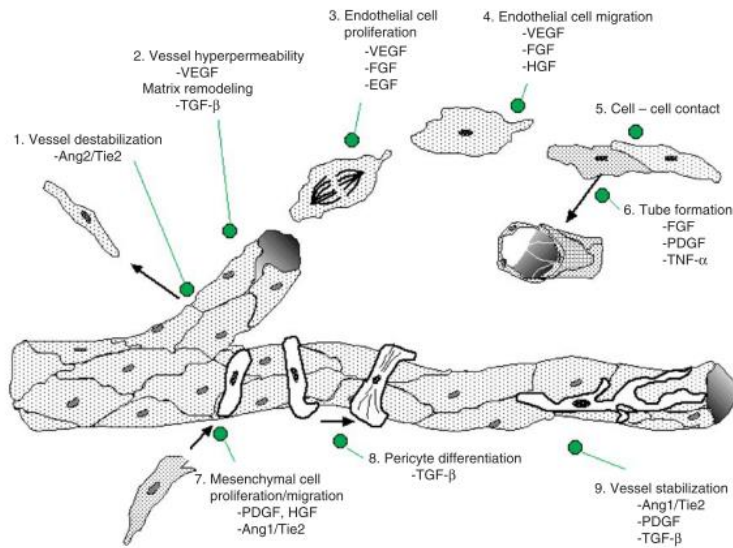


Figure 2.1. Schematic of the angiogenesis process and the growth factors utilized in each step. The schematic was adapted from Papetti and Herman and is used with permission.²⁸

In continuation of the angiogenesis process, arteriogenesis, also called collateral growth, may occur. Arteriogenesis results in the enlargement of newly formed capillaries to compensate for the flow lost in other vessels, forming arterioles.^{17,19} Arteriogenesis is mostly initiated and regulated by the flow shear stress caused as the result of vessel occlusion. The vessel diameter increases until the radial wall stress is normalized.^{19,29,30} During this process, shear forces activate endothelial cells that subsequently stimulate the production of adhesion molecules and chemokines such as monocyte chemoattractant protein-1 (MCP-1), granulocyte-macrophage colony-stimulating factor-10, tumor necrosis factor- α and stem cell-derived factor-1 (SDF-1).^{24,31,32} Circulating monocytes are recruited by the cytokines and collected around the developing artery where they invade the interstitial space and differentiate to macrophages.³³ In addition to other cellular elements the resulting macrophages release more MCP-1, nitric oxide, as well as growth factors

including PDGF, TNF- α , VEGF, FGF-1 and FGF-2.^{24,34} The secreted matrix proteases degrade the tissue surrounding the growing vessel and produce a space into which the collateral vessels can expand. Released growth factors recruit endothelial cells, pericytes and SMCs from the surrounding tissue to the abluminal surface of the endothelium, which envelop the vessel wall. To form mature blood vessels, mural cells differentiate, interact with endothelial cells, and form a matrix which stabilizes the new vessels and prevents their regression. Later the endothelial cells become quiescent, improve cell-cell contacts, and complete ECM synthesis.^{13,14,20}

2.2 Therapeutic Angiogenesis

The body is naturally capable of developing blood vessel networks to treat ischemia, but this process occurs very slowly, and is not capable of compensating for the lost blood flow completely. Therapeutic angiogenesis via local delivery of stem cells or progenitor cells (cell therapy)^{7,13,36} and/or angiogenic growth factors^{7,37} in the lower limb has been examined in efforts to overcome the limits of the natural angiogenesis response by promoting endothelial cell proliferation, migration, and blood vessel formation.

2.2.1 Cell therapy

In cell therapy, transplantation of cells such as adipose tissue-derived stem/stromal cells (ASC),^{38,39} bone-marrow derived endothelial, hematopoietic stem and progenitor cells,^{40–42} and bone-marrow mononuclear cells⁴⁰ can induce tissue revascularization at the ischemic sites. These cells not only restore tissue revascularization, but also secrete a number of

angiogenic growth factors such as VEGF, SDF-1, FGF-2, Ang-1 and HGF that facilitate incorporation of endothelial progenitor cells (EPC) into the newly sprouting blood vessels.^{38–40,42,43}

Recent clinical and pre-clinical studies proved that angiogenic cell therapy is a feasible, and potentially effective therapeutic strategy for PAD patients with evidences of increasing lower limb perfusion, decreasing the pain score, relevant improvement in ankle brachial index (ABI), and promoting foot ulcer healing.^{7,40,44,45} Despite the potential advantages of cell therapy, this method showed low therapeutic efficacy due to the low survival level of cells transplanted into the hypoxic tissue. In fact the direct exposure of cells to the ischemic site caused a high level of cell apoptosis within a few days of transplantation due to the lack of initial vasculature.⁴⁶ This method also has other challenges such as difficulties in *ex vivo* proliferation and differentiation of EPCs and side effects caused by different hematopoietic and irrelevant tissue-specific pluripotent stem and progenitor cells of bone-marrow mononuclear cells such as aberrant hemorrhage-prone vessels, fibrosis, abnormal tissue remodeling and arrhythmias.⁴²

2.2.2 Gene therapy

Angiogenic gene therapy is based on the therapeutic delivery of specific growth factor DNA sequence into the target cells to encode the localized and sustained secretion of a specific growth factor depending on the tissue transfected and the vector used.^{7,47} Nowadays, genes are transferred using plasmids and viral vectors. Plasmids have low transfection efficiency and reduced transgene expression. Adenoviral vectors and adeno-

associated virus (AAV) are the most effective way of delivering angiogenic growth factors by transducing nonproliferating cells. However, the high cytotoxicity of adenoviral vectors due to the adenovirus products and inflammatory reaction against adenovirus limits their application.⁴⁸ In contrast, AAVs with low immunogenic potential and prolonged expression may provide higher efficiency than adenoviral vectors.^{49–51}

Preclinical models of gene therapy revealed promising results on improving angiogenesis, but the clinical studies on overexpression of angiogenic growth factors have not achieved significant success in decreasing amputation rate and improving ulcer healing. Proposed explanations for these disappointing clinical results include: low level of gene expression especially in elderly patients with diabetes and hyperlipidemia, gene persistence, and low efficiency of single growth factor administration as it is known that several growth factors are contributing to angiogenesis.^{47,51–53}

2.2.3 Protein therapeutics

As demonstrated by the natural angiogenesis process, multiple growth factors are involved in forming new and stable blood vessels. Therefore, an approach based on local administration of various growth factors at the ischemic site via a delivery device could be introduced to achieve angiogenesis. In comparison to cell therapy and gene therapy, the protein therapeutics approach provides several advantages, including the ability to combine several growth factors in a single formulation as well as the ability to control the delivered dose and duration of growth factors.

Growth factors are soluble signaling proteins that can control cellular responses in a very wide range of cell actions including cell survival, migration, proliferation, and differentiation. The cell behavior is directed through binding the growth factor to specific transmembrane receptors on the target cells. The resulting binding transfers a signal to the cell nucleus. The transfer mechanism involves a complex array of events, which engages cytoskeleton protein phosphorylation, ion fluxes, changes in metabolism, gene expression, protein synthesis, and finally an integrated biological response.^{54,55}

However, growth factors have a rapid, local effect because of their slow and short-range diffusion through, and short half-life time in, the ECM. The diffusion behaviour of growth factors is regulated by the extent of their binding to ECM components and the resulting spatiotemporal gradient.^{35,56} The ability of a growth factor to instruct cell behavior not only depends on its half-life and diffusion properties through the ECM, but is also determined by the number of target cells, types of receptors and the nature of intracellular signal transduction subsequent to growth factor binding. Depending on the type of cell the same receptor can produce different intracellular transduction pathways and subsequently translate different messages. Finally, interaction between the target cell and a specific growth factor is controlled by external factors including ECM degradation rate, target cell location, and the concentration of the growth factor.²⁵ According to the critical role of growth factors in regulating the cellular behaviour and tissue regeneration, a wide range of growth factors such as VEGF,^{13-15,57,58} FGF,^{13,57,59} PDGF,^{58,59,60,61} HGH^{15,62,63} and placental growth factor (PlGF)⁶⁴⁻⁶⁷ have been studied for therapeutic angiogenesis. In the next section, the family of VEGF will be introduced as the most utilized growth factor for

angiogenesis, and a brief discussion about the challenges of protein therapeutics will be presented.

2.3 Angiogenic Growth Factors

2.3.1 Vascular Endothelial Growth Factor (VEGF)

There are six known members of the VEGF family: VEGF-A, B, C, D, E and PlGF. VEGF-B, C, D and E are mitogenic growth factors for ECs as is VEGF-A, but are significantly less potent than VEGF-A. VEGF-A is a disulfide-bonded dimeric glycoprotein with a molecular weight of 34-45 kg/mol (kDa) that is the major player in angiogenesis. It is expressed by various cell types such as SMCs, macrophages, tumor cells, cardiomyocytes and ECs at low levels under normal conditions; however, its concentration reaches higher level at angiogenic conditions such as within fetal tissue, the placenta, human tumors, and during tissue repair. The local oxygen concentration affects the level of VEGF-A secretion as its production is dramatically upregulated by hypoxia.^{56,68,69} There are four isoforms of VEGF-A composed of 121, 165, 189, and 206 amino acids, which are known as VEGF₁₂₁, VEGF₁₆₅, VEGF₁₈₉, VEGF₂₀₆. The C-terminal domains of VEGF₁₆₅, VEGF₁₈₉ and VEGF₂₀₆ are highly basic, bind to heparin-rich proteoglycans of the ECM, and consequently these growth factors diffuse more slowly than VEGF₁₂₁, which has no affinity for heparin. MMPs can cleave the VEGF-ECM bond and form a stable and active form of the growth factor. This released active growth factor can interact with its cognate receptors inducing angiogenesis, increasing vascular permeability, facilitating paracrine/autocrine growth factor release, enhancing cell motility and inhibiting cell apoptosis.^{35,56} Within the

VEGF family, VEGF₁₆₅ is the most common and most biologically active isoform that is secreted into the extracellular environment.⁷

The activities of VEGF-A are predominantly regulated by its binding to two tyrosine kinase receptors, vascular endothelial growth factor receptor 1 (Flt-1 or VEGFR-1) and vascular endothelial growth factor receptor 2 (KDR/Flk-1 or VEGFR-2). VEGFR-1 shows the highest affinity to VEGF-A, and is found on ECs, vascular smooth muscle cells, and monocytes. VEGFR-1 does not cause direct migratory, proliferative, or cytoskeletal effects.^{28,70} In contrast, VEGFR-2 has a lower affinity than VEGFR-1 for VEGF-A, is expressed on ECs and its hematopoietic precursors affects EC mitogenesis.^{71,72} The resulting activity of VEGF-A caused by binding to VEGFR-2 leads to the EC specific action of VEGF-A.

2.4 Angiogenic Growth Factor Delivery

Effective angiogenesis through growth factor administration requires an optimized dosage, sequence, and release duration of bioactive growth factors.^{18,55,67,73-77} Growth factors can be administered directly by bolus injection or through incorporation into delivery devices. However, growth factors typically have short half-lives following injection; for example, the plasma half-life of VEGF is 1 h.^{18,78} Therefore, for effective therapy, large doses would need to be systemically administered by daily bolus injection.⁷⁹ This approach is not recommended because high concentrations of angiogenic growth factors within a local environment may cause abnormal vessel growth and immune dysfunction resulting in edema, hypotension, or hemangioma.^{57,64,67,80} Therefore, controlled delivery strategies

should be utilized to provide prolonged release of low and localized doses of angiogenic growth factors into the ischemic site, while maintaining their bioactivity. For this purpose growth factors have been incorporated into biomaterials with characteristics that provide gradual *in vivo* release.^{18,55,74-77} Previous studies have revealed that 3-4 weeks of sustained and local delivery of bioactive growth factors into the hypoxic tissue is necessary to form a stable vascular network and provide effective blood flow.^{13,14}

Clinical trials have consistently demonstrated that administration of a single growth factor is not sufficient to provide a stable and effective blood vessel network.^{18,57,73} This is not surprising as multiple growth factors are involved in the natural angiogenesis process to induce EC activation, proliferation, migration, and tube formation as well as attracting pericytes/SMCs to stabilize the newly formed blood vessels.^{7,43,81} Therefore, several studies were completed on co-administration of angiogenic growth factors such as VEGF/FGF-2,^{59,82} VEGF/PDGF-BB,^{58,60,61} PDGF/FGF-2,⁵⁹ VEGF/HGF,^{15,63} VEGF/PIGF⁶⁷ to improve therapeutic angiogenesis.

2.5 Protein bioactivity

Protecting growth factor bioactivity is one of the most important parameters that should be considered when designing a growth factor delivery device. Proteins have primary, secondary, tertiary and sometimes quaternary structures that determine their biological activity. These structures may exhibit both chemical and physical instability (denaturation) in solution and in the solid state that subsequently leads to a decrease in the protein bioactivity.⁸³

Protein chemical instability refers to reactions such as deamidation, oxidation, and disulfide exchange in which covalent bonds are cleaved and reformed, yielding a new chemical substance.⁸⁴ In contrast, protein physical instability occurs without breaking or reforming covalent bonds, but rather by disruption of the native folded conformation of the protein, aggregation, and formation of insoluble particles.^{84,85} Physical denaturation occurs due to various stresses experienced during purification, processing, storage, and release from the delivery device. These stresses include exposure to extreme pH, adsorption to surfaces, exposure to shear strains caused by agitation and filtration, and temperature fluctuations during different steps such as freezing, lyophilization, thawing, and protein release.^{79,86-90}

Proteins can be formulated as either solutions or lyophilized solids using excipients called osmolytes such as sugars, salts, polyols, amino acids, and amines to preserve their bioactivity. Osmolytes preserve the protein bioactivity by reducing aggregation of unfolded proteins in solution via the thermodynamically unfavorable mechanism of preferential hydration in which osmolytes are preferentially excluded from the vicinity of the protein.^{83,91-95} Preferential hydration increases the free energy of both the native and unfolded protein structure. However, the unfolded protein structure is expected to have a greater preferential hydration because it possesses a greater surface area compared to the native structure. Therefore, the presence of osmolytes leads to a greater energy difference between the native and unfolded structure, and subsequently higher energy is required to unfold proteins. On the other hand, proteins prefer self-association in the presence of osmolytes to decrease their surface area and reduce the unfavorable interaction with

osmolytes which enhances aggregation.⁹³ Therefore, the osmolyte concentration should be optimized to preserve the protein bioactivity.

Proteins are most often lyophilized with osmolytes such as sugars as cryoprotectants and lyoprotectants to enhance the protein stability. Lyophilization involves two processes including freezing and drying which both may cause damage to the protein structure. Thus, the selected excipients must stabilize the protein effectively against the applied stresses of lyophilization as well as the other stresses discussed previously. Many excipients can provide cryoprotection, but they are not effective against drying. Typically, disaccharides such as trehalose^{90,96,97} and sucrose⁹⁷ are effective lyoprotectants and are the most commonly used excipients. These sugars, with high glass transition temperatures, reduce the motion of the protein during the drying stage by forming highly viscous glassy matrices that stabilize the labile protein molecule and maintain their native conformation.^{93,95,98} Salts are also present in the formulation for lyophilizing proteins to act as a buffer to control the solution pH.^{83,95} Salts may enhance the stability of the protein solution before lyophilization, but they are not typically employed to preserve the protein stability in the solid formulation.⁹⁹

2.6 Growth Factor Delivery Approaches

Physical encapsulation of growth factors in biodegradable polymers is a favoured approach to preserve the biological activity of proteins and provide a sustained effective local release of growth factors with a minimal initial rapid release, called the burst effect. The protein

release rate is regulated by a number of potential parameters such as the degradation of the polymer and transport by diffusion and/or osmotic pressure.

When designing such a delivery approach, the following criteria should be considered. The polymer used should initiate a moderate tissue response without significant ongoing inflammation or irritation,^{100,101} while preserving the bioactivity of the growth factor. Also, it should be biodegradable through a mechanism producing nontoxic and soluble components that can be completely cleared from the body by metabolism or via the kidney's glomerular filtration. Previous studies have revealed that 3-4 weeks of sustained and local delivery of bioactive growth factors into the hypoxic tissue is necessary to form a stable vascular network and provide effective blood flow.^{13,14,35} Using these results, the desired degradation time frame is 6-10 weeks, which provides effective growth factor release while the delivery device does not remain for a prolonged time at the injection site after completing the treatment period. In fact, the slow degrading delivery devices are able to cause an extended inflammation response and block tissue from the forming blood vessels.¹⁸ The manufacturing process cost should also be considered as growth factors are expensive. Efficient growth factor incorporation into the device while preserving their bioactivity throughout the manufacturing process is necessary. Also, administration of the delivery device directly to the intended site should be minimally invasive. Therefore, non-surgical methods such as injection are favourable. In addition, it would be ideal for growth factors to be sequentially released from the delivery device in a manner that mimics the temporal profile of the healing process *in vivo*.

2.6.1 Microspheres

Biodegradable and biocompatible polymeric microspheres are one of the most common injectable delivery platforms. These microspheres are generally composed of poly(lactide-co-glycolide) (PLGA) containing growth factors as solid particles. This formulation have received attention because PLGA is widely available at different molecular weights and monomer ratios which offers possibilities to determine its degradation and drug release kinetic.^{18,102} Moreover, PLGA does not need any environmental signals or externally applied cues such as changes in pH or temperature, or application of enzymes and ions to regulate the release rate. PLGA microspheres degrade by gradual, random, and non-enzymatic hydrolysis of the polyester backbone into water soluble oligomers and monomers that are eliminated from the body.^{103,104} PLGA Microspheres have been fabricated primarily by emulsion/solvent evaporation techniques using slightly water soluble toxic and carcinogenic organic solvents, such as methylene chloride and ethyl acetate, to dissolve the polymer. An aqueous phase containing the growth factor is then mixed with the organic polymer solution to form a water-in-oil emulsion.^{102,105–107}

protein release rate from PLGA microspheres depends on polymer characteristics such as composition and crystallinity, hydrophilicity, molecular weight, and degradation rate, as well as microsphere properties such as size and porosity, and the nature and amount of any excipients and growth factors loaded in the microsphere. Long-term protein release from microsphere matrices has been difficult to achieve. Release is usually rapid in the first 24 h causing a large burst effect^{105,106,108} followed by a sustained incomplete release.^{106,107,109,110} In general, protein release profile is classified in three phases including

an initial burst release due to dissolution of surface resident protein particles, diffusion-controlled release due to the dissolution of the protein particles within the PLGA microspheres and their diffusion out through the pores and channels, and erosion-controlled release resulted from the degradation of the microspheres providing new pores and channels within the microsphere.^{18,106–110} Also, microspheres are free to move independently at the site of injection. Thus, a method should be considered to prevent their migration from the defect/implantation site. To achieve local treatment, microspheres are often incorporated in scaffolds¹¹¹ or hydrogels^{112,113} in composite delivery systems.

However, the main challenge of using PLGA microspheres is protecting the growth factor bioactivity. Previous studies showed that the degradation process generates acidic species, monomeric lactic and glycolic acid, resulting in a decrease in pH of the surrounding aqueous solution and within the polymer bulk to below 3.^{114–117} Acidic degradation products trapped inside the polymer bulk facilitate the degradation process affecting the release kinetics,^{115,116,118} cause growth factor denaturation,^{119,107} inhibit cell viability,¹²⁰ and may cause tissue inflammation surrounding the implant.¹²¹

Several methods have been utilized to control the local pH within PLGA microspheres including incorporation of basic salts,^{122,123} and blending poly(ethylene glycol) (PEG)^{124,125} into the PLGA matrix. Incorporation of basic salts did not control pH changes, which significantly decreased over 3 weeks.¹²³ Blending with PEG stabilized the pH between 5 and 5.8 over 4 weeks incubation of the microspheres in PBS.¹²⁴ However, a significant VEGF burst of ~70% was observed from the resulting microspheres over the first 4 days.¹²⁶ To control the local pH within PLGA microspheres, another delivery system

was also suggested which is based on decreasing the amount of degradation products by blending PLGA with slower degrading materials such as poly(3-hydroxybutyrate-co-3-hydroxyvalerate)(PHBV).¹²⁷ However, while PHBV degrades remarkably more slowly than PLGA, it could not provide an effective therapeutic release rate. The release profile of FGF-2 encapsulated in the resulting blend microsphere was biphasic, with release over the first 6 days reaching 33%, with a slow release plateau between 7 to 30 days due to the slower degradation rate of a PHBV/PLGA shell than PLGA, and then a second release phase to complete release within 60 days. The released HGF from PLGA/PHBV microspheres maintained its bioactivity for at least 40 days; however, this biphasic release mechanism is not suitable for therapeutic angiogenesis.⁶² These techniques could improve the protein bioactivity and adjust the release kinetics from PLGA microspheres but none of them could prevent PLGA degradation and growth factor denaturation.

2.6.2 Hydrogels

Hydrogels are crosslinked three-dimensional networks of hydrophilic polymers containing large amounts of water. Absorption of significant amounts of water by hydrogels and their soft nature can provide hydrogels the same mechanical properties as the natural ECM which prevents inflammation caused by tissue irritation.¹²⁸ In addition, the porous structure and high water content of hydrogels provide suitable conditions for the incorporation of water-soluble compounds like growth factors. In comparison to PLGA microspheres, it is possible to prepare hydrogel under mild condition using an aqueous environment and body temperature which helps preserve growth factor bioactivity. In general, the growth factor release mechanism from hydrogel can be diffusion controlled

and/or polymer degradation controlled^{74,75,129–132} as well as controlled by affinity binding^{133,134} depending on polymer characteristics (composition, hydrophilicity, molecular weight, charge, and degradation mechanism), hydrogel characteristics (polymer concentration, hydrogel formation/decomposition mechanism, pore size, and the density/nature of the crosslinks) as well as the protein properties (isoelectric point, molecular weight and water solubility).

Injectable hydrogels are one of the favored formulations for growth factor delivery. Injectable hydrogels provide several advantages over the pre-formed implantable hydrogels including minimally invasive nonsurgical administration *in vivo* and the ability to fill nearly any cavity or defect providing a good fit and interface between the hydrogel and the surrounding tissue. In this way the injectable hydrogel remains localized at the site of injection.^{74,135}

In general, injectable hydrogels are classified into two groups as gel-forming materials and pre-formed injectable hydrogels. Gel-forming materials start in the form of a polymer solution which turns into a viscoelastic crosslinked depot at the site of administration upon injection in response to chemical or physical stimuli. Chemical gels formed by covalent crosslinks are not suitable for use as an injectable platform for growth factor release as achieving compatibility between the crosslinking conditions and the incorporated growth factors as well as the surrounding tissue is challenging.^{74,75,135} In contrast, physical gels formed by physical association between polymer chains are more favored. The most common formulation approach for injectable physical hydrogels is based on block copolymers with lower critical solution temperatures (LCST) around 37 °C such as

poly(ethylene oxide)-poly(propylene oxide)-poly(ethylene oxide) (PEO-PPO-PEO),¹³⁶ PEG-PLGA-PEG,¹³⁷ and poly(N-isopropylacrylamide-co-propylacrylic acid).¹³⁸ These formulations convert to a gel via hydrophobic interactions in which hydrophobic domains aggregate at body temperature. Thermosensitive gels demonstrate a high burst effect due to the initial time required for *in vivo* gel formation followed by rapid and short duration release, especially for water soluble drugs, due to the high water content of the hydrogels formed and their fast decomposition. Decomposition of the hydrogel occurs through water influx from the surrounding environment diluting the polymer to below its critical gelation concentration.^{74,75} Physical gels can also be formed based on hydrogen bonding between two or more natural polymers with rheological synergism in mixture such as gelatin-agar¹³⁹, starch-carboxymethyl cellulose¹⁴⁰, and hyaluronic acid-methylcellulose.¹⁴¹ These blend formulations provide excellent biocompatibility, but can also be diluted and dispersed over a few hours to a few days *in vivo* due to water influx from surrounding environment, which leads to limited usage as short-acting drug release systems.⁷⁴

Pre-formed injectable hydrogels are visco-elastic solids that can be syringe delivered. One of the favored formulation approaches of pre-formed injectable hydrogels is shear-thinning hydrogels. Shear-thinning hydrogels have the ability to flow with low viscosity while under stress in the syringe and quickly recover elastic properties after being released from the applied stress. The effect of the local *in vivo* environment on crosslinking of the gel is negligible as these hydrogels are formed *ex vivo*. Also, the recovery of the solid properties after injection may be faster for shear-thinning hydrogels than the rate of gelation after injection of gel-forming materials.¹⁴²⁻¹⁴⁴ Self-assembly is the main crosslinking mechanism for shear-thinning hydrogels, which is achieved as a balance between weak

forces that favor assembly (e.g., hydrophobic interactions, hydrogen bonding and electrostatic attraction) and forces which are against assembly (electrostatic repulsion and solvation).¹⁴⁵ Peptide-based β -hairpin hydrogels such as MAX 8^{146,147} and heparinized star PEG (PEG-LMWH) associated with star PEGs functionalized with heparin-binding peptides (PEG-HBP), PEG-LMWH : PEG-HBP hydrogels¹⁴⁸ are examples of successful shear-thinning hydrogels used for growth factor delivery. The encapsulation of the growth factors within these shear-thinning hydrogels do not negatively affect the gel formation and rehealing after injection, and the applied shear stress did not cause burst effect. A sustained release of bioactive growth factors was observed in the first hours to days of the incubation; however, an incomplete release was finally achieved.^{146,148}

2.6.3 Osmotic Delivery Strategies

Osmotic delivery formulations are based on hydrolysable polymers in which the growth factor is distributed as separate and independent particles. In this approach, protein release is independent of polymer degradation, and a complete and nearly constant release can be achieved before significant degradation of the polymer occurs, thereby preserving the growth factor bioactivity.^{18,149,150} To achieve this goal the growth factor is lyophilized with a cryoprotectant/lyoprotectant excipient such as trehalose which also acts as the osmotic pressure-generating compound. As proteins generate low osmotic pressures in solution, mixing trehalose with the growth factor can effectively generate the osmotic pressure necessary.¹⁴⁹ Complete release can be achieved as the excipient osmotic activity increases,¹⁵¹ or the particle size¹⁵² and tensile strength decreases¹⁵³, and reaches a maximum value at or near the percolation threshold.¹⁵¹ However, the highly osmotic

solution released from the growth factor particles may cause osmotic injury by inducing shrinkage of the cell wall and plasma membrane as well as rehydration of organelles within the cell which subsequently would have resulted in a loss of the cell viability.¹⁵⁴ Osmotic delivery strategies have included both solid and injectable formulations as described below.

2.6.3.1 Solid Osmotic Delivery Formulations

To prepare solid formulations an elastomeric device based on photo-crosslinked star-poly(ϵ -caprolactone-co-DL-lactide) (50:50 molar ratio) with terminal acrylate groups was studied.¹⁵⁵ This formulation provided a constant release and high bioactivity of VEGF for the first 2 weeks, but a significant decrease in VEGF bioactivity occurred rapidly in the later weeks due to a decrease in the internal pH to below 5.¹⁵⁶ Incorporating trimethylene carbonate (TMC) in the elastomer of poly(ϵ -caprolactone-D,L-lactide-trimethylene carbonate) (25-25-50 molar ratio) eliminated the acidic degradation issue,¹⁵⁷ and provided a nearly constant release rate of VEGF and HGF with bioactivity higher than 80 % throughout the release period.¹⁵ However, the solid form possessed, some deficiencies, such as the slow degradation of the elastomer, which had 80 wt% of the initial mass remaining at week 28 long after the release had plateaued at 60% of the initially loaded VEGF. The remaining growth factor would require degradation of the elastomer to be released.¹⁵ The prolonged degradation rate may also cause an extended inflammation response and block tissue from the forming blood vessels.¹⁸

2.6.3.2 Viscous Liquid Osmotic Delivery Formulations

To overcome the deficiencies of solid state delivery formulations, some viscous liquid injectable vehicles were studied recently. The viscous liquid polymers used in these studies with amorphous structure and T_g lower than $-30\text{ }^\circ\text{C}$, are injectable polymers through standard gage needles at $37\text{ }^\circ\text{C}$ with viscosity lower than $150\text{ Pa}\cdot\text{s}$.^{63,158,159} This formulation has some of the same advantages as hydrogels and microspheres such as minimally invasive administration and reduced irritation when implanted in soft tissue. In addition, the growth factor is loaded into the vehicle by simple mixing in the absence of water and organic solvents.

A variety of viscous liquid polymer compositions have been used to prepare injectable delivery depots for protein drug delivery such as poly(ortho esters),^{160,161} low molecular weight poly(α -hydroxy acids),^{162,163} hexyl-substituted poly(lactide),¹⁶⁴ poly(trimethylene carbonate) (PTMC),^{150,158} branched, ester linked, fatty acid polymers from the reaction of glyceryl monolinoleate with succinic anhydride, and low molecular weight fatty-acid based polyanhydrides.¹⁶⁵ Degradation of all these polymers except PTMC results in the accumulation of acidic degradation products within the depot which may cause denaturation of growth factors,^{1,105,108} local tissue irritation.^{121,166}, and also catalyzes the degradation process which affects the growth factor release kinetics.^{116,167,168}

Towards the aim of producing a viscous liquid polymer with no acidic degradation products for growth factor delivery, low molecular weight PTMC with an amorphous structure and glass transition temperature (T_g) of -40 to $-17\text{ }^\circ\text{C}$ has been studied. This formulation

showed an *in vitro* release of VEGF co-lyophilized with trehalose and bovine serum albumin (BSA) matching an osmotic release mechanism with a sustained release of 15 to 20 ng/day over 40 days, followed by a monotonically decreasing rate with time. The released VEGF retained over 90% bioactivity during the release period.¹⁵⁹ However, the *in vivo* degradation rate of injectable PTMC and its depot forming behaviour were highly dependent on the polymer molecular weight. At 620 Da, the PTMC formed dispersed droplets in the tissue following subcutaneous implantation and was absorbed within a week. In contrast at 1600 Da and 2400 Da, PTMC formed a coherent depot upon implantation, but degraded very slowly, reaching only 10 % and 55% weight loss after 40 weeks, respectively.¹⁵⁸

To overcome the slow *in vivo* degradation rate and difficulties of forming a cohesive depot observed for low molecular weight PTMC, low molecular weight injectable poly(5-ethylene ketal ϵ -caprolactone-co-D,L-lactide) (PEKCDLLA) with viscosity below 130 Pa·s at 37 °C was studied. The copolymers exhibited surface erosion degradation kinetic with a nearly linear degradation rate,^{169,170} formed a cohesive depot after subcutaneous injection in rats and were well tolerated *in vivo*.¹⁷⁰ VEGF and HGF co-lyophilized with BSA and trehalose were incorporated into PEKCDLLA by simple mixing. The *in vitro* release study revealed that VEGF and HGF were released in a sustained near zero-order release profile with a minimal burst effect, achieving complete release within 7 and 14 weeks for VEGF and HGF, respectively.⁶³ The release mechanism was also studied and explained as follows (Figure 2.2).¹⁷¹

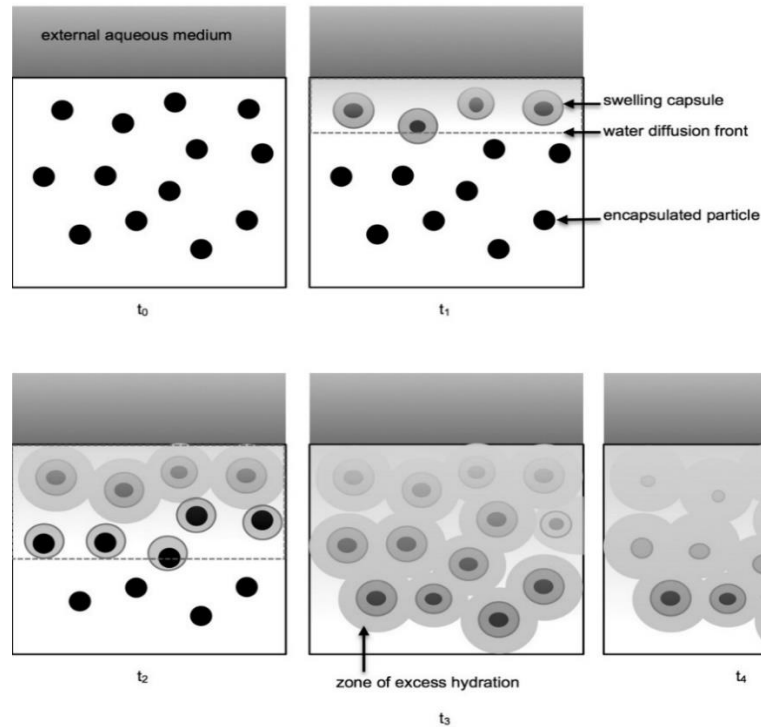


Figure 2.2. Pictorial representation of the osmotic release mechanism that involves the formation of zones of excess hydration wherein solute transport occurs.¹⁷¹

After implantation, water absorbs into and diffuses through the device until reaching the incorporated particles (time t_1). Then water dissolves the solid at the water/polymer interface to form a saturated solution. Subsequently, the water activity gradient between the external solution and the solution formed at the particle surface draws water into the polymer and generates a pressure equal to the osmotic pressure of the saturated solution. Depending on the resulting osmotic pressure and polymer viscosity, capsules form around the particles. The resulting capsules swell because of the osmotic pressure. At some point, the maximum swelling of the capsule is reached but due to the water activity gradient water is still diffusing into the capsule region. The generated pressure and the low molecular weight of the polymer, force water into the polymer region surrounding the capsule,

forming superhydrated polymer regions. In these regions the water concentration is higher than the fully hydrated polymers in the absence of the encapsulated particles. The superhydrated regions surrounding the polymer are referred to as zones of excess hydration (t_2). The resulting zones eventually overlap as water diffuses further through the polymer (t_3). Then solute is driven by convection and/or diffusion through the superhydrated region to the polymer/aqueous medium interface. This convection results from the pressure difference between the osmotic pressure in the swollen capsules and the osmotic pressure of the surrounding release medium. Once the solid particles have completely dissolved, the osmotic driving force decreases and capsules are no longer present.¹⁷¹ Based on this mechanism, the release rate depends on the osmotic activity of the entrapped particles determined by the excipient content and/or water solubility of the incorporated protein, and the relaxation ability of the polymer chains to tolerate the swelling pressure, as reflected by the polymer glass transition temperature.

PEKCDLLA degraded to form acidic degradation products.¹⁷⁰ Nevertheless, the bioactivity of the released VEGF and HGF was greater than 80%. The high bioactivity was due to the remove of acidic degradation products through the superhydrated regions formed around the incorporated particles which ensured close to neutral local pH surrounding the particles.⁶³ However, the PEKCDLLA degraded slowly, with 20-50% of the initial mass still remaining *in vivo* long after complete release of the growth factors.

2.7 Injectable Drug Delivery Vehicle Based on aliphatic polycarbonates

As mentioned above, low molecular weight PTMC is a promising biomaterial for growth factor delivery as it does not generate acidic degradation products. PTMC does not degrade appreciably via hydrolysis, and *in vivo* degradation is molecular weight dependent.¹⁷²⁻¹⁷⁴ Under *in vivo* condition, upon failure to engulf PTMC, macrophages attach to PTMC surface releasing hydrolytic enzymes and oxygen species which degrade the surface of PTMC.^{174,175} Studies on the degradation of 60 kDa and 100 kDa PTMC in the presence of cholesterol esterase and lipase revealed that the surface stiffness and polymer chain flexibility affect the enzymatic adsorption, conformation and activity as cholesterol esterase and lipase caused 98% and 39% mass loss of 100 kDa PTMC within 9 weeks, respectively, while mass loss of 60 kDa PTMC was negligible.¹⁷⁴ Injectable low molecular weight PTMC, 2400 Da and 1600 Da, showed much slower degradation, losing only 10 to 55 % of the initial mass after 50 weeks implantation in rats. Mass loss for these low molecular polymers was due to their absorption into the tissue and/or blood stream.¹⁵⁸ Therefore, it is necessary to modify PTMC based formulations with hydrophilic/hydrolysable units to achieve an appropriate degradation rate .

It was reported that the presence of hydroxyl pendent groups along the backbone of aliphatic polycarbonates would enhance their degradation by increasing the polymer hydrophilicity and cleavage of the carbonate bond via intramolecular nucleophilic attack of a hydroxy substituent at a carbonate function.¹⁷⁶ In an attempt to provide hydrolytic degradation to polycarbonates, a glycerol-derived polycarbonate named poly(2-hydroxy trimethylene carbonate) (PHTMC) has been synthesized. PHTMC is prepared from

polymerization of 5-benzyloxy trimethylene carbonate (BTMC), followed by debenylation of the benzyloxy group to an hydroxyl group.¹⁷⁷⁻¹⁷⁹ Figure 2.3 shows the chemical structure BTMC and PHTMC. An examination of the degradation of PHTMC by Dr. Chen from the Amsden group showed that the presence of the pendant hydroxyl group resulted in a rapid rate of degradation, with a 42 kDa homopolymer reaching complete mass loss within 24 hours at neutral or alkaline pH producing glycerol and carbon dioxide as degradation products,¹⁸⁰ both of which are natural components of physiological systems.^{181,182}

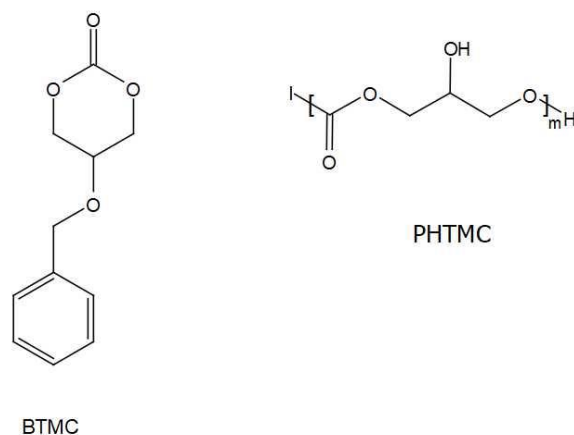


Figure 2.3. Chemical structure of BTMC and PHTMC, “I” in PHTMC structure represents the initiator.

Copolymerization has been known as one of the most used approaches to adjust the properties of polymeric materials. Based on the rapid degradability of PHTMC, it was hypothesized that introduction of HTMC units into the PTMC chain may provide a new pathway to adjust degradation rate of PTMC-based drug delivery formulations for short term release applications. However, the presence of hydroxyl groups along the polymer backbone would also result in a higher glass transition temperature and higher viscosity in

the final copolymer. To achieve the desired injectable drug delivery device, copolymer properties such as monomer content, monomer distribution along the polymer chain, and molecular weight would need to be examined.

2.8 Polymerization Catalysts

PTMC is typically produced by ring-opening polymerization (ROP) of the cyclic carbonate monomer with various metal alkoxides including tin(II) 2-ethylhexanoate ($\text{Sn}(\text{Oct})_2$) at high temperature.^{183–185} $\text{Sn}(\text{Oct})_2$ is still the most frequently used and most efficient catalyst in TMC polymerization, but tin complexes have shown potential toxicity due to tin residues and subsequently extensive purification is required for biomedical applications.¹⁸⁶ Therefore less toxic metal complexes such as calcium, magnesium, iron and zinc,^{187–189} as well as several organic compounds such as 1,8-diazabicyclo-7-undecene (DBU)^{184,190–193} and a hydrogen chloride solution in diethyl ether ($\text{HCl}\cdot\text{Et}_2\text{O}$)^{184,194,195} have been investigated for a low toxicity preparation of PTMC for biomedical applications.^{186,196} Both DBU and $\text{HCl}\cdot\text{Et}_2\text{O}$ catalyze TMC polymerization at room temperature under solution conditions with reasonable control over molecular weight and molar mass dispersity. The ROP of TMC proceeds by different mechanisms with each of these catalysts, as described in the following section.

$\text{Sn}(\text{Oct})_2$ is generally considered to act in a coordination-insertion manner, in which the stannous dialkoxide initiator, compound 2 in Figure 2.4 produced by the reaction between alcoholic initiator and $\text{Sn}(\text{Oct})_2$, becomes coordinated with the carbonyl of a carbonate monomer, ultimately causing it to be inserted between the Sn group and the rest of the

polymer chain. With this mechanism, several side reactions are possible. First, the initiator can be deactivated with a reaction with water present in the polymerization environment (Figure 2.4, compound 4). Also, the hydroxyl group of water can initiate polymerization. Second, there is a possible reaction between the active polymerizing center and water or the alcoholic initiator as well as transesterification can convert the active propagating chain to an inactive alcohol (Figure 2.4, compound 6). Third, at the high temperatures of polymerization back-biting of the propagating chain end leading to the formation of TMC as well as TMC auto-initiation is possible. All these reactions may affect the end group fidelity, a parameter that quantifies the proportion of the polymer chains that contain the expected end-groups, and cause difficulties in achieving the desired molecular weight with narrow dispersity that subsequently affects the final physical and mechanical properties of polymer.^{184,185}

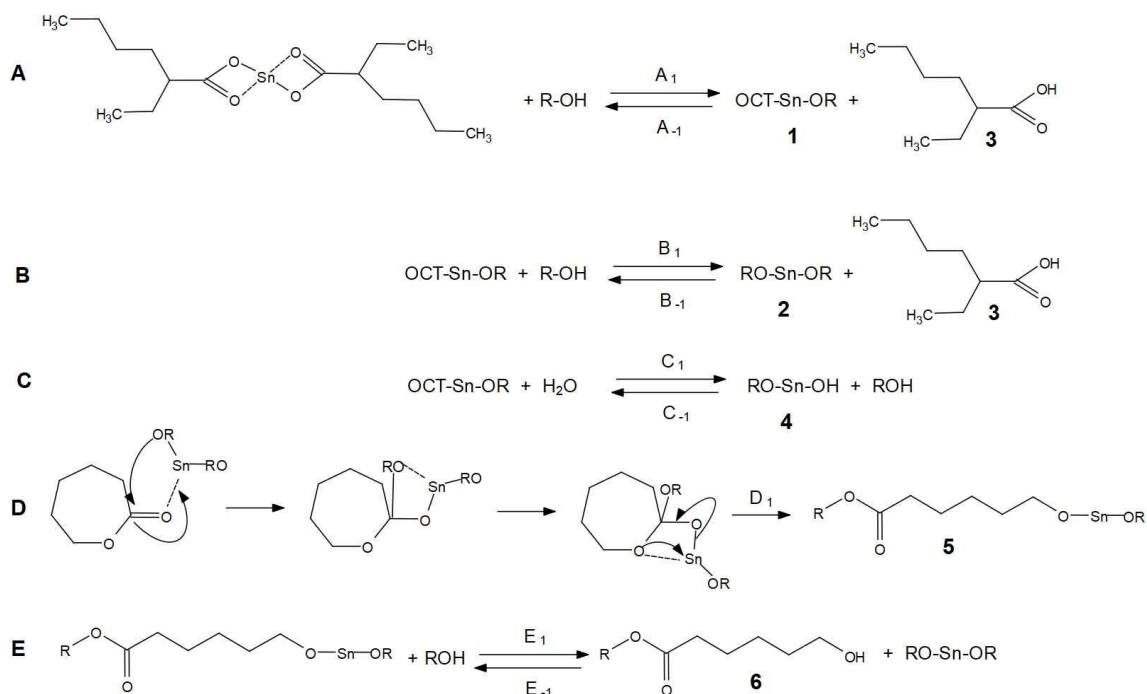


Figure 2.4. Mechanism of polymerization of ϵ -caprolactone in the presence of $\text{Sn}(\text{Oct})_2$ as a catalyst, including (A,B) formation of stannous alkoxide initiator, (C) catalyst deactivation by water, (D) propagation step via coordination/insertion of monomer into the stannous alkoxide bond, (E) deactivation of polymerizing center via reaction with water or alcoholic initiator as well as transesterification.¹⁸⁵

It is reported that TMC undergoes cationic polymerization with various alcohol/ $\text{HCl}\cdot\text{Et}_2\text{O}$ initiator systems via a monomer activation mechanism (Figure 2.5). This mechanism could suppress unfavorable reactions such as disproportionation and decarboxylation. Also, conducting the reaction at room temperature decreases the chance of TMC auto-initiation and back-biting. According to this mechanism, initially the hydrogen ion of $\text{HCl}\cdot\text{Et}_2\text{O}$ activates the TMC monomer by conjugating to the carbonate bond. The resulting activated monomer is more susceptible to a nucleophilic attack by the hydroxyl group on the alcoholic initiator or the growing chain end.^{195,197}

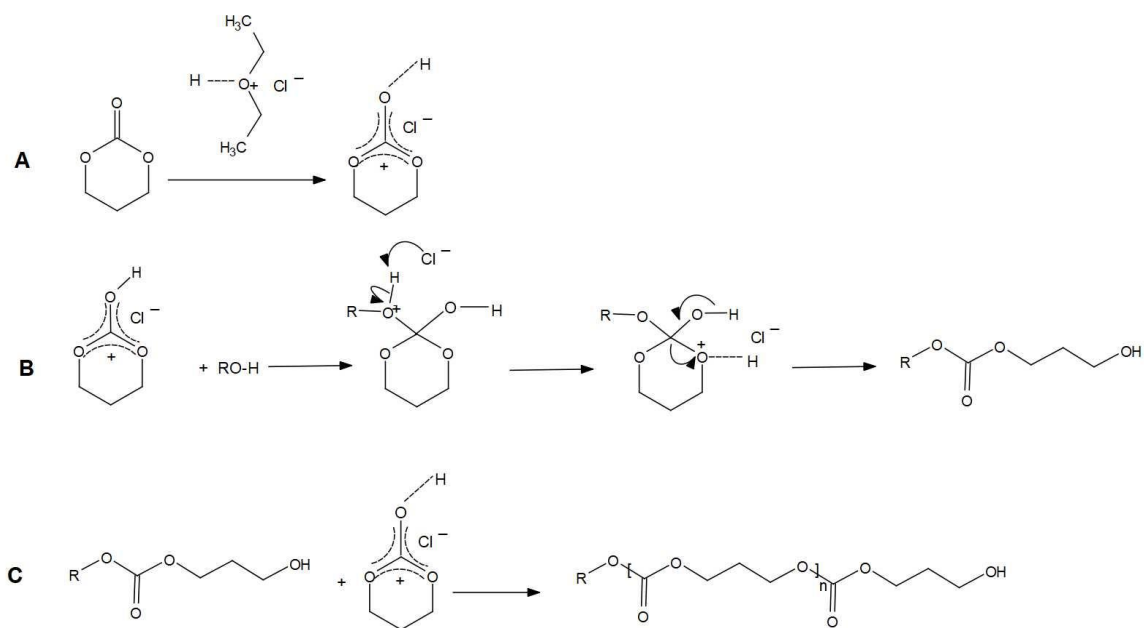


Figure 2.5. Mechanism of polymerization of TMC in the presence of HCl·Et₂O as a catalyst, including (A) activation of monomer, (B) polymer initiation step via nucleophilic attack of the hydroxyl group on the alcoholic initiator, (C) propagation step via nucleophilic attack of the hydroxyl group on the growing chain end.^{195,197}

DBU catalyzes polymerization of carbonate monomers via two different mechanisms including activation of the initiating/propagating hydroxyl group via hydrogen bonding (Figure 2.6.A),^{198,199} and an anion mechanism in which DBU conjugates with TMC, forming an alkoxide anion. The resulting alkoxide anion serves as an initiator that can attack the carbonyl group of TMC monomers (Figure 2.6.B).^{184,190,199,241}

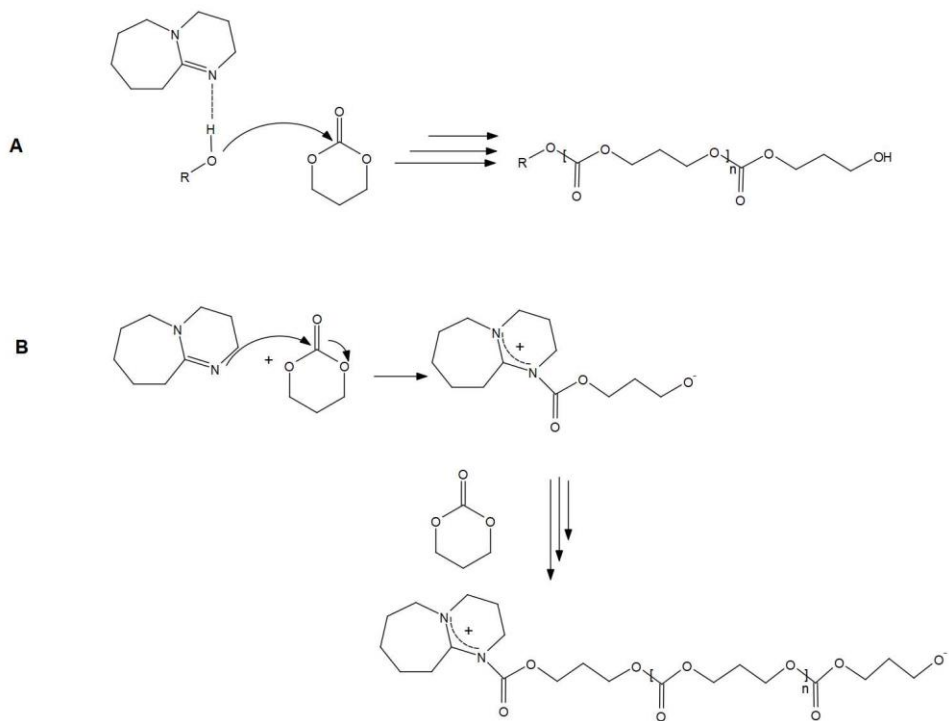


Figure 2.6. Mechanism of polymerization of TMC in the presence of DBU as a catalyst, including (A) activation of the initiating/propagating hydroxyl group,¹⁹⁸ (B) formation of alkoxide anion initiator and propagation step via the attack of anion to the carbonyl bond of TMC.¹⁸⁴

These studies have highlighted the fact that the choice of catalyst may determine the polymerization conditions, purification process, polymer dispersity, and the end group fidelity, and subsequently adjusts the physical/mechanical properties and biocompatibility of the final polymer. There are several studies on successful copolymerization of TMC with functionalized monomers for biomedical applications.^{175,183,184,194} The presence of pendant groups on TMC such as the benzyloxy group of BTMC may affect the activity of the carbonate bond in the presence of each catalyst, which influences the BTMC polymerization rate and subsequently the conformation of its copolymer with TMC. A BTMC homopolymer as well as its random and block copolymers were also fabricated via ROP of cyclic carbonate monomers, most frequently with Sn(Oct)₂ as a catalyst.^{177–179,200–}

²⁰⁴ However, given the potential toxicity of residual Sn in the polymer, it is necessary to determine the effect of the pendent benzyloxy group of BTMC on polymerization rates in the presence of less toxic catalysts such as DBU and HCl·Et₂O.

2.9 Tissue response

All delivery vehicles induce a tissue response when implanted into living tissue. The tissue response continuum is the series of body responses that are initiated by the administration procedure followed by the presence of the delivery device including responses to the biomaterial, its degradation products, and the released growth factor. Therefore, it is necessary to initially study the effect of the biomaterial and its degradation products on the surrounding tissue. The tissue response to the delivery device is characterized by multiple factors including the extent of injury and the loss of basement membrane caused via the administration process, blood-material interactions, provisional matrix formation, acute inflammation, chronic inflammation, granulation tissue and fibrosis/fibrous capsule development at the tissue-biomaterial interface.^{100,101,205,206} All biomaterials initiate an inflammatory response, but materials resulting in stable healing without significant ongoing inflammation or irritation are deemed to be biocompatible.

In the first hours after implantation, the damage incurred to the vascularized tissue causes blood-material interactions and inflammatory cell recruitment, specifically neutrophils and monocytes. The blood-material interactions cause blood protein deposition onto the surface of the biomaterial leading to the formation of a transient provisional matrix consisting of the initial thrombus/blood clot, at and around the tissue-biomaterial interface. The

provisional matrix is a natural sustained release environment rich in activating and inhibiting substances such as mitogens, chemoattractants, cytokines and growth factors that are capable of modulating macrophage activity along with the proliferation and activation of other cells in the inflammatory response and wound healing process. The tissue response to the biomaterial is indirectly induced by the surface chemistry and hydrophobicity of the biomaterial surface that determines the composition of the adsorbed layer of proteins.^{207,208} In addition, the charge of the biomaterial determines neutrophil and macrophage adhesion and foreign body giant cells (FBGC) formation.^{209,210}

Following the coagulation around the implanted biomaterial, fibrinogen is hydrolyzed to fibrin by thrombin, forming a dense fibrin network. The hydrolysis process activates fibrin stabilizing factor (factor XIII) to catalyze the formation of crosslinks within the deposited fibrin network.²⁰⁶ The fibrin network improves leukocyte, neutrophil and macrophage adhesion,^{211,212} and plays the role of a transient matrix for leukocyte extravasation.²¹³ Fibrinogen adsorbs most abundantly to the surface of hydrophobic biomaterials which are progressively denaturing over time, leading to the exposure of the P1 fragment of fibrinogen.²¹⁴ Exposure of the P1 fragment induces biomaterial binding to the phagocyte integrin complement receptor (CR3) leading to the adhesion of tissue phagocytes to the biomaterial. Subsequently, these phagocytes release cytokines and chemokines such as interleukin-1 (IL-1), tissue necrosis factor (TNF- α), VEGF and C-C chemokine ligand (CCL)-2/MCP-1 that activate the proximal vasculature and attract leukocytes and fibroblasts.²¹⁵

Finally, complement factor C3b can bind to the biomaterial inducing the complement system.^{216,217} The adsorbed C3b is recognized by infiltrating phagocytes through binding to the CR1 receptor. In addition, complement factor Bb can bind to C3b forming C3 convertase C3bBb. C3bBb can splice many C3 molecules to C3a and C3b convertase inducing the opsonization process which leads to the release of the potent leukocyte chemoattractant C5a, and leukocyte infiltration during the acute phase of inflammation as well as the release of oxidative metabolites.²⁰⁶ The presence of C3a and C5a also increases the permeability of the capillaries and induces the release of histamine and interleukin-13 (IL-13) by mast cells in the surrounding tissue, which amplifies the inflammatory response and consequently the foreign body reaction by recruiting phagocytic cells including macrophages.^{100,206} Also, antibodies may bind to the biomaterial surface activating the classical complement pathway. The Fc domain of these antibodies is recognized by complement factor C1q that subsequently deposits and activates C3b on the biomaterial causing a similar response as seen with spontaneously adsorbed C3b.^{206,215} The provisional matrix and the adsorption of fibrin, complement and antibodies activates the following inflammatory process. Therefore, the initial foreign body reaction against the biomaterial depends on the physiochemical characterization of the biomaterial and the extent of the injury caused via administration.

Acute inflammation begins by the infiltration of neutrophil granulocytes (polymorphonuclear leukocytes, PMNs) that are attracted to the implantation site within 24-48 hours. This phase is characterized by the presence of neutrophils as the first set of phagocytic cells to infiltrate the site of implantation. Neutrophils are attracted by the secretion of TGF- β , platelet factor 4 (PF4), TNF- α and IL-1 by platelets. Neutrophils kill

any bacteria around the site of implantation by secreting lysosomal agents and oxygen free radicals.^{206,218} Redundant neutrophils are cleared from the implantation site by extrusion to the wound surface as slough or by phagocytosis by macrophages. The main function of PMNs is specific to the first days after implantation to prevent infection, and they are considered to have little influence beyond this stage.^{100,101,205,206,218}

The chronic inflammation phase follows the acute inflammation and extends for 2-3 weeks. During this stage, the blood monocytes are attracted to the tissue by a variety of chemoattractants including complement, clotting components, fragments of immunoglobulin G, leukotriene B₄, platelet factor IV, PDGF and TGF- β , and undergo a phenotypic change to convert to tissue macrophages.²¹⁸ Macrophages are the key regulatory cells at this stage of the inflammatory process. The assembled macrophages are phagocytic cells and the primary producers of growth factors including PDGF, TNF- α , interleukin 6 (IL-6), granulocyte-colony stimulating factor (G-CSF) and granulocyte macrophage-colony stimulating factor (GM-CSF). These growth factors are responsible for attracting more macrophages and fibroblasts to the site of implantation to proliferate and produce replacement ECM by fibroblasts as well as the proliferation of SMCs and ECs resulting in angiogenesis.^{206,218}

The secreted cytokines in the acute and chronic inflammatory phases induces the formation of granulation tissue, which has a pink, soft, granular gross appearance as a hallmark of healing inflammation. Histologically, the granulation tissue is characterized by proliferating fibroblasts and vascular endothelial cells in a loose ECM. This process involves proliferation and maturation of ECs into capillary tubes, and proliferation of

fibroblasts and myofibroblasts, which are responsible for synthesizing collagen, especially collagen type I and III, fibronectin and proteoglycans around the implanted biomaterial.^{100,206,218} The thickness of the resulting collagenous capsule formed around the implanted biomaterial would directly affect the kinetic of the growth factor release to the ischemic site as the released growth factors need to diffuse through the fibrous layer to initiate angiogenesis.²¹⁹ If the implanted polymer and its degradation products cause irritation to the surrounding tissue, macrophages and FBGCs will persist around the biomaterial to phagocytose the degradation products by attracting more macrophages and forming FBGCs. Therefore, the tissue response may continue till the polymer degrades completely and its degradation products are eliminated from the body.^{100,219,220}

2.10 Summary

The sustained and local delivery of bioactive angiogenic growth factors at optimized dosage and sequence using a delivery vehicle is a promising clinical approach for treating critical limb ischemia. As demonstrated by the natural angiogenesis process, multiple growth factors are involved in forming new and stable blood vessels. VEGF-A is the most potent angiogenic growth factor initiating angiogenesis via binding to VEGFR-2 expressing on ECs, and subsequently affects EC mitogenesis. When designing such a delivery device multiple issues should be considered including biocompatibility of the biomaterial and its degradation products as well as the degree and extent of the tissue damage caused via the administration process determining the tissue response, the manufacturing process affecting the bioactivity of the incorporated growth factor, and the release mechanism determining the dosage, sequence and bioactivity of the released

growth factor. Injectable delivery vehicles possess a number of advantageous and so may be a promising approach in therapeutic angiogenesis.

Chapter 3

Proposed Approach and Objectives

3.1 Proposal

A delivery formulation for treating critical limb ischemia should be biocompatible and biodegradable and able to be administered directly to the affected site via a minimally invasive approach. This delivery vehicle should provide a sustained release at the effective local dose of the target growth factor with a minimal initial burst effect while the bioactivity of the growth factor is preserved.^{14–16}

To achieve these goals, fabrication of a viscous and biodegradable delivery formulation based on modified low molecular weight PTMC was proposed in which VEGF would be incorporated as a lyophilized powder by simple mixing. The rationale of introducing modified low molecular weight PTMC to make a delivery device was as follows. The low molecular weight PTMC homopolymer, number average molecular weight (M_n) lower than 2400 Da, has a low glass transition temperature (T_g) of -40 to -17 °C and an amorphous structure, which makes it a relatively low viscosity polymer at room temperature and at 37 °C.¹⁵⁸ Also, its amorphous structure prevents incomplete release of loaded growth factor that results from the presence of polymer crystallinity as well as tissue inflammation caused by exposing polymer crystals to tissue.²²¹ However, its depot forming behavior, degradation rate, and subsequently the growth factor delivery capacity and release rate are highly dependent on the polymer molecular weight.^{221,222} Previous studies showed that at 620 Da, PTMC was dispersed into numerous droplets in the tissue upon subcutaneous

implantation, which were rapidly absorbed by the body (80% within the first 7 days). In contrast, at a higher molecular weight of 1600 Da, PTMC formed a cohesive single depot in the body that degraded very slowly, reaching only 55% weight loss after 40 weeks.²²¹

Clinical trials have consistently demonstrated that administration of a single growth factor is not sufficient to provide a stable and effective blood vessel network.^{18,57,73} According to the natural angiogenesis process, multiple growth factors are involved to induce EC activation, proliferation, migration, and tube formation as well as attracting pericytes/SMCs to stabilize the newly formed blood vessels.^{7,43,81} Therefore, several studies have examined the co-administration of angiogenic growth factors such as VEGF/FGF-2,^{59,82} VEGF/PDGF-BB,^{58,60,61} PDGF/FGF-2,⁵⁹ VEGF/HGF,^{15,63} VEGF/PIGF⁶⁷ to improve therapeutic angiogenesis. However, this study focused on the release behavior of VEGF as the most potent angiogenic growth factor stimulating the proliferation and migration of endothelial cells^{56,69,82,223} to determine the feasibility of releasing bioactive growth factors from the designed formulation.

3.2 Objective

The main objective of this project was to determine the ability of a delivery formulation based on modified low molecular weight PTMC for localized and sustained release of bioactive VEGF.

3.3 Specific Aims

To achieve the above objective the following 4 specific aims were studied:

1. The synthesis, characterization and assessment of the *in vitro* degradation of a hydrolysable and injectable ester or anhydride-linked low molecular weight PTMC.
2. The synthesis, characterization and assessment of the *in vitro* degradation of low molecular weight poly(trimethylene carbonate-co-2-hydroxy trimethylene carbonate) (P(TMC-co-HTMC)).
3. Determination of the influence of the copolymer composition of P(TMC-co-HTMC) on its *in vivo* degradation rate and tissue response.
4. Determination of the effect of P(TMC-co-HTMC) composition, degradation rate and the protein particle composition on *in vitro* release of VEGF and its bioactivity.

Chapter 4

Hydrolysable, Conjugated, Low Molecular Weight Poly(trimethylene carbonate) (PTMC): Synthesis, Characterization and *In Vitro* Degradation

4.1 Abstract

In this chapter, Specific Aim 1 is addressed, namely the synthesis, characterization and *in vitro* degradation study of a hydrolysable ester or anhydride-linked low molecular weight PTMC, as an injectable delivery vehicle. PTMC was prepared via melt ring opening polymerization initiated with either a hydrophobic (1-octanol) or hydrophilic initiator (350 Da poly(ethylene glycol) methyl ether, P350) using tin(II) 2-ethylhexanoate as a catalyst. The ester or anhydride linked PTMCs were prepared using sebacyl chloride and diglycolyl chloride as conjugation molecules. An *in vitro* mass loss study of the conjugated samples showed that the anhydride bond cleaved within the first 24 hours, generating acidic products that lowered the pH of the buffered degradation medium. In contrast, due to the slower reactivity of the ester bond, ester hydrolysis did not result in an acidic pH within the incubation medium. However, the ester bond degraded too slowly for the intended application. Using P350 as an initiator increased the total mass loss to about 26 wt% within 28 days; however, using P350 caused a large initial mass loss of solubilized polymer followed by a very slow mass loss. Based on these results the conjugation approach was considered to not provide a desirable polymer degradation profile.

4.2 Introduction

With the objective of producing a viscous liquid polymer with no acidic degradation products for growth factor delivery, low molecular weight poly(trimethylene carbonate) (PTMC) with amorphous structure and glass transition temperature of $-40\text{ }^{\circ}\text{C}$ to $-17\text{ }^{\circ}\text{C}$ has been introduced recently. However, the *in vivo* degradation rate of injectable PTMC was not controllable, and its depot forming behaviour was highly dependent on the polymer molecular weight. Previous studies showed that at 620 Da, PTMC was dispersed into numerous droplets in the tissue upon subcutaneous implantation, and rapidly absorbed by the body (80% within the first 7 days). In contrast at a higher molecular weight of 1600 Da, PTMC formed a cohesive single depot in the body, but one that degraded very slowly, reaching only 55% weight loss after 40 weeks.¹⁵⁸ Therefore, in this chapter a strategy of linking low molecular weight PTMC chains in the range of 600-1000 Da, with a hydrolysable ester or anhydride linkage (Figure 4.1) was examined. In this way, a molecular weight large enough to form a cohesive depot would be attained, while still providing biodegradability.

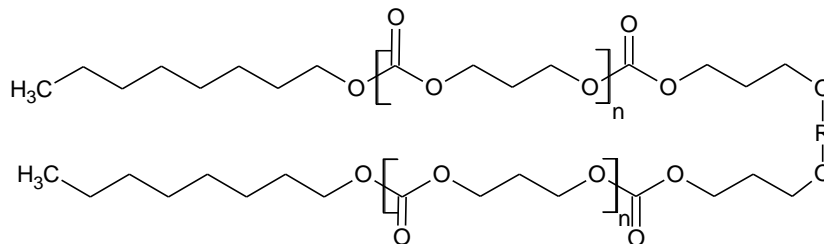


Figure 4.1. General chemical structure of low molecular weight PTMC blocks conjugated with a hydrolysable linkage (R).

Based on this strategy, cleavage of the hydrolyzable linkage would form two water soluble PTMC chains, which would be readily eliminated from the body.¹⁵⁸ To adjust polymer degradation rate, the hydrophilicity of the initiator used, the molecular weight of the PTMC blocks, and the susceptibility of the linking bond to cleavage in an aqueous environment are important parameters. Therefore, different initiators generally recognized as safe for *in vivo* use, such as 1-octanol and low molecular weight poly(ethylene glycol) methyl ether (Figure 4.2.A), were used in combination with the diacid halides as sebacoyl chloride (SC) or diglycolyl chloride (DGC) (Figure 4.2.B) to form conjugated PTMC.^{224,225} It was reasoned that the degradation products formed from the hydrolysis of the resulting polymer, sebacic acid and glycolic acid, which are naturally present in the body, would not cause an adverse tissue response.²²⁶⁻²²⁹

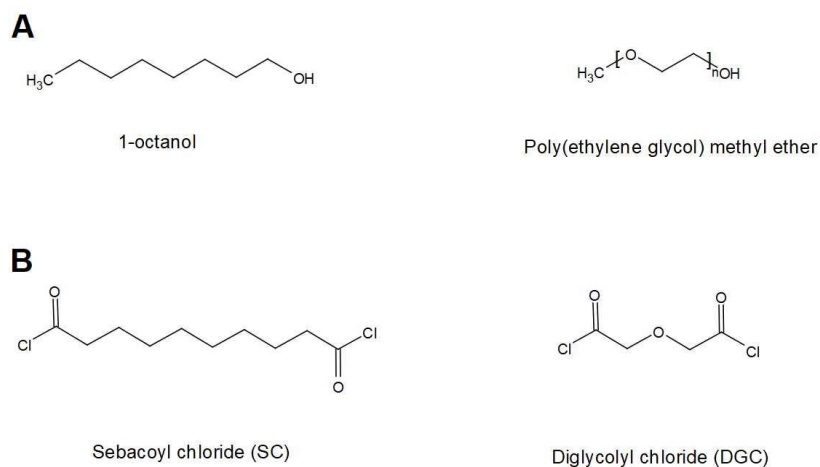


Figure 4.2. Chemical structure of A) initiator molecules, B) conjugation molecules used.

The objective of this chapter was to synthesize, characterize and determine the *in vitro* degradation of hydrolysable ester and anhydride conjugated low molecular weight PTMC

to assess the potential of this polymer approach for forming a suitable liquid injectable vehicle for VEGF delivery.

4.3 Materials

1,3-trimethylene carbonate (Boehringer Ingelheim) (TMC) was obtained from Leapchem, Hangzhou, China. Stannous 2-ethylhexanoate ($\text{Sn}(\text{Oct})_2$) was purchased from Alfa Aesar, USA. Succinic anhydride, sebacoyl chloride (SC), diglycolyl chloride (DGC), triethylamine (TEA), 1-octanol, 350 Da poly(ethylene glycol) methyl ether (P350), deuterated dimethyl sulfoxide (DMSO-d_6) were purchased from Sigma-Aldrich Ltd, Canada. Phosphate buffered saline (PBS) powder, dichloromethane (DCM), ethyl acetate (EtOAc), and toluene were purchased from Thermo Fisher Scientific, Canada. Water used was of type 1 purity, obtained from a Millipore Milli-Q Plus ultrapure water filtration system. Solvents were dried over activated 3 Å molecular sieves. All other materials were used as received.

4.4 Methods

4.4.1 Synthesis of poly(trimethylene carbonate) (PTMC)

Low molecular weight PTMC was synthesized by a ring opening melt polymerization of TMC at 125 °C. In this reaction, 1-octanol and P350 were used as initiators to adjust both PTMC molecular weight and hydrophilicity, and $\text{Sn}(\text{Oct})_2$ was used as a catalyst. A monomer to catalyst mole ratio (M/C) of 800:1 was used based on a previous protocol for TMC polymerization.¹⁵⁸ The following is a representative procedure for preparing PTMC

at a monomer to initiator mole ratio (M/I) of 5:1. 1-octanol (1.27 g, 9.8 mmol), TMC (5 g, 49 mmol), and 57 μ L of 50 % Sn(Oct)₂ solution (24.8 mg, 0.06 mmol of catalyst) in dry toluene were added to a previously flame-dried glass ampoule. The ampoule was purged with argon then evacuated under vacuum, for 3 cycles. Finally, the ampoule was vacuum sealed and placed in a 60 °C oven for 10-15 min to melt the monomer. The resulting melt was mixed using a vortexer and placed in an oven maintained at 125 °C under 20 mm Hg vacuum overnight. Different monomer to initiator ratios were used to achieve polymers of different molecular weight.

4.4.2 Synthesis of carboxylic acid terminated PTMC (PTMC-COOH)

Without any purification, PTMC was transferred to a newly dried glass ampoule with a stoichiometric amount of succinic anhydride to terminal PTMC hydroxyl. The ampoule was purged with argon, and flame-sealed under vacuum. The mixture was placed at 160 °C under 20 mm Hg vacuum for 4 h. The resulting functionalized polymer is referred to hereafter as PTMC-COOH.

4.4.3 Ester and anhydride conjugation

To prepare ester-linked PTMC, it was reacted with diacid halides (DGC or SC) in dry DCM in the presence of TEA as a catalyst and acid scavenger at a TEA/polymer molar ratio of 1.05. All steps were done in dry glassware at low humidity (between 5-8%) in a glove box to prevent the hydrolysis of the reactants and the final product. Anhydride linked PTMC was prepared in the same manner, with the exception that PTMC-COOH was used instead

of PTMC. To purify the conjugated polymers, DCM was extracted completely by evaporation on a rotary evaporator, and then the resulting precipitate was dissolved in EtOAc to a concentration of 10 wt%. The TEA·HCl salt was filtered out and the polymer solution was concentrated to 20 wt%. The concentrated solution was placed at -20 °C overnight to force the remaining TEA·HCl salt to precipitate. Then the top layer was separated and centrifuged for 8 min. Finally, EtOAc was extracted by evaporation on the rotary evaporator, and the final polymer dried at 40 °C under 20 mm Hg vacuum.

4.4.4 Polymer Characterization

A Bruker Avance-400 MHz spectrometer was used to measure ^1H NMR spectra of the polymers in DMSO- d_6 (10 mg/mL) at room temperature after the initial polymerization, conjugation reaction and throughout *in vitro* degradation. The conversion rate of TMC to PTMC and the number average molecular weight (M_n) of the resulting PTMC (conjugated and non-conjugated PTMC) were calculated by comparing the signal intensity of the methylene groups adjacent to the carbonate bond ($\delta = 4.4$ ppm) of the unreacted TMC and the central methylene groups from the alkane region of PTMC ($\delta = 1.9$ ppm and 1.72 ppm), respectively, to the signal intensity of the methyl group of 1-octanol ($\delta = 0.8$ ppm), or to the methylene group of P350 ($\delta = 3.6$ ppm). The degree of conversion of the hydroxyl chain ends to carboxylic acid in the formation of PTMC-COOH, as well as the extent of the ester conjugation reaction were calculated by comparing the signal intensity of the remaining central methylene group of the end unit of PTMC ($\delta = 1.72$ ppm) to the signal intensity of the methyl group of 1-octanol ($\delta = 0.8$ ppm), or to the methylene group of P350 ($\delta = 3.6$ ppm). The extent of the anhydride conjugation reaction was calculated by

comparing the signal intensity of the methylene group linked to anhydride bond ($\delta = 2.76$ ppm) to the signal intensity of the methyl group of 1-octanol ($\delta = 0.8$ ppm).

Thermal properties were determined using a Mettler-Toledo DSC1 differential scanning calorimeter. A heating and cooling rate of 10 °C /min was applied over a temperature range of -100 °C to 80 °C. The glass transition temperature (T_g) was taken as the midpoint of the inflection in the second heating cycle. The initial water solubility of ester and anhydride-linked PTMCs was measured by adding 1 mL of 37 °C distilled water at an initial pH of ~7 to 50 mg of each polymer. The samples were then continuously mixed on a rotary mixer for 24 h at 37 °C. After this time, the supernatant was extracted and freeze-dried. The dry mass of the dissolved polymer was measured, and the solubility reported as a wt% concentration.

4.4.5 *In vitro* Polymer Degradation

The *in vitro* degradation rate was assessed in pH 7.4 phosphate buffered saline (PBS). Approximately 50 mg of each polymer was placed at the bottom of a 1 mL glass vial and then 1 mL of 37 °C PBS was added. To add the polymer, it was pre-heated to 37-40 °C while within a plastic 1 mL syringe and injected into the bottom of the glass vial. The exact initial weight of polymer in each vial was measured and recorded. The vials were then placed in a thermomixer at 37 °C with horizontal shaking at 300 rpm. The solution pH was measured at each time point to assess the effect of the degradation products on the pH of the PBS. At specific time points, 3 samples were collected, the PBS was removed by aspiration using a pipette, the remaining polymer was washed 3 times with distilled water

to remove residual buffer salts, and then the polymer was dried to a constant weight on a Modulyo D lyophilizer (Thermosavant, USA) at -50 °C and 100 mbar. The resulting dry samples were analyzed at each time point for weight loss, molecular weight, and chemical composition as described in section 4.4.4.

The dissolution trend of PTMC and PTMC-COOH at the initial molecular weight of 640 Da was also studied at the same condition as the control samples for ester and anhydride-linked samples, respectively.

4.4.6 Statistics

All data are reported as the average \pm the standard deviation about the average.

4.5 Results and Discussion

4.5.1 Polymer Synthesis

The main goal was to prepare PTMC and PTMC-COOH to subsequently conjugate through an ester or anhydride bond, respectively. For these studies, PTMC was synthesized via ring opening melt polymerization initiated with either a hydrophobic (1-octanol) or hydrophilic (P350) initiator to adjust the hydrophilicity, and thus the hydrolytic degradation rate, of the resulting polymer. The monomer to initiator molar ratio was chosen to achieve targeted number average molecular weights of 600-1000 Da. This range of molecular weight was chosen based on previous studies that showed rapid absorption of octanol initiated PTMC ($M_n = 620$ Da) following subcutaneous implantation in rats.¹⁵⁸

Figure 4.3 shows a representative ^1H NMR spectrum of PTMC initiated with 1-octanol along with peak assignments. The ^1H NMR spectra corresponds well to the spectra of TMC and PTMC reported in the literature.¹⁵⁸ Based on the integration of the methylene groups linked to the carbonate bond of unreacted TMC, almost complete (97-99%) monomer conversion was achieved. A representative ^1H NMR spectrum of PTMC initiated with P350 is given in Appendix A, Figure A.1.

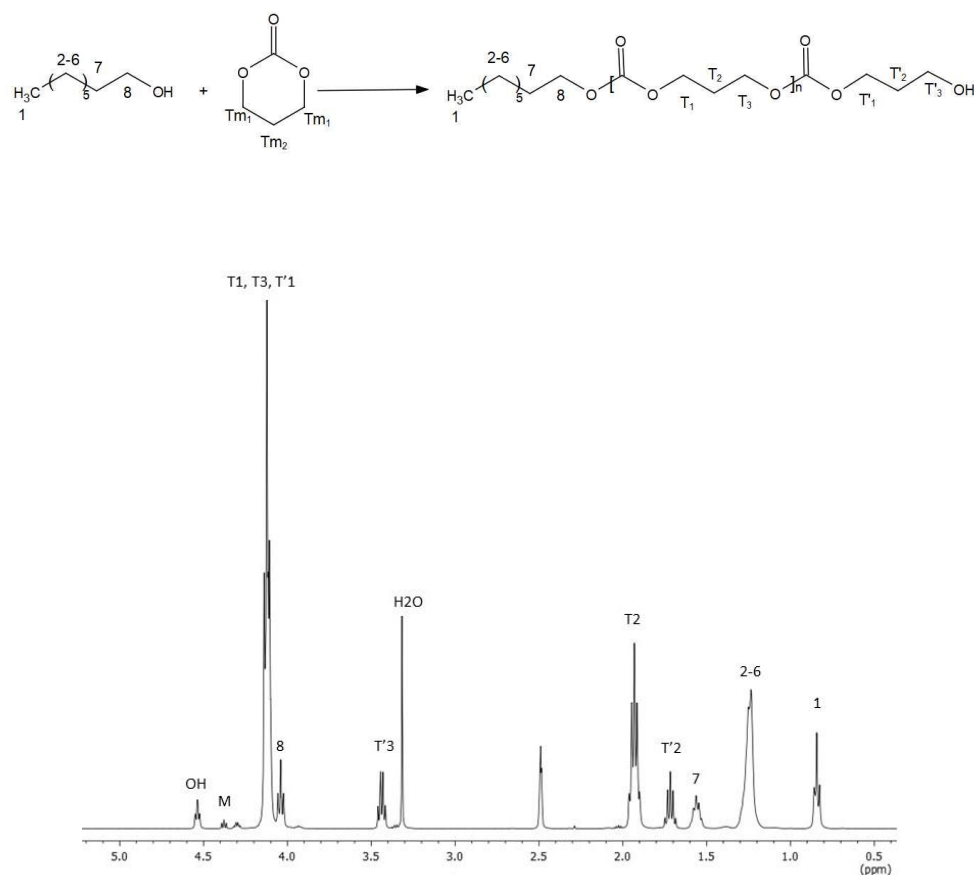


Figure 4.3. ^1H NMR spectrum of PTMC initiated with 1-octanol obtained in DMSO-d_6 . $M/I = 5$, $M_n = 640$ Da. Peak “M” corresponds to the methylene groups linked to the carbonate bond of TMC monomer.

To form the carboxylic acid terminated PTMC (PTMC-COOH), 1-octanol initiated PTMC was reacted with a stoichiometric amount of succinic anhydride. A representative ^1H NMR

spectrum along with peak assignments is shown in Figure 4.4. A significant decrease in the peaks corresponding to the protons on the end unit PTMC central methylene group ($\delta = 1.72$ ppm), the methylene group linked to the terminal hydroxyl ($\delta = 3.45$ ppm) and the hydroxyl group ($\delta = 4.55$ ppm), as well as the appearance of new peaks corresponding to the carboxylic acid protons ($\delta = 12.25$ ppm) and the protons on the methylene groups of the end group of PTMC-COOH ($\delta = 2.55$ ppm) confirmed the success of the reaction. Based on the integration of the remaining central methylene group of the end unit of PTMC at 1.72 ppm in Figure 4.4, a 90% conversion of hydroxyl end group to carboxylic acid end group was achieved.

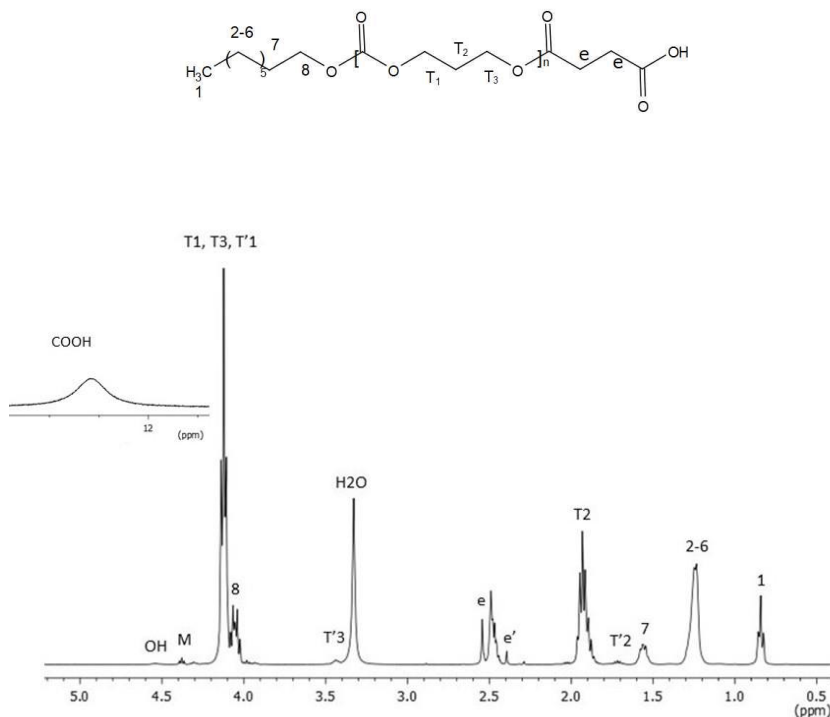


Figure 4.4. ¹H NMR spectrum obtained in DMSO-d₆ of PTMC-COOH initiated with 1-octanol, M/I=5, M_n = 724 Da. T'2 and T'3 are the peaks corresponding to the methylene groups of the remaining end unit of PTMC, and e' is the unreacted succinic acid.

4.5.2 PTMC Conjugation

Ester-linked PTMC was prepared by reaction between PTMC, initiated either with 1-octanol or P350, and diacid halides (DGC or SC). Hereafter, the conjugated polymers will be referred to as initiator-linkage-linker molecule. For example, octanol initiated PTMCs linked via an ester using sebacoyl chloride will be referred to as OCT-CE-SC. Figure 4.5 shows a representative ^1H NMR spectrum of OCT-CE-SC along with peak assignments. A significant decrease in the peaks corresponding to the end unit PTMC including central methylene group ($\delta = 1.72$ ppm), the methylene group linked to hydroxyl ($\delta = 3.45$ ppm) and the hydroxyl group ($\delta = 4.55$ ppm), as well as the appearance of new peaks corresponding to the central methylene groups of the linker molecule ($\delta = 1.25$ and 1.6 ppm) and the methylene groups linked to the ester bond ($\delta = 2.27$ ppm) confirmed the success of the reaction. Based on the integration of the central methylene groups of PTMC end unit ($\delta = 1.72$ ppm), a high rate of esterification ($> 90\%$) was achieved. ^1H NMR spectra of the other ester-linked PTMCs initiated with either 1-octanol or P350 are given in Appendix A, Figure A.2 and Figure A.3.

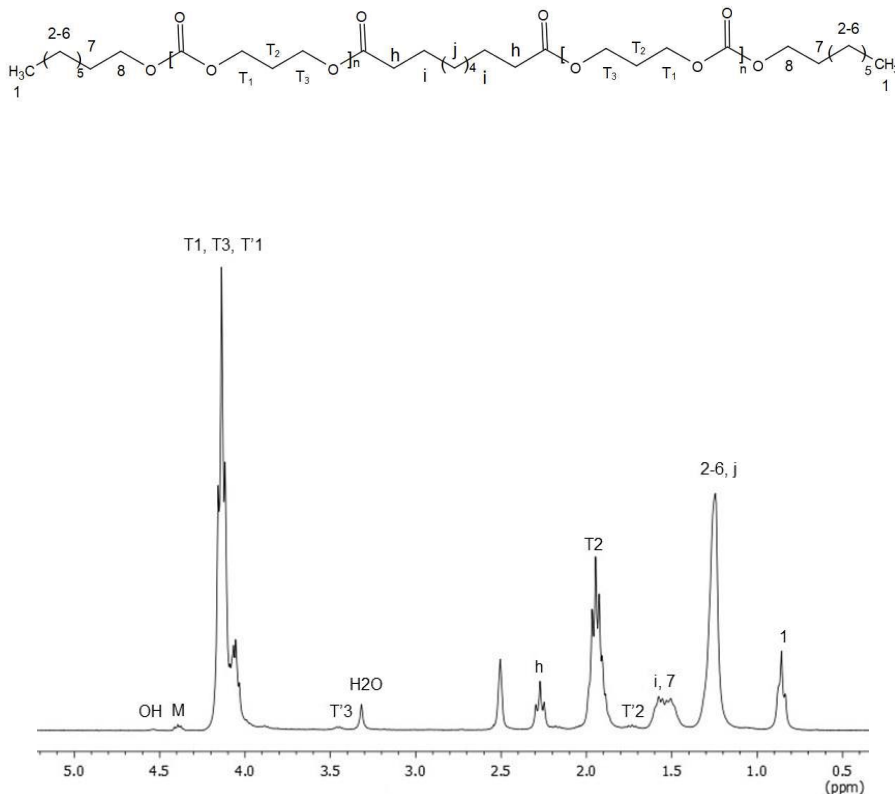


Figure 4.5. ^1H NMR spectrum of ester-linked PTMC (OCT-CE-SC) obtained in DMSO-d_6 .

The anhydride-linked PTMC was prepared by the reaction of PTMC-COOH with sebacoyl chloride. Figure 4.6 shows a representative ^1H NMR spectrum of the anhydride-linked PTMC, OCT-CA-SC, along with assignments. The appearance of new peaks corresponding to the central methylene groups of the linker molecule ($\delta = 1.25$ and 1.6 ppm) and the methylene groups linked to the anhydride bond ($\delta = 2.6$ and 2.76 ppm) confirmed the success of the reaction. Based on the integration of peak h at 2.76 ppm, corresponding to the methylene protons adjacent to the anhydride, a moderate rate of formation of the anhydride-linked PTMC of 75% was obtained, which decreased to 66% after purification.

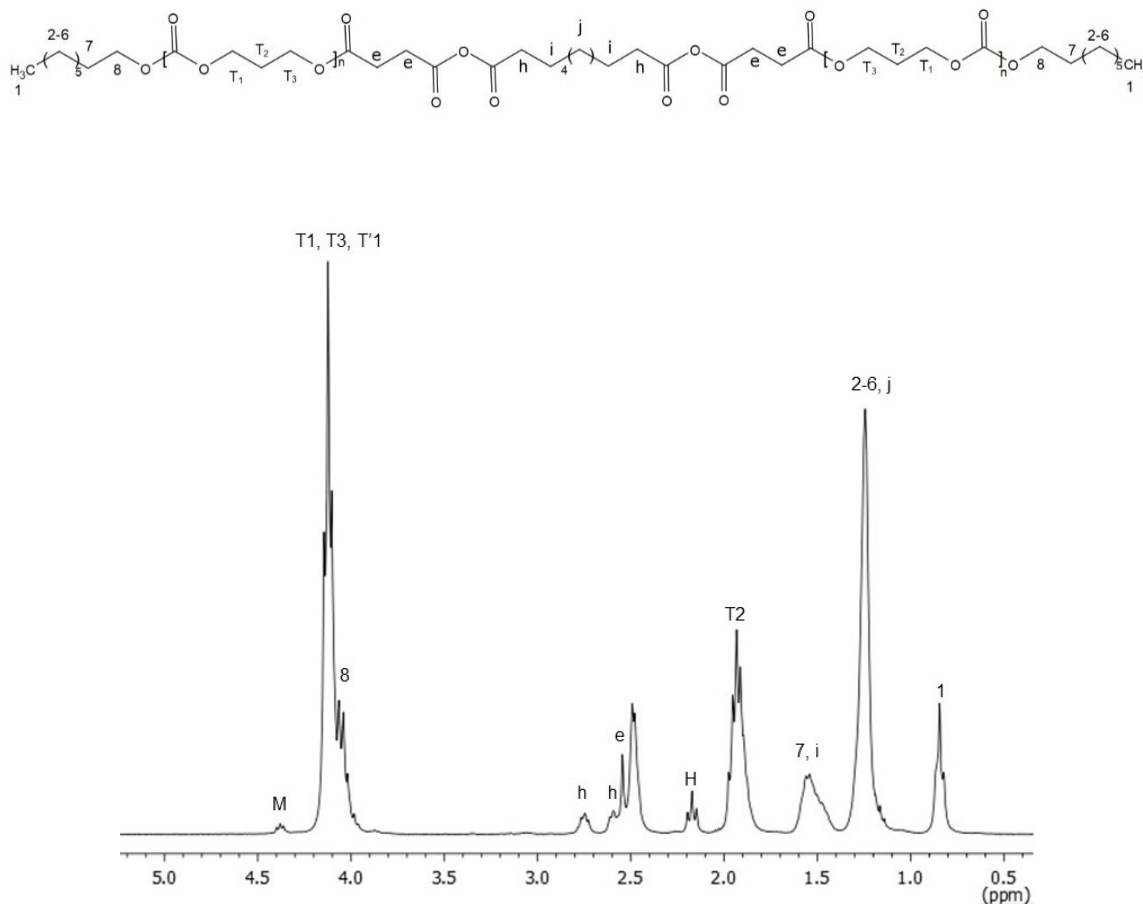


Figure 4.6. ^1H NMR spectrum of anhydride-linked PTMC (OCT-CA-SC) obtained in DMSO-d_6 . Peak “H” at 2.17 ppm represents the unreacted end methylene group of SC.

Table 4.1 lists the physical-chemical properties of the resulting ester and anhydride-linked PTMCs. Conjugation via anhydride or ester linkage provided products with number average molecular weights close to the desired target values, while the glass transition temperatures were low enough to allow the polymers to be injectable (-57 to -47 $^{\circ}\text{C}$).¹⁵⁸ The anhydride-linked PTMC, OCT-CA-SC, showed nearly 5 times higher water solubility than the ester-linked PTMC with the same linker and initiator, OCT-CE-SC. Also, using the hydrophilic initiator, P350, significantly increased the initial water solubility of the ester-linked PTMCs by 12-15 times; however, increasing the molecular weight of PTMC

and subsequently decreasing the ethylene glycol to TMC molar ratio (EG/TMC) did not cause a significant change in initial water solubility of the resulting conjugated PTMC.

Table 4.1 Physical-chemical properties of conjugated PTMCs

Sample	Initial Polymer			Conjugated Polymer			
	Mn (Da)	Tg (°C)	(EG/TMC)	Conversion (%)	Mn (Da)	Tg (°C)	Water solubility (wt%)
OCT-CA-SC	640	-53	...	66	1040	-54	0.25 ± 0.003
OCT-CE-SC	640	-60	...	90	1440	-56.5	0.045 ± 0.003
OCT-CE-DGC	640	-60	...	90	1340	-51	0.052 ± 0.001
P350-CE-SC-4	760	-62	2	90	1600	-57	0.74 ± 0.02
P350-CE-DGC-4	760	-62	2	91	1510	-53	0.8 ± 0.035
P350-CE-SC-6	950	-58	1.3	90	2080	-52	0.63 ± 0.015
P350-CE-DGC-6	950	-58	1.3	92.5	2000	-47	0.79 ± 0.017

4.5.3 *In vitro* Mass Loss of Conjugated PTMC

In vitro degradation of the ester- and anhydride-linked PTMC samples initiated by 1-octanol or P350 was studied in pH 7.4 PBS at 37 °C to gain an understanding of the effect of the hydrolysis rate of the linkage bond, hydrophilicity of the initiator and the influence of degradation products on the degradation rate of the conjugated polymer and the change in pH of the degradation medium. Changes in sample weight, polymer composition and pH were studied over time.

Measurements of pH during the degradation experiment showed that an acidic degradation medium (pH = 4.5) existed very early for the anhydride-linked PTMC sample, OCT-CA-SC, which gradually increased to neutral pH in 5 weeks (Figure 4.7). OCT-CA-SC showed

approximately 80 wt% mass loss within 3 weeks, and finally completely dissolved in week 5 (Figure 4.8). In parallel, the mass loss by dissolution of the 640 Da PTMC-COOH used to prepare OCT-CA-SC was studied as a control, and the pH of the PBS medium during the degradation study was monitored to determine the influence of PTMC-COOH water solubility and carboxylic acid end group on mass loss and pH. The medium pH during the dissolution of PTMC-COOH was 5.5 at day 1 and gradually increased to neutral by 2 weeks (Figure 4.7), and a complete mass loss by dissolution of PTMC-COOH was observed within 5 weeks (Figure 4.8). Therefore, the mass loss of OCT-CA-SC is the result of hydrolysis of anhydride bond leading to release of the water-soluble PTMC-COOH chains.

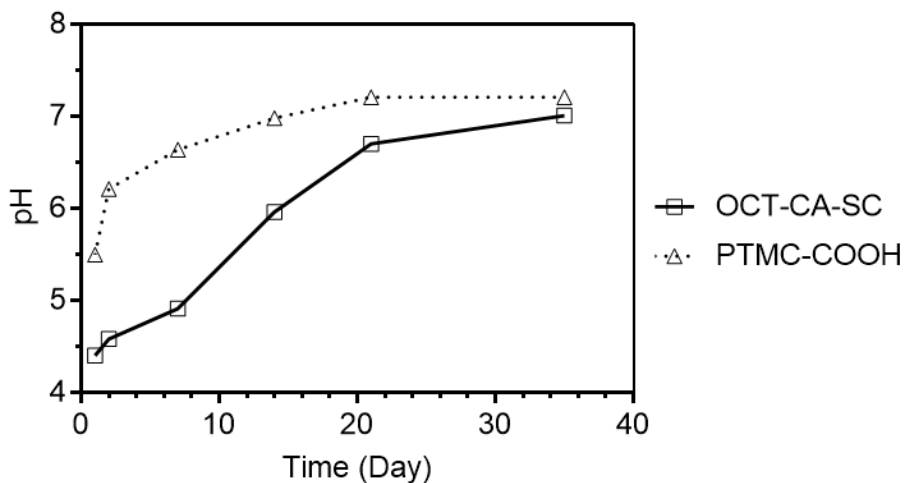


Figure 4.7. pH of PBS during the *in vitro* degradation of anhydride-linked PTMC and dissolution of PTMC-COOH at 37 °C. The initial pH of the medium, replaced at each time point, was 7.4.

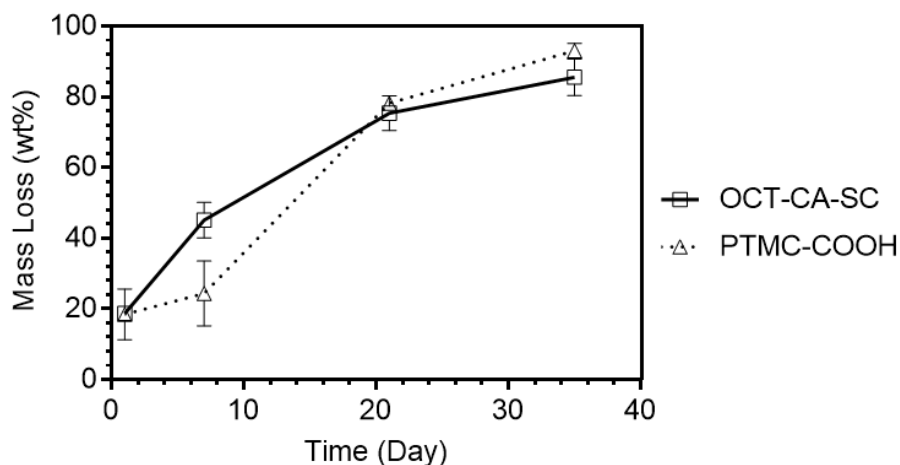


Figure 4.8. Mass loss (%) of anhydride-linked PTMC and unlinked PTMC-COOH in 37 °C PBS at the initial pH of 7.4.

To determine the factors causing the acidic pH and mass loss of OCT-CA-SC in PBS, the ^1H NMR spectra of the remaining as well as dissolved OCT-CA-SC were analyzed and compared to the ^1H NMR spectrum and the mass loss trend of the control sample, PTMC-COOH. According to Figure 4.9 which shows the ^1H NMR spectrum of the OCT-CA-SC remaining at 24 h, the peak corresponding to the methylene group linked to the anhydride bond ($\delta = 2.6$ and 2.76 ppm in Figure 4.6) had disappeared completely. Also, new peaks appeared corresponding to the methylene groups linked to the carboxylic acid end group in sebacic acid ($\delta = 2.17$ ppm) and succinic acid ($\delta = 2.4$ ppm) as well as the carboxylic acid end group of PTMC-COOH ($\delta = 2.55$ ppm), (Figure 4.9). Therefore, the anhydride bond linking the PTMC-COOH chains was completely cleaved in less than 24 h, forming short non-conjugated PTMC-COOH chains. Subsequently, the low molecular weight PTMC-COOH chains dissolved in PBS, as indicated by the fact that PTMC-COOH and OCT-CA-SC showed essentially the same mass loss rate (Figure 4.8).

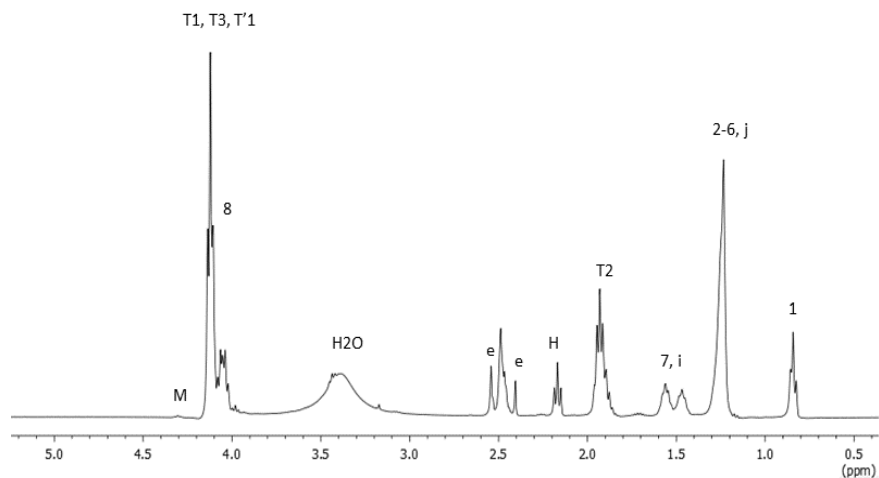


Figure 4.9. ^1H NMR spectrum obtained in DMSO-d_6 of the OCT-CA-SC remaining at 24 h in 37 °C PBS at an initial pH of 7.4.

Furthermore, the ^1H NMR spectrum of the dissolved fraction of the degraded OCT-CA-SC after 24 h showed peaks related to sebacic acid at 1.25, 1.5 and 2.2 ppm, and a peak at 2.4 ppm arising from succinic acid (Figure 4.10). The succinic acid peak was also observed in the ^1H NMR spectrum of the soluble fraction of PTMC-COOH. Therefore, the ester bond linking the succinic acid to PTMC was also cleaved under the resulting acidic conditions. According to this evidence, the resulting acidic pH during the degradation of OCT-CA-SC was due to the rapid cleavage of the anhydride bond subsequently releasing low molecular weight acidic products and the hydrolysis of a portion (15-20 wt%) of the ester linked succinic acid. The remaining insoluble fraction of the OCT-CA-SC and PTMC-COOH samples retained a succinic acid end group in the last days of the study. At these time points, the aqueous medium surrounding the samples had a neutral pH; however, less than 20 wt% of the initial polymer mass remained.

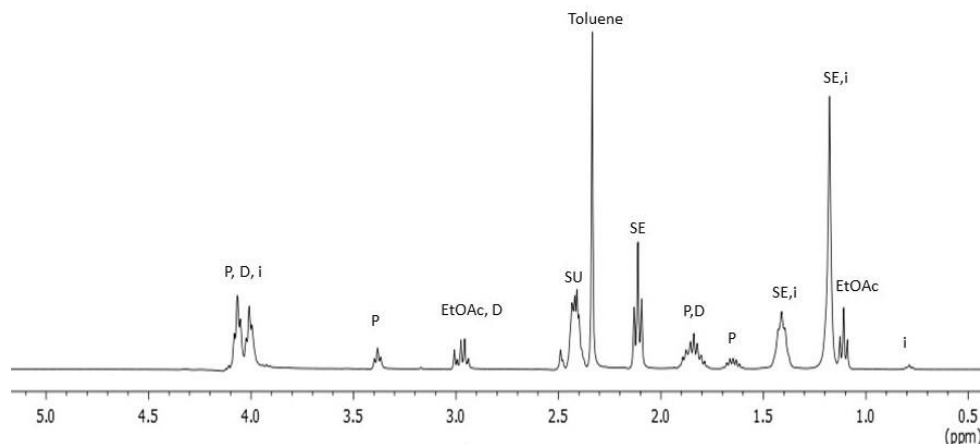


Figure 4.10. ^1H NMR spectrum of dissolved fraction of OCT-CA-SC at 24 h under *in vitro* degradation condition obtained in DMSO-d_6 . In this figure abbreviations are as “SE”: sebacic acid, “SU”: succinic acid, “P”: polymer, “D”: 1,3-propanediol, i: initiator.

Based on these results, anhydride-linked PTMC was not considered a suitable candidate for growth factor delivery because of the acidic pH generated during its degradation, which would likely affect the growth factor bioactivity.^{107,119} Also, the high sensitivity of the anhydride bond to environmental humidity, which made forming and storing the anhydride-linked polymer difficult, is another limitation of using the anhydride-linked PTMC.

In contrast, the degradation medium of the ester-linked PTMC samples initiated either with 1-octanol or P350 had a fairly constant pH that varied between 6.8-7.3, values comparable with the initial pH of PBS and a control medium containing the control sample, non-conjugated PTMC. The ester-linked PTMC chains initiated with 1-octanol showed a much slower degradation rate compared to the anhydride-linked PTMC, reaching approximately 30 wt% mass loss within 84 days (Figure 4.11). The lower mass loss rate of the ester-linked polymers compared to the anhydride-linked polymers is due to the slower rate of cleavage

of the ester bond compared to the anhydride bond,¹⁶⁷ and the preservation of a neutral aqueous media.

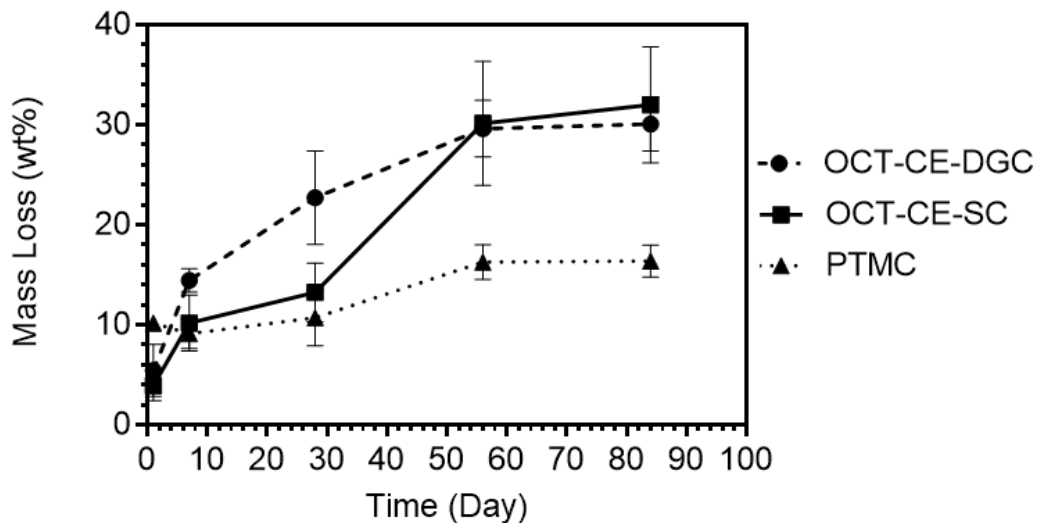


Figure 4.11. Mass loss (%) of ester-linked PTMC and unlinked PTMC in 37 °C pH 7.4 PBS.

The mass loss of the 640 Da PTMC used to prepare the ester linked polymers was also studied to determine the influence of PTMC water solubility on mass loss. As PTMC does not degrade appreciably by hydrolysis,^{221,174} a depot formed from 640 Da PTMC could only lose mass by the slow dissolution of its water-soluble mass fraction. Over 84 days, the 640 Da samples lost 16 ± 1.6 wt% of their initial mass.

According to the lower number average molecular weight and higher water solubility of PTMC compared to the ester-linked PTMC, it can be concluded that hydrolysis of the ester bond produced PTMC chains with carboxylic acid end groups, which increased the mass loss over that of the 640 Da PTMC samples. However, most of the non-degraded polymer

remaining after 12 weeks consisted of ester linked PTMC blocks. Figure 4.12 shows a representative ^1H NMR spectrum of OCT-CE-SC remaining after 12 weeks degradation in PBS. Based on the integrations of the central methylene group of PTMC end unit ($\delta = 1.72$ ppm) and PTMC chain ($\delta = 1.9$ ppm), the remaining OCT-CE-SC at 84 days still showed 89% ester-linkage and an M_n equal to 1540 Da.

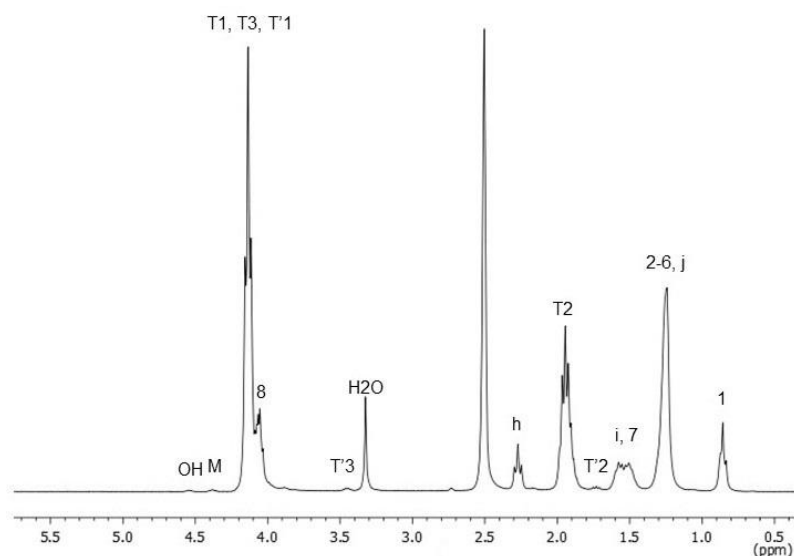


Figure 4.12. ^1H NMR spectrum obtained in DMSO-d_6 of OCT-CE-SC remaining at 84 days under *in vitro* degradation conditions.

To increase the mass loss rate of the ester-linked PTMC, P350 initiated PTMC was prepared at different EG/TMC ratio, and conjugated using both DGC and SC. The resulting ester-linked polymers showed approximately 20-40 wt% mass loss within 1 day in pH 7.4 PBS at 37 °C. The mass loss increased up to 2 weeks, then slowed, reaching a final value of 40-60 wt% by 84 days (Figure 4.13). Except for the difference in the initial mass loss in day 1, all samples showed almost the same mass loss trend with time, which was independent of the EG/TMC ratio and linker molecule used. The higher initial mass loss

of PEG-initiated ester-linked PTMCs was due to the higher water solubility of PEG-initiated PTMC. The integration of the central methylene group of the PTMC end unit ($\delta = 1.72$ ppm) showed that the remaining polymer chains were still highly linked via an ester bond (Appendix A, Figure A.5). Therefore, the rate of ester hydrolysis was considered too slow for the intended purpose, with the desired degradation time of 6-10 weeks not attainable even for the P350 initiated ester-linked PTMC.

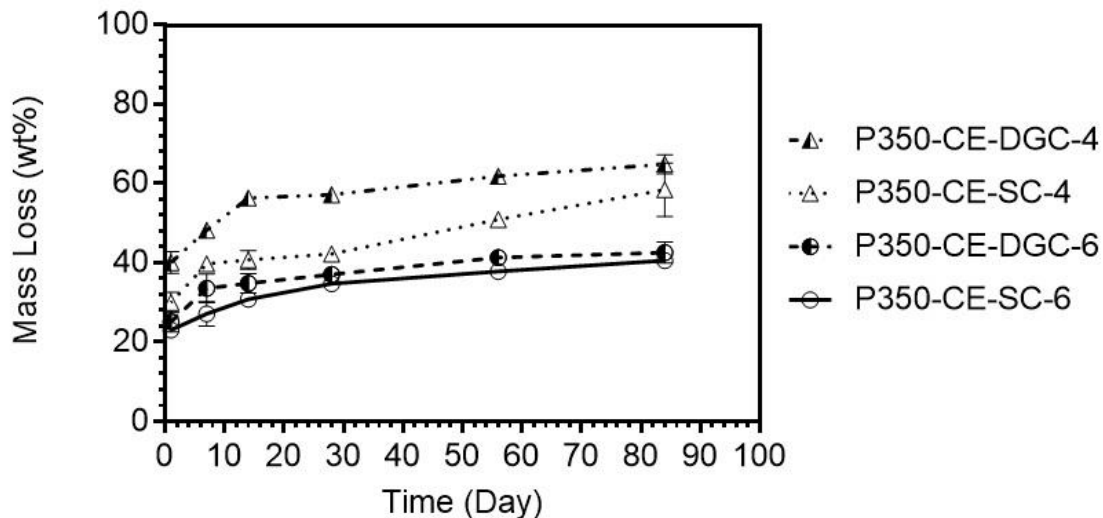


Figure 4.13. Mass loss (%) of ester-linked PEG-initiated PTMC-OH in 37°C pH 7.4 PBS.

4.6 Conclusion

In this chapter, an approach was explored based on increasing the overall molecular weight of the injectable PTMC via conjugation by either hydrolysable ester or anhydride linkages. It was reasoned that the linkage would cleave in aqueous media over time, thereby releasing free PTMC chains that would slowly dissolve within 6 to 10 weeks. An *in vitro* mass loss

study of the conjugated samples showed that for the anhydride-linked PTMC all the anhydride bonds cleaved within the first 24 hours, generating acidic products that lowered the pH of the buffered degradation medium. The resulting mass loss was then due to the dissolution of the PTMC-COOH chains formed. In contrast, due to the slower reactivity of the ester bond within the ester-linked PTMC, ester hydrolysis did not result in an acidic pH within the incubation medium. However, the ester bond degraded too slowly for the intended application. Using P350 as an initiator to increase the water solubility of the ester-linked PTMC increased the total mass loss to about 26 wt% within 28 days. However, the increased polymer water solubility resulting from the incorporation of the P350 caused a large initial mass loss of solubilized polymer followed by a very slow mass loss. Based on these results the conjugation approach was considered to not provide desirable complete and gradual degradation within the target time frame of 6-10 weeks.

Chapter 5

Hydrolysable injectable delivery vehicle based on low molecular weight poly(trimethylene carbonate-co-5-hydroxy trimethylene carbonate): Synthesis, characterization and *in vitro* degradation

5.1 Abstract

In this chapter, Specific Aim 2 is addressed, namely the synthesis, characterization and *in vitro* degradation of poly(trimethylene carbonate-co-5-hydroxy trimethylene carbonate), P(TMC-co-HTMC), as an injectable delivery vehicle. Ring opening polymerization under melt and solution conditions and initiated with hydrophobic initiators (1-octanol and 1-butanol) was explored using different catalysts. Specifically, hydrogen chloride in ether (HCl·Et₂O), 1,8-diazabicyclo-7-undecene, and tin(II) 2-ethylhexanoate were examined. The polymerization kinetics for each catalyst and its effect on copolymer microstructure were determined. Also, the nature of the initiator, the molecular weight and the copolymer composition were studied for their effects on copolymer glass transition temperature (T_g), *in vitro* degradation rate, and the incubation medium pH during degradation. Of the catalysts studied, HCl·Et₂O provided a random comonomer distribution and low toxicity burden. Copolymers prepared with HCl·Et₂O as catalyst and of different molecular weights, 5-hydroxy trimethylene carbonate (HTMC) content, and using varying initiators were injectable at room temperature having T_g 's less than -20 °C. Moreover, the *in vitro* degradation of random copolymer was tailored by adjusting the HTMC content, initial molecular weight and the choice of initiator. During *in vitro* degradation, the pH of the

medium surrounding the copolymer always remained near neutral, which is a safe condition for preserving the bioactivity of the released growth factor.

5.2 Introduction

The strategy of utilizing anhydride or ester linked poly(trimethylene carbonate) did not result in a polymer that met the desired features for the intended application. Thus, based on recent findings in the Amsden laboratory, a new polymer strategy was developed, involving a copolymer of trimethylene carbonate (TMC) with 5-hydroxy trimethylene carbonate (HTMC),^{177,179,230} P(TMC-co-HTMC). In this approach, P(TMC-co-HTMC) was prepared through two steps. In the first, 5-benzyloxy trimethylene carbonate (BTMC) was copolymerized with TMC via ring-opening polymerization (ROP) under melt or solution conditions. Following copolymerization, the BTMC repeating units were debenzylated to yield HTMC repeating units along the backbone (Figure 5.1).^{177,230}

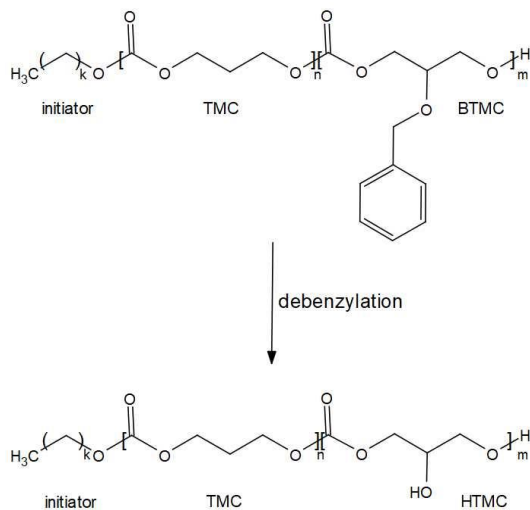


Figure 5.1. Copolymer chemical structure; n and m refer to the number of repeating units of TMC and BTMC or HTMC along the copolymer backbone, k refers to the number of methylene (CH₂) groups within the initiator (*e.g.* k = 3 is 1-butanol, k = 7 is 1-octanol).

An examination of the degradation of HTMC homopolymers (PHTMC) by Dr. Chen from the Amsden group showed that the presence of the pendant hydroxyl group resulted in a rapid rate of degradation, with a 42 kDa homopolymer reaching complete mass loss within 24 hours at neutral or alkaline pH. According to the degradation mechanism of PHTMC proposed by Dr. Chen, the final degradation products of PHTMC are glycerol and carbon dioxide,^{176,180,231} both of which are natural components of physiological systems.^{181,182} The degradation of PHTMC also did not result in a significant lowering of the local pH in a solution buffered at physiologic conditions.

Based on the proposed degradation mechanism and fast degradation of PHTMC within 24 h, it was therefore proposed that introducing HTMC units distributed randomly along the backbone of a low molecular weight copolymer of HTMC and TMC would result in a liquid viscous polymer with a controllable degradation rate while preserving the local neutral pH.

In ROP, the choice of catalyst dictates the polymerization rate, polymerization conditions, purification process, polymer dispersity, and end group fidelity (the number of polymer chains that incorporate the initiator),^{232,233} and thus warrants careful consideration based on the intended application for the polymer. To achieve a random structure, TMC and BTMC copolymerization was studied using different catalyst systems including hydrogen chloride solution in diethyl ether ($\text{HCl}\cdot\text{Et}_2\text{O}$),^{184,194,234,235} 1,8-diazabicyclo-7-undecene (DBU),^{184,190–193,236} and tin(II) 2-ethylhexanoate ($\text{Sn}(\text{Oct})_2$) (Figure 5.2).^{185,237}

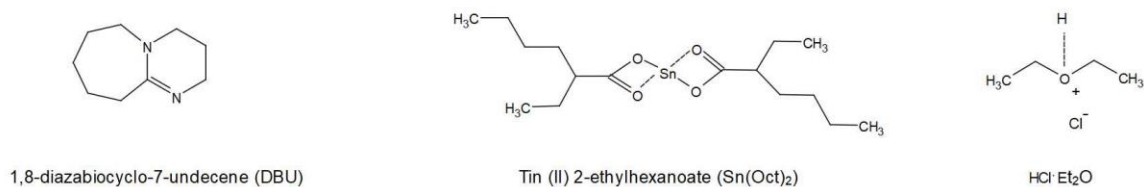


Figure 5.2. Chemical structure of monomers and catalysts.

Sn(Oct)₂ is the most frequently used and most efficient catalyst in ROP of cyclic carbonate monomers at high temperature, but tin complexes have shown a potential toxicity due to tin residues and subsequently extensive purification is required for biomedical applications.¹⁸⁶ Also, side reactions including initiation with water as well as monomer auto-initiation, chain transesterification and backbiting at high temperatures of polymerization may affect the end group fidelity and molecular weight dispersity.^{184,185} Therefore, potentially less toxic catalysts such as DBU and HCl were also explored.^{186,196} Both DBU and HCl·Et₂O are reported to catalyze the polymerization of cyclic carbonate monomers at room temperature under solution conditions with suitable control over molecular weight and molecular weight dispersity.²³⁴ All three catalysts used in this study are effective in the ROP of cyclic carbonate, but function through different mechanisms. The Sn(Oct)₂ catalytic mechanism is considered a coordination-insertion in which the Sn group attaches to the hydroxyl group of the growing polymer chain or the alcoholic initiator and coordinates with the carbonyl group of the monomer.¹⁸⁵ DBU catalyzes polymerization via an anionic mechanism in which DBU conjugates with TMC forming an alkoxide anion,^{184,190,199} and activation of the initiating/propagating hydroxyl group via hydrogen binding.^{198,199} In contrast, HCl·Et₂O activates the monomer by conjugating to its carbonate

bond. The resulting activated monomer is susceptible to a nucleophilic attack by the hydroxyl group on the alcoholic initiator or the growing chain end.^{234,197} The presence of the benzyloxy group in the BTMC monomer as an electronegative group provides a positive charge density around the carbonate bond which may affect the monomer stability under the polymerization conditions provided by each catalyst and subsequently determine the copolymer microstructure.

Therefore, the effect of each catalyst and polymerization condition on the monomer conversion rate as well as copolymer microstructure, molecular weight, and end group fidelity of the final copolymer was studied. The objective was to obtain a random copolymer with high purity, high end group fidelity, controlled molecular weight and narrow molecular weight distribution with hydrolysable HTMC units distributed randomly along the backbone. Finally, copolymers were prepared using the most suitable of these catalysts, with different initiators and at different molecular weight to adjust the degradation rate, T_g and viscosity of the final copolymer.²³⁷

5.3 Materials

1,3-trimethylene carbonate (TMC) was obtained from Leapchem, Hangzhou, China. 5-benzyloxy trimethylene carbonate (BTMC) was purchased from Obiter research LLC, USA. Tin(II) 2-ethylhexanoate ($\text{Sn}(\text{Oct})_2$) was purchased from Alfa Aesar, USA. 1 M hydrogen chloride solution in diethyl ether ($\text{HCl}\cdot\text{Et}_2\text{O}$), 1,8-diazabicyclo-7-undecene (DBU), palladium on carbon (Pd/C), palladium hydroxide on carbon ($\text{Pd}(\text{OH})_2/\text{C}$), 1-octanol, 1-butanol, celite, deuterated chloroform (CDCl_3) and deuterated dimethyl

sulfoxide (DMSO- d_6) were purchased from Sigma-Aldrich Ltd, Canada. Phosphate buffered saline (PBS) powder, anhydrous potassium carbonate (K_2CO_3), tetrahydrofuran (THF), methanol (MeOH), dichloromethane (DCM), and diethyl ether were purchased from Thermo Fisher Scientific, Canada. Hydrogen gas (H_2) (99.99% purity) was purchased from Linde Ltd, Canada. Water used was of type 1 purity, obtained from a Millipore Milli-Q Plus ultrapure water filtration system. THF and MeOH were dried over activated 3 Å molecular sieves. All other materials were used as received.

5.4 Methods

5.4.1 Synthesis of P(TMC-co-BTMC) via different polymerization methods

5.4.1.1 Melt polymerization using $Sn(Oct)_2$

Prescribed amounts of TMC and BTMC at a molar ratio of 50/50 were put in glass ampoules to prepare compositions of copolymer with 40 total repeating units. In this reaction, 1-octanol and $Sn(Oct)_2$ were used as initiator and catalyst, respectively. A monomer to catalyst mole ratio (M/C) of 800:1 was used based on a previous protocol for TMC polymerization.¹⁵⁸ The following is a representative procedure for preparing a copolymer with a monomer to initiator molar ratio (M/I) of 40:1 and BTMC/TMC molar ratio of 50/50. In a flame-dried glass ampoule was mixed 1-octanol (0.318 g, 2.45 mmol), TMC (5 g, 49 mmol), BTMC (10.2 g, 49 mmol), and 100 μ L of 50% $Sn(Oct)_2$ solution (50 mg, 0.12 mmol of catalyst) in dry toluene. The ampoule was purged with argon and connected to vacuum for 3 cycles. Finally, the ampoule was vacuum sealed and placed in

a 60 °C oven for 10-15 min to melt the monomer. The resulting melt was mixed using a vortex and placed in an oven at 130-135 °C under 20 mm Hg vacuum. To determine the kinetics of copolymerization, 4 individual ampoules were removed from the oven at specific time points and cooled to 5 °C in a refrigerator for 10 min to quench the polymerization. The resulting copolymer will be referred to as OCT-P40-50B-Sn. After complete monomer conversion, the resulting copolymer was purified by precipitation in cold methanol.

5.4.1.2 Solution polymerization using HCl·Et₂O and DBU

The following is a representative procedure for preparing copolymer with a M/I of 18:1 and BTMC/TMC molar ratio of 50/50 using HCl·Et₂O as a catalyst at a M/C molar ratio of 3:1. 1-octanol (0.71 g, 5.4 mmol) was added to a 1.5 M solution of TMC (5 g, 49 mmol) and BTMC (10.2 g, 49 mmol) in dry DCM. Following this addition, 33 mL of 1 M HCl·Et₂O was added to the glass vial to achieve a final monomer concentration of 1 M and a M/C ratio of 3:1. To avoid auto-initiation and initiation with water the polymerization reaction was performed under argon at room temperature. The same procedure was used for copolymerization with DBU but with a M/I of 40:1 and a M/C of 80:1 using a 1 M solution of monomer in dry DCM. The M/C molar ratio was chosen based on preliminary experiments. According to the higher catalytic activity of DBU and Sn(Oct)₂ than HCl·Et₂O in these preliminary results, a higher M/I was chosen for the copolymerization in the presence of these catalysts to be able to track the monomer conversion over time.

To study the kinetics of copolymerization using HCl·Et₂O, the collected polymerization solution at each time point was quenched using a flow of air over the sample for 2-3 min following the addition of 10-fold diethyl ether as a non-solvent to completely precipitate the polymer. The kinetics of copolymerization using DBU was also determined via quenching the collected polymerization solution at each time point by adding 2 equivalents of acetic acid to catalyst.¹⁹¹ The solvent was removed under a flow of air. Finally, all samples were stored at -20 °C until analyzed. The resulting copolymers prepared using DBU and HCl·Et₂O will be referred to as OCT-P40-50B-DBU and OCT-P18-50B-HCl, respectively.

After complete monomer conversion, the copolymer prepared with HCl·Et₂O was purified/neutralized by washing in cold MilliQ water 3 times at 4 °C. After each wash, the water pH was checked and adjusted to neutral using K₂CO₃. The copolymer prepared with DBU was purified by precipitation in cold methanol at -20 °C. For studies examining the influence of HTMC content and initiator structure on polymer degradation rate, copolymers with BTMC/TMC molar ratios of 30/70 and 50/50, initiated with 1-octanol or 1-butanol were prepared using HCl·Et₂O as a catalyst.

5.4.2 Debenzylation of P(TMC-co-BTMC)

The BTMC units of the final pure copolymer were debenzylated to hydroxyl groups using a Pd/C and Pd(OH)₂/C mixture (1:1 w/w ratio). For this purpose the copolymer dissolved in a THF/MeOH solvent mixture was added to the catalyst dissolved in THF under Ar in a water-free autoclave reactor.²³⁸ The final ratio of THF to MeOH and the final copolymer

concentration were adjusted to 4 v/v and 0.1 w/v, respectively. A Pd/C and Pd(OH)₂/C mixture of 34 g catalyst/mol of BTMC was used. The autoclave reactor was charged with H₂ at 120 psig and then continuously agitated for 24 h at room temperature.^{201,202} The resulting copolymer, P(TMC-co-HTMC), was filtered through a celite cake, washed with anhydrous THF and dried on a roto-evaporator. Finally, the copolymer was washed with neutral MilliQ water to extract the initial water-soluble fraction and dried on a Modulyo D lyophilizer (Thermosavant, USA) at -50 °C and 100 mbar.

5.4.3 Polymer Characterization

The monomer conversion rate, the final chemical composition and number average molecular weight (M_n) of P(TMC-co-BTMC) were determined by ¹H NMR spectroscopy (Bruker Avance 400 MHz) using CDCl₃ as the solvent at room temperature. The M_n and chemical composition of P(TMC-co-HTMC) were determined by ¹H NMR spectroscopy using DMSO-d₆ as the solvent at room temperature.

In the kinetics study of the copolymerization of TMC and BTMC, the TMC conversion rate was calculated by comparing the signal intensity of the central methylene group of TMC units along the copolymer chain ($\delta = 2.06$ ppm) with the signal intensity of the central methylene group of the TMC monomer ($\delta = 2.16$ ppm). To calculate the BTMC conversion rate, the signal intensity of the methylene groups linked to the carbonate bond of the BTMC units in the copolymer chain ($\delta = 4.1 - 4.25$ ppm) was compared with the signal intensity of the methylene group of the pendent benzyloxy group ($\delta = 4.67$ ppm) of the BTMC monomer and the BTMC of the growing copolymer. The percentage of BTMC repeating

units in the copolymer chain was calculated by comparing the signal intensity of the methylene group of the pendent benzyloxy group of the BTMC ($\delta = 4.67$ ppm) with the signal intensity of the central methylene group of the TMC units ($\delta = 2.06$ ppm). The M_n was calculated by comparing the signal intensity of these two peaks with the signal intensity of the methyl group of the initiator ($\delta = 0.9$ ppm). End group fidelity (α) was calculated as shown in Equations 1 to 4.²³² The terminal group ratio (τ) was calculated by dividing the signal intensity of the methylene groups of a BTMC end unit ($\delta = 3.75$ ppm) and a TMC end unit ($\delta = 1.93$ and 3.66 ppm) by the signal intensity of the methylene group of initiator ($\delta = 0.9$ ppm, Equation 1). If no chains were initiated by another source, such as residual water, and no transesterification occurred, τ would be 1. The amount by which τ exceeds 1 represents the integration contribution from polymer chains without an attached initiator. This quantity is then halved to account for the fact that non-alcohol initiated-polymer chains will have an identical terminal CH_2 group on both chain ends due to decarboxylation of the carbonic ester end. α is then obtained by normalizing the number of alcohol initiated-polymer chains to the total number of polymer chains (initiated plus non-initiated, Equation 2), and M_n was calculated by Equation 3. If $\tau < 1$, then $\alpha = \tau$, and M_n was calculated using Equation 4.

$$\tau = \frac{\left(\frac{I_{B12} + I_{B13}}{3} + \frac{I_{T12} + I_{T13}}{4} \right)}{\frac{I_1}{3}} \quad (1)$$

If $\tau > 1$, then:

$$\alpha = \frac{1}{1 + \frac{\tau - 1}{2}} \quad (2)$$

and M_n is calculated as:

$$M_n = (M_{w(\text{TMC})} \cdot \frac{I_{T2}}{2} + M_{w(\text{BTMC})} \cdot I_{B2} + M_{wi}) \cdot \alpha \quad (3)$$

If $\tau < 1$, then $\alpha = \tau$, and M_n is calculated as:

$$M_n = (M_{w(\text{TMC})} \cdot \frac{I_{T2}}{2} + M_{w(\text{BTMC})} \cdot I_{B2} + M_{wi}) \cdot \alpha + 2 \cdot (M_{w(\text{TMC})} \cdot \frac{I_{T2}}{2} + M_{w(\text{BTMC})} \cdot I_{B2} + M_{wi}) \cdot (1 - \alpha) \quad (4)$$

In these equations, $M_{w(\text{TMC})}$, $M_{w(\text{BTMC})}$ and M_{wi} are the molar mass of TMC, BTMC and initiator (either 1-octanol or 1-butanol), respectively. To characterize P(TMC-co-HTMC), the same methodology was utilized; however, corresponding HTMC units were analyzed instead of BTMC units.

In the resulting P(TMC-co-BTMC), the microstructure was determined by ^{13}C NMR spectroscopy (Bruker Avance 400 MHz) using CDCl_3 as the solvent at room temperature. The degree of randomness was calculated by comparing the signal intensity of the methylene groups linked to the carbonate bond of BTMC-TMC pairings ($\delta = 64.5$ and 66.25 ppm) with the analogue signals of BTMC-BTMC pairings ($\delta = 66.5$ ppm) and of TMC-TMC pairings ($\delta = 64.25$ ppm).

Copolymer dispersity was measured using a Waters gel permeation chromatography system (GPC) equipped with a 2690 GPC separation module equipped with four Waters Styragel HR columns in series, and a Waters 410 Differential Refractometer. Refractive index measurements were collected at 25 °C using distilled THF as the eluent and calibrated to polystyrene standards. The solution used for GPC measurement was prepared at 3-10 mg/mL using HPLC grade THF and filtered through a 0.2 µm syringe filter. Thermal properties were determined by a Mettler-Toledo DSC1 differential scanning calorimeter. A heating and cooling rate of 10 °C/min was applied for temperature range of -100 °C to 80 °C. The T_g was taken as the inflection point of the second heating cycle.

5.4.4 *In vitro* degradation

1 mL of pH 7.4 PBS at 37 °C was added to 50 mg of each copolymer within a glass vial. The glass vials were then placed in a thermomixer at 37 °C with horizontal shaking at 300 rpm. At specific time points, 3 samples were collected, washed 3 times with distilled water to remove residual salt and then dried to a constant weight on a Modulyo D lyophilizer (Thermosavant, USA) at -50 °C and 100 mbar. The resulting dry samples were weighed and analyzed for number average molecular weight and composition as described in section 5.4.3. The solution pH was also measured using pH meter to assess the effect of the degradation products on the aqueous environment pH.

5.4.5 Viscosity measurement

Melt viscosity was measured using a Reological Visco Tech controlled stress rheometer at 25 °C and 37 °C. A parallel plate stainless steel fixture with a diameter of 20 mm and a 0.5 mm plate gap was used.

5.4.6 Statistical analysis

The viscosity, *in vitro* degradation rate, and the chemical composition and number average molecular weight of the remained copolymers during the degradation study were assessed using 3 samples. All the data are reported as the average \pm the standard deviation about the average. Statistical differences were determined using a one-way ANOVA. Differences were considered significant for p values less than 0.05.

5.5 Results and Discussion

5.5.1 Influence of catalyst on copolymer conformation

The objective was to prepare a copolymer with high purity, high end group fidelity, low molecular weight and narrow molecular weight distribution with hydrolysable HTMC units distributed randomly along the backbone. To examine the control over polymerization and determine the copolymer conformation, the conversion rate of each monomer was studied in the presence of the different catalysts chosen: HCl·Et₂O, DBU, and Sn(Oct)₂. Each of these catalysts reportedly functions differently, which would affect the microstructure of

the final copolymer. In these experiments, 1-octanol was used as the initiator, while an equimolar ratio of TMC and BTMC was used in the feed.

After complete conversion of the monomers, the ^1H NMR spectra of copolymers made using different catalysts possessed the anticipated peaks based on chemical structure as compared to the spectra of the corresponding homopolymers. Figure 5.3 shows a representative ^1H NMR spectrum of OCT-P18-50B-HCl after complete monomer conversion along with peak assignments. In this spectrum, there are two signals corresponding to the central methylene group ($\delta = 2.06$ ppm), and the methylene groups linked to the carbonate bond ($\delta = 4.1 - 4.25$ ppm) from the alkane region of the TMC units. Copolymerizing BTMC with TMC revealed new signals corresponding to the central methine group ($\delta = 3.88$ ppm), methylene group linked to the benzyl group ($\delta = 4.67$ ppm), and the signal related to the protons of the benzyl group ($\delta = 7.36$ ppm) for the BTMC units. The representative ^1H NMR spectra of OCT-P40-50B-DBU and OCT-P40-50B-Sn are given in Figure B.1 and Figure B.2 of Appendix B, respectively.

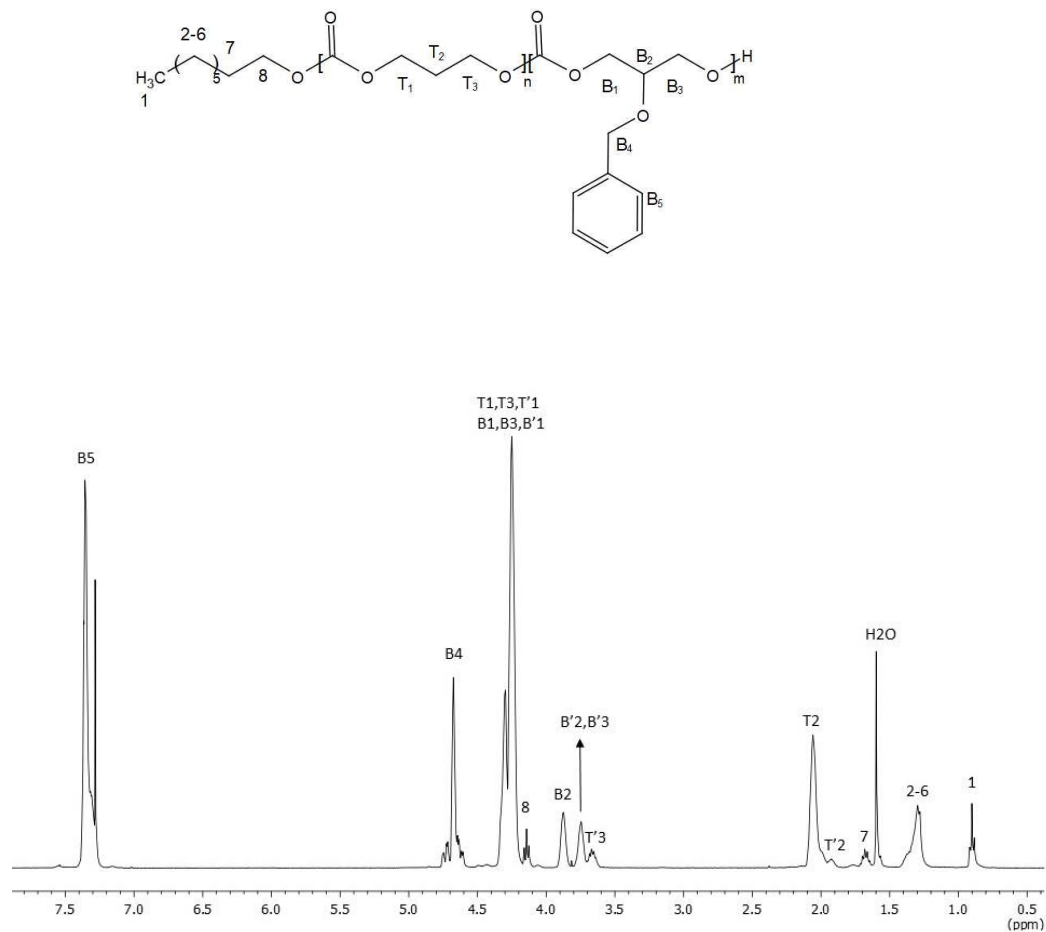


Figure 5.3. ^1H NMR spectrum of OCT-P18-50B-HCl obtained in CDCl_3 , $M/I=18$, $M_n = 1440$, Da, BTMC: 46%. Protons labelled with a prime correspond to the copolymer end group.

The monomer conversion rate was determined by quenching the copolymerizing samples at a given time point and monitoring the integration area of peaks corresponding to the monomers and the resulting copolymers via following the ^1H NMR spectra as explained in section 5.4.3. Figure 5.4 shows a representative stacked ^1H NMR spectra of the copolymerization of TMC and BTMC in the presence of $\text{HCl}\cdot\text{Et}_2\text{O}$ as the catalyst. The monomer conversion (%) versus time using the different catalysts is shown in Figure 5.5.

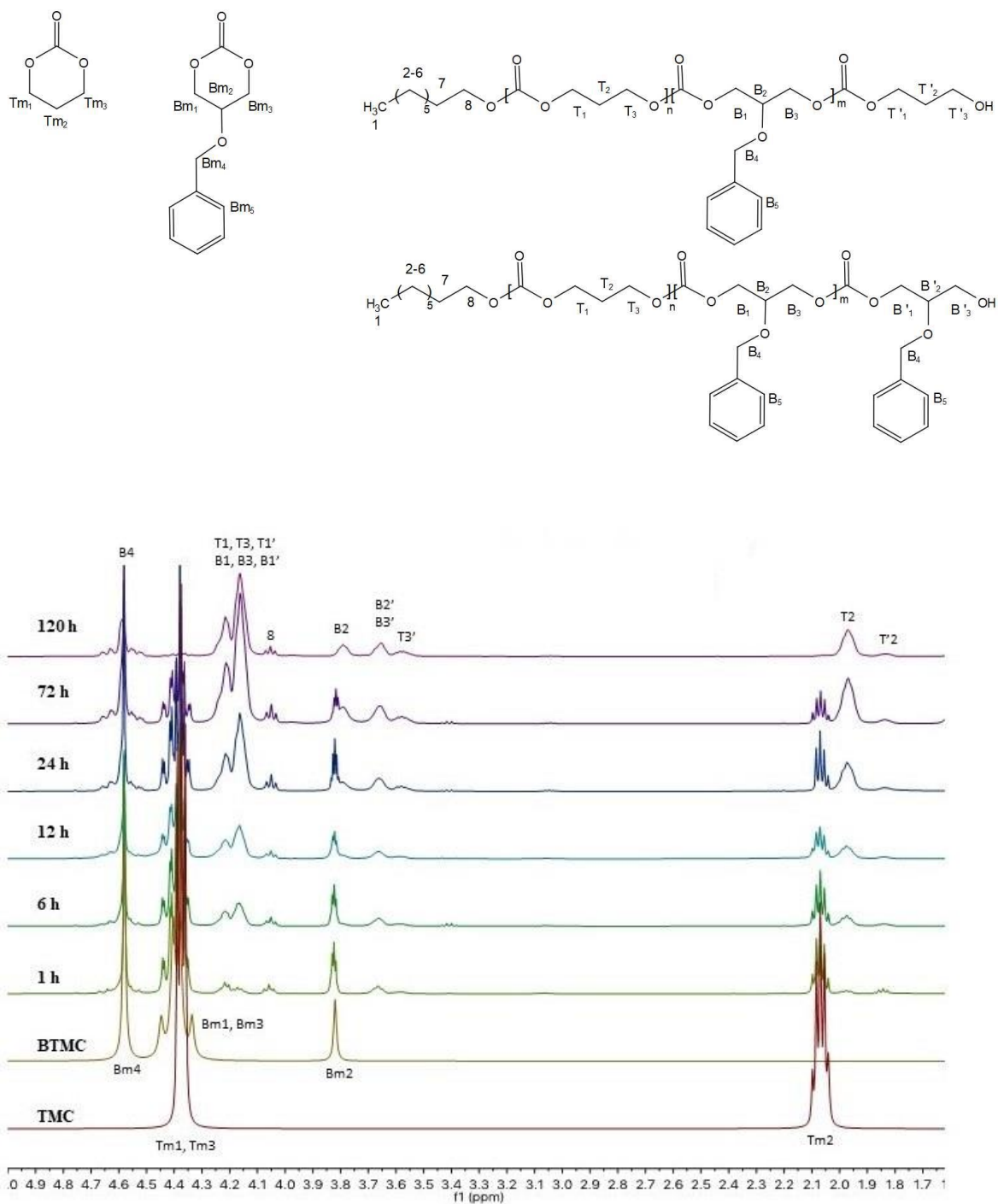


Figure 5.4. Stacked ^1H NMR spectra obtained in CDCl_3 of TMC and BTMC conversion versus time during copolymerization. The initiator was 1-octanol, and the catalyst was $\text{HCl}\cdot\text{Et}_2\text{O}$.

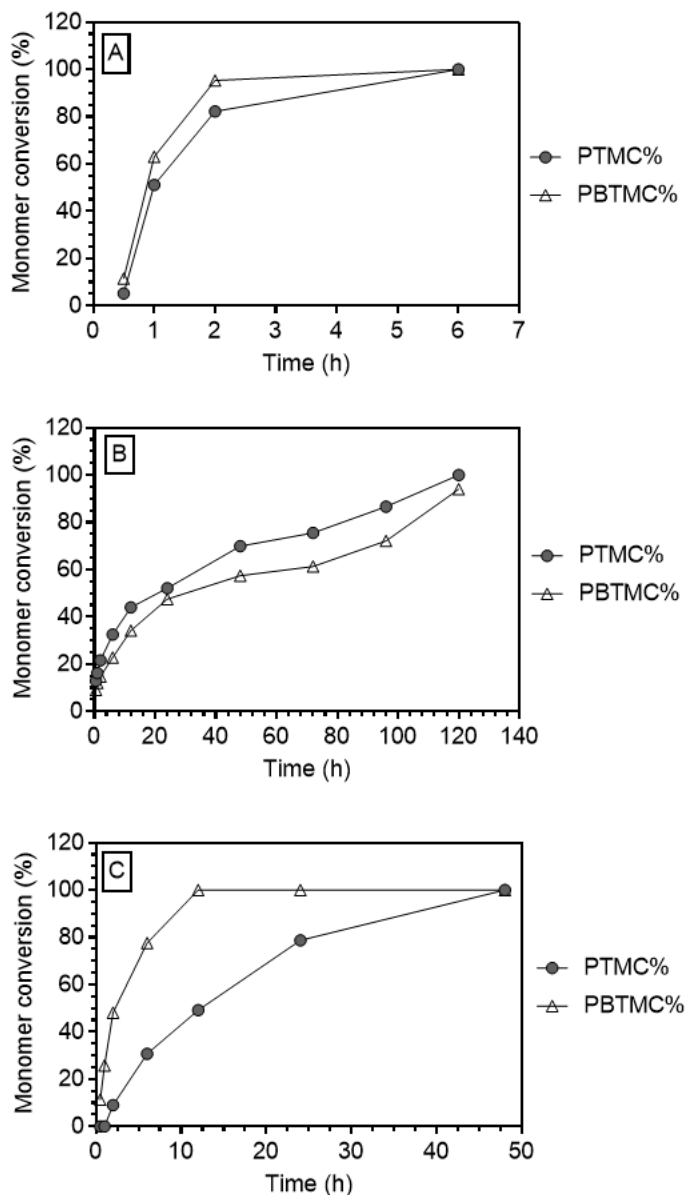


Figure 5.5. Monomer conversion versus time for the copolymerization of TMC and BTMC using different catalysts: (A) Sn(Oct)₂, 130-135°C; (B) HCl·Et₂O, room temperature and (C) DBU, room temperature.

The presence of the benzyloxy group in the BTMC monomer as an electronegative group provides a positive charge density around the carbonate bond which may affect the monomer stability under the polymerization conditions. The monomer conversion results revealed that TMC and BTMC monomers do polymerize coincidentally in the melt in the

presence of $\text{Sn}(\text{Oct})_2$, and that BTMC polymerizes slightly faster than TMC (Figure 5.5A). $\text{Sn}(\text{Oct})_2$ is considered to act in a coordination-insertion manner, in which the Sn group becomes attached to the initiator or the growing end of the polymer chain forming stannous alkoxide and coordinates with the carbonyl of a carbonate monomer, ultimately causing monomer to be inserted between the Sn group and the rest of the polymer chain (Figure 5.6A).¹⁸⁵ According to the propagation step in the presence of $\text{Sn}(\text{Oct})_2$, it is expected that the partial positive charge density around the carbonate bond in BTMC would facilitate the nucleophilic attack of stannous alkoxide to the carbonate bond of BTMC, increasing the BTMC conversion rate. However, our results showed a negligible difference between TMC and BTMC conversion under ROP condition at 130-135 °C.

When the monomers were copolymerized in solution using $\text{HCl}\cdot\text{Et}_2\text{O}$ as the catalyst, both monomers were also incorporated into the copolymer at nearly the same rate, with TMC reacting slightly faster (Figure 5.5B). According to the proposed mechanism of $\text{HCl}\cdot\text{Et}_2\text{O}$ catalyzed ring-opening polymerization, initially the hydrogen ion of the $\text{HCl}\cdot\text{Et}_2\text{O}$ activates the monomer by conjugating to the carbonate bond. The resulting activated monomer is more susceptible to a nucleophilic attack by the hydroxyl group on the alcoholic initiator or the growing chain end (Figure 5.6B).^{234,197} In this mechanism, the carbonate bond of the cyclic monomer is already activated and positively charged by $\text{HCl}\cdot\text{Et}_2\text{O}$; thus the higher partial positive charge density around the carbonate bond of BTMC does not affect the BTMC affinity significantly in comparison to TMC. As such, with both $\text{Sn}(\text{Oct})_2$ and $\text{HCl}\cdot\text{Et}_2\text{O}$, a random distribution of TMC and BTMC was expected. The polymerizations with $\text{HCl}\cdot\text{Et}_2\text{O}$, however, proceeded much more slowly, reaching

complete conversion in 120 h, in contrast to the complete conversion within 6 h found using $\text{Sn}(\text{Oct})_2$ in a melt copolymerization at 130-135 °C.

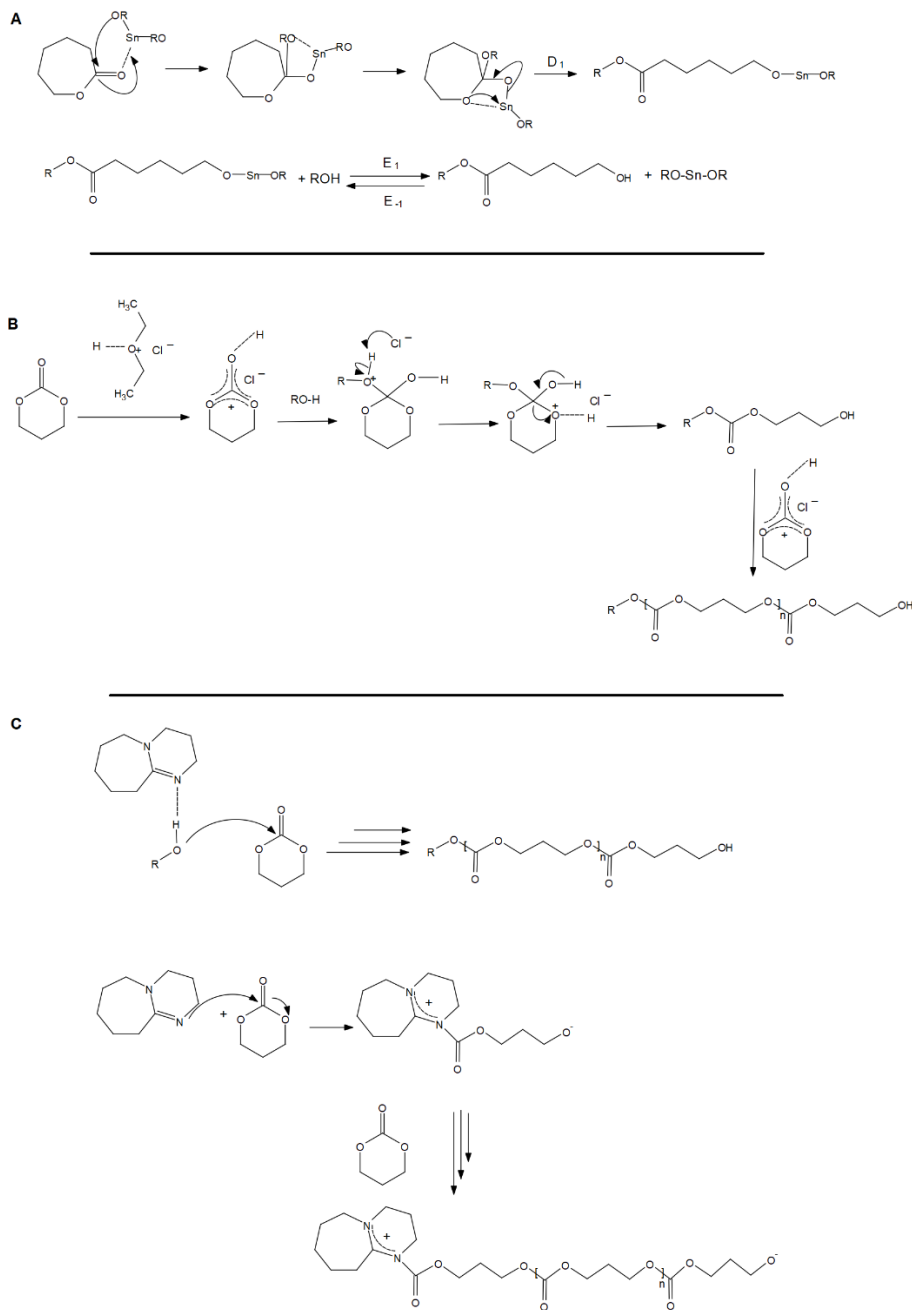


Figure 5.6. Mechanism of polymerization of cyclic carbonate monomer in the presence of (A) $\text{Sn}(\text{Oct})_2$, (B) $\text{HCl}\cdot\text{Et}_2\text{O}$, (C) DBU as a catalyst.

In contrast, BTMC polymerized much faster than TMC in the presence of DBU, as it reached complete conversion in 12 h, at which time the TMC conversion was only 50%. Thus, blocky copolymers were formed (Figure 5.5C).

DBU catalyzes polymerization via activation of the initiating/propagating hydroxyl group^{198,199} and an anionic mechanism causes auto-initiating of TMC (Figure 5.6C).^{184,190,199} According to the monomer conversion achieved in this study, the partial positive charge around the carbonate bond caused by the benzyloxy group in the BTMC monomer provided higher reactivity and thus a higher monomer conversion rate for BTMC than for TMC in the presence of DBU. For all three catalysts, monomer conversion slowed near the end of the polymerization, due to the low concentration of monomers in the polymerization solution.

In the copolymerization of TMC and BTMC, eight possible sequences of repeating units may form as described in Figure 5.7. In this figure, BTMC units and TMC units are referred to as B and T, respectively.

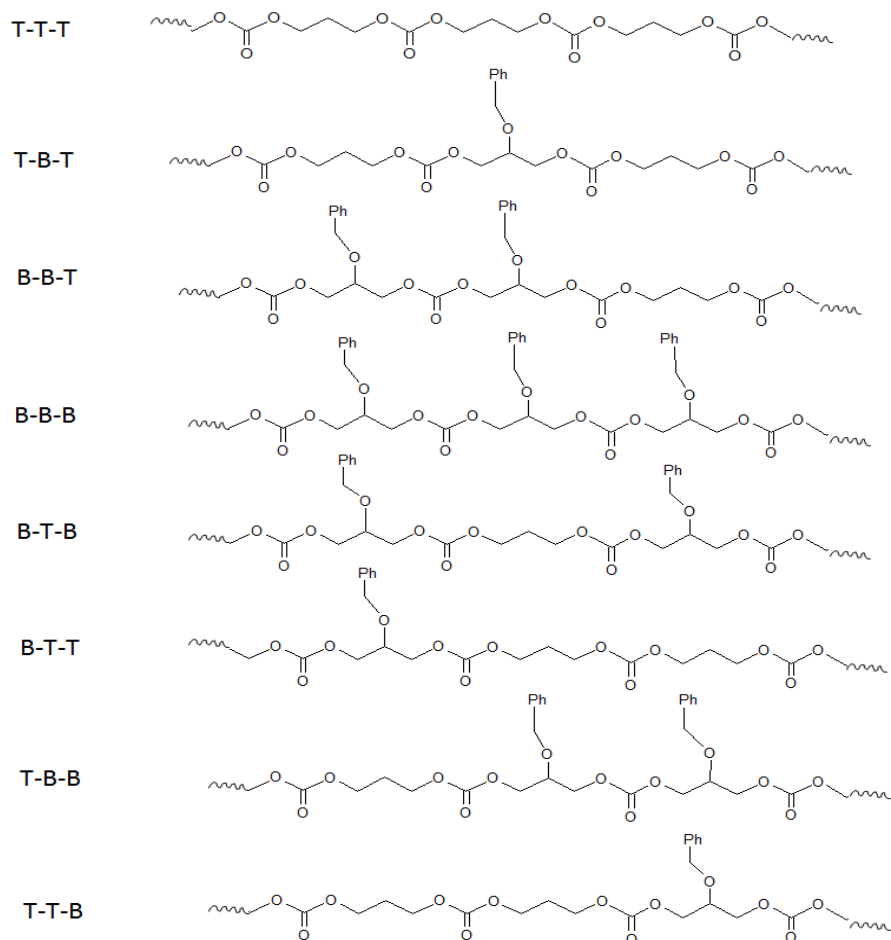


Figure 5.7. Possible sequences of carbonate bonds in the copolymer structure.

To calculate the degree of randomness of the copolymer backbone, the ^{13}C NMR spectrum of P(TMC-co-BTMC) was compared with the ^{13}C NMR spectra of PTMC and PBTMC (Figure 5.8). The peaks of triad sequences that do not overlap the peaks of homopolymers (B-B-B and T-T-T) determine the randomness in the sequences.^{200,239}

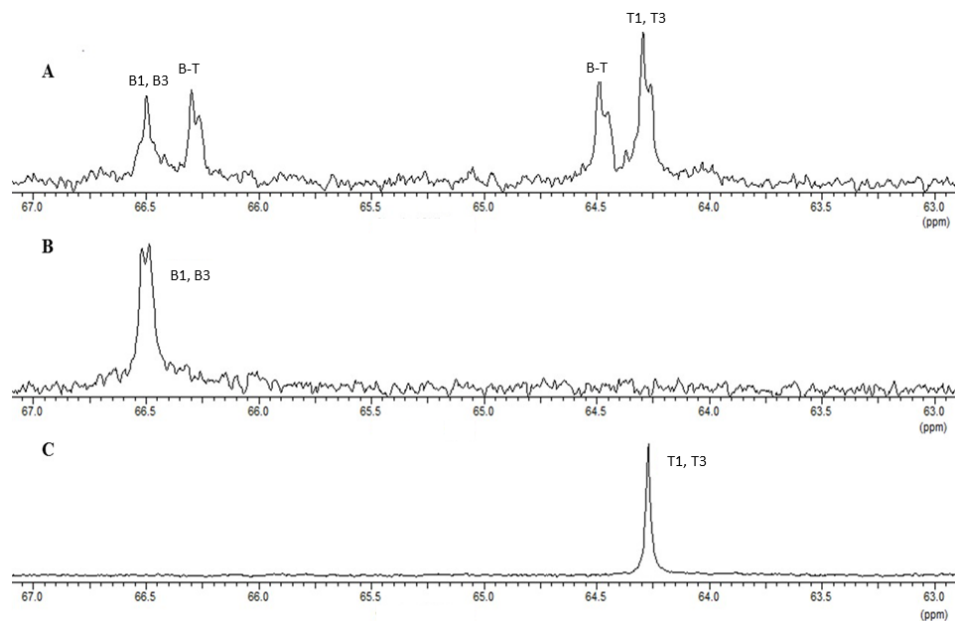


Figure 5.8. ^{13}C NMR spectra of A) OCT-P18-50B-HCl ($M_n = 1440$ Da), B) PBTMC ($M_n = 5100$ Da), C) PTMC ($M_n = 12600$ Da), NMR solvent: CDCl_3 .

Referring to the ^{13}C NMR spectrum of each homopolymer the resonance signals of ^{13}C nuclei were attributed to the carbon atoms at different sites of each kind of carbonate comonomer. In these spectra, resonances of the carbonyl group for the PTMC backbone appeared as separate signal for carbons of the methylene groups linked to the carbonate bond at $\delta = 64.25$ ppm (Figure 5.8.C). In contrast, PBTMC showed signals for carbons of the methylene groups linked to the carbonate bond at $\delta = 66.5$ ppm (Figure 5.8.B). As seen in Figure 5.8.A, which shows a representative spectrum of a copolymer (OCT-P18-50H-HCl) two new peaks appeared for carbons of the methylene groups linked to the carbonate bond at 64.5 ppm and 66.25 ppm. These peaks can be related to B-T pairings in different sequences showing that BTMC and TMC are linked together instead of linking to the corresponding homo-monomer. Similar peaks were observed in the ^{13}C NMR spectra of OCT-P40-50H-Sn and OCT-P40-50H-DBU (Figure B.3 and Figure B.4 in Appendix B).

Comparison of the relative intensities allowed for the calculation of the degree of randomness in each copolymer (Table 5.1). According to the ^{13}C NMR spectra, use of $\text{Sn}(\text{Oct})_2$ and $\text{HCl}\cdot\text{Et}_2\text{O}$ as catalysts yielded higher degrees of randomness (46-50 %) than the use of DBU as a catalyst (33 %, Table 5.1). These results are in agreement with the monomer conversion rates shown in Figure 5.6.

Table 5.1. Characterization of the pure copolymers prepared with different catalysts

Sample	Theoretical M_n (Da)	Actual M_n (Da)	Dispersity	BTMC (%)	T_g (C)	Randomness (%)	α (%)
OCT-P18-50B-HCl	2900	1440	1.2	46	-21	46	60
OCT-P40-50B-Sn	6300	3920	1.6	48	-7	50	55
OCT-P40-50B-DBU	6300	3200	1.3	50	-7	33	42

The monomer composition, number average molecular weight, end group fidelity, molecular weight distribution, and T_g of the resulting copolymers are also given in Table 5.1. Polymerization with all three catalysts yielded copolymer compositions similar to the target composition of equimolar TMC and BTMC. However, the number average molecular weight determined from ^1H NMR end group analysis was significantly lower than the theoretical molecular weight. This difference in molecular weight was due to the poor end group fidelity (α), which ranged from 42% for DBU catalyzed polymerization to 60% for the $\text{HCl}\cdot\text{Et}_2\text{O}$ catalyzed polymerizations. End group fidelity quantifies the proportion of the polymer chains that initiated with the initiator and contain the expected end group. In these copolymers, 100% end group fidelity is referred to as those copolymer chains containing a methyl group from the alcohol initiator at one end and a terminal

hydroxyl group on the other end. End group fidelity can be reduced by side reactions such as initiation with water, catalyst and impurities, auto-initiation of the monomer, backbiting and trans-esterification. Unexpected polymer chain initiation is possible for all three catalysts used in this study from sources other than the initiator, including residual water in the reactants,^{184,185} and potentially residual TEA or TEA·HCl in the BTMC as an impurity.^{177,178} In addition, poor end group fidelity may be the result of auto-initiation of the cyclic monomer, trans-esterification and backbiting at the elevated temperature of 130 °C used with the Sn(Oct)₂ catalyzed polymerization,^{184,185} and initiation with DBU at room temperature.^{190,199,241} (add Ref 190, 199) Also, side reactions affected the molecular weight dispersity as Sn(Oct)₂ with higher possibility of auto-initiation, backbiting and trans-esterification showed higher molecular weight dispersity of 1.6 in comparison with DBU and HCl·Et₂O with molecular weight dispersity of 1.3 and 1.2, respectively.

The DSC thermographs of the copolymers are shown in Figure B.4 in Appendix B. All the copolymers were amorphous and exhibited only one T_g which was -21 °C for the lower molecular weight copolymer, OCT-P18-50H-HCl, and -7 °C for the higher molecular weight copolymers OCT-P40-50H-DBU and OCT-P40-50H-Sn. The difference in microstructure of the copolymers did not affect their T_g's; however, decreasing the molecular weight diminished the T_g significantly.

Of the catalysts studied, HCl·Et₂O was chosen for further polymerizations. This catalyst yielded random copolymers with a narrow molecular weight distribution and reasonably high end group fidelity while being readily removed by purification and thus contributing low toxicity.

5.5.2 Preparation and characterization of P(TMC-co-HTMC)s

A series of copolymers of different molecular weight and monomer ratio were prepared using $\text{HCl}\cdot\text{Et}_2\text{O}$ as a catalyst, and debenzylated using Pd/C and Pd (OH)/C, yielding pendant hydroxyl groups along the copolymer backbone.^{177,179,202} Figure 5.9 shows the ^1H NMR spectrum of OCT-P18-30H; the copolymer contains 18 monomer units with 30 mol% of those monomers HTMC. The resulting copolymers were purified by precipitation in MilliQ water at room temperature. Complete disappearance of the signals corresponding to the methylene group linked to the benzyl group ($\delta = 4.67$ ppm, Figure 5.4) and the protons of the benzyl group ($\delta = 7.36$ ppm, Figure 5.4) in the ^1H NMR spectrum of the copolymer as well as the appearance of a new peak at 5.45 ppm corresponding to the pendant hydroxyl group along the backbone, confirmed complete conversion of the benzyloxy groups to hydroxyl groups.

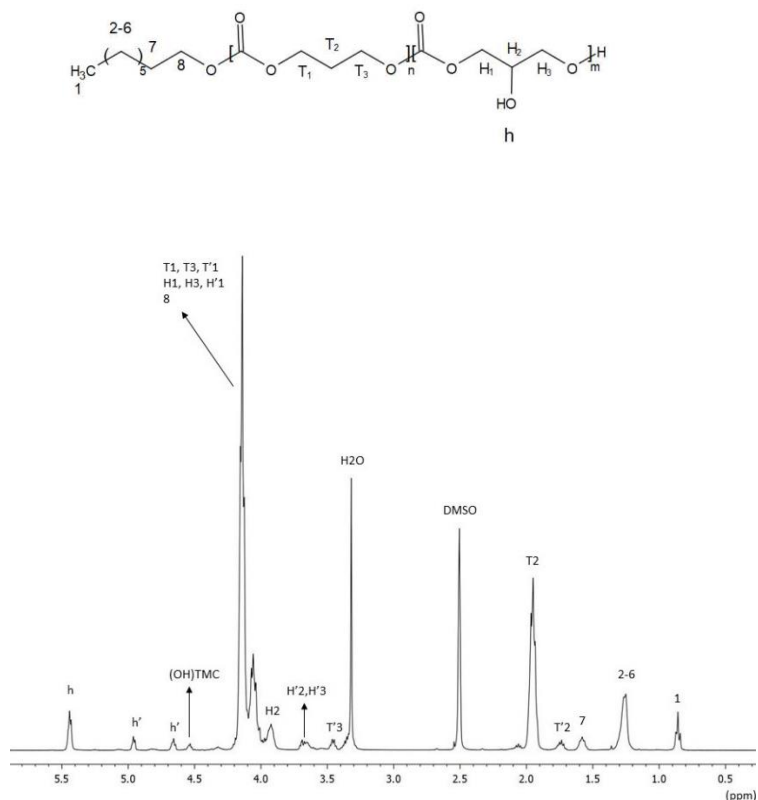


Figure 5.9. ^1H NMR spectrum of copolymer OCT-P18-30H obtained in DMSO-d_6 . $M/I=18$, $M_n = 1600$ Da, HTMC: 30%. Labels with a prime correspond to the copolymer end group and the label (OH)TMC corresponds to the hydroxyl group of TMC end unit.

The end group fidelity increased upon debenzoylation and purification (Table 5.2). This result is attributed to the loss of low molecular weight fractions during the purification step in MilliQ water. All the resulting copolymers had low T_g 's in the range of -23 °C to -50 °C and were amorphous. The T_g of the resulting debenzylated copolymers increased as molecular weight increased. For copolymers of approximately the same molecular weight (those of M_n between 1460 and 1600 Da) but with different amount of HTMC, the T_g did not change significantly as the amount of HTMC in the copolymer increased. This result reflects the limited influence of hydrogen bonding provided by the pendant hydroxyl group of the HTMC on T_g . The initiator used had no influence on the glass transition temperature as well. For example, for copolymers with a molecular weight of approximately 1800 Da

and a monomer composition of 50 mol% HTMC, the T_g was $-23\text{ }^\circ\text{C}$, regardless of whether 1-butanol or 1-octanol was used as the initiator. In contrast, samples with the same amount of HTMC but of lower molecular weight, *e.g.* OCT-P10-30H *vs.* OCT-P18-30H, showed significantly lower T_g .

Table 5.2. Characterization of the pure copolymers prepared using HCl·Et₂O as catalyst.

Sample	Feed moles of BTMC (%)	Before debenzoylation				After debenzoylation and purification			
		BTMC molar (%)	M_n (Da)	α (%)	T_g ($^\circ\text{C}$)	HTMC molar (%)	M_n (Da)	α (%)	T_g ($^\circ\text{C}$)
BU-P6-50H	50	49	610	56.2	-40	46	580	75	-50
BU-P18-50H	50	50.2	1920	70.6	-16	50	1500	90	-23
OCT-P18-50H	50	50.6	1690	63	-20	49	1560	95	-23
OCT-P10-30H	30	29.6	940	74	-34	27	1160	100	-35
OCT-P18-30H	27.8	24.7	1650	71	-24	30	1600	83	-25
BU-P18-30H	27.8	27.3	1690	72	-25	26	1580	86	-26

5.5.3 *In vitro* degradation

In vitro degradation studies were undertaken in pH 7.4 PBS under mild agitation at 300 rpm. The degradation rate of the copolymer under these conditions was dependent on copolymer composition, copolymer molecular weight, and the nature of the initiator used (Figure 5.10). The amount of HTMC in the copolymer had the greatest effect on the copolymer mass loss rate. Copolymers with 50 mol% HTMC lost more than 60 wt% of

their initial mass before 2 weeks; in contrast, copolymers possessing 30 mol% HTMC required 16 weeks to reach approximately the same extent of mass loss. For copolymers with 50 mol% HTMC, molecular weight and initiator also affected the mass loss trends, with shorter chains and chains of the same molecular weight but initiated with the more hydrophilic initiator, 1-butanol, showing a higher mass loss rate. On the other hand, copolymers consisting of 30 mol% HTMC content exhibited almost the same mass loss trend, regardless of initiator or initial molecular weight, reaching a plateau of between 47-55 % after 16 weeks. For all copolymers examined, the rate of mass loss decreased with time.

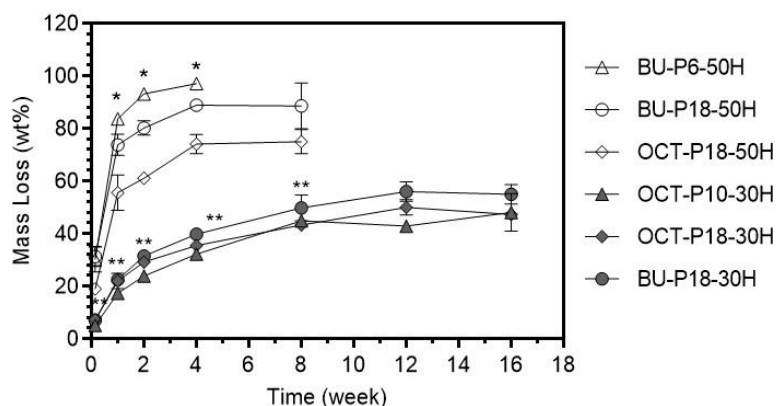


Figure 5.10. Mass loss of the samples in PBS (pH 7.4) at 37 °C under horizontal agitation of 300 rpm. The PBS was replaced every second day. Statistical difference between copolymers containing 50 mol% initial HTMC over time (*), statistical difference of the copolymers containing 50 mol% initial HTMC with copolymers containing 30 mol% initial HTMC (**), $p < 0.05$, one-way ANOVA, $n=3$.

To obtain insight into the degradation mechanism, the monomer composition and the number average molecular weight of the remaining copolymer were monitored with time. The effect of HTMC content as well as the effect of initiator and molecular weight on the degradation mechanism and trend were studied (Figure 5.11 and Figure 5.12). The HTMC content of the copolymer mass that remained as a separate phase from the buffer medium

decreased with time for all cases. As shown in Figure 5.11A, the HTMC content decreased significantly in the first week for the samples containing 50 mol% HTMC then remained nearly constant at between $12 \pm 6\%$ to $22 \pm 2.4\%$. Also, samples containing 30 mol% HTMC showed a significant decrease in HTMC content within the first 2 weeks, after which the HTMC content remained nearly constant at between 6-15% (Figure 5.11B). This result is a product of the hydrolytic resistance of the TMC carbonate linkage,²⁴² and the hydrophilicity/ degradation of the HTMC units distributed along the copolymer backbone.¹⁷⁷

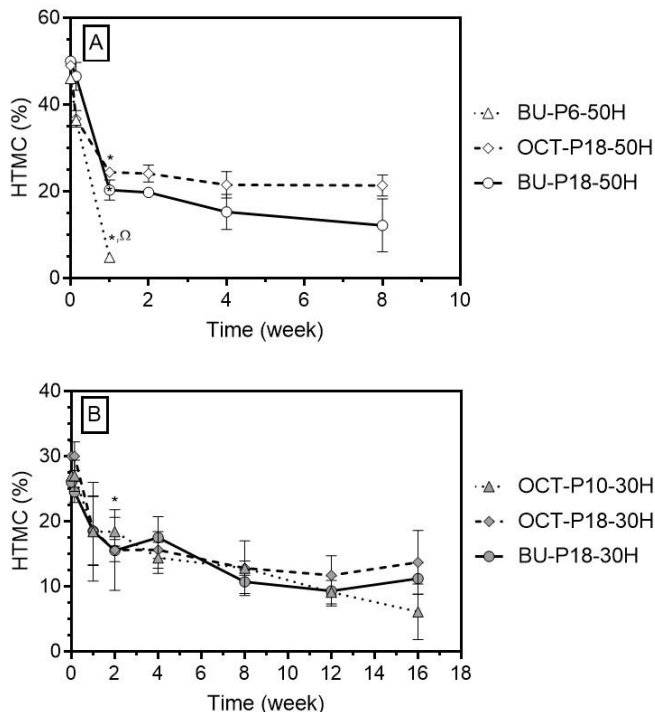


Figure 5.11. HTMC percentage of the samples in PBS (pH 7.4) at 37 °C under horizontal agitation of 300 rpm. The PBS was changed every other day. A: 50% HTMC, B: 30% HTMC. Statistical difference with day 1 (*), Statistical difference of BU-P6-50H with other copolymers in week 1 (Ω), $p < 0.05$, One-way ANOVA, $n=3$.

In a similar fashion as the change in HTMC content with time, the average molecular weight of the copolymers decreased over time by 12 to 38 % depending on the initial

copolymer molecular weight (Figure 5.12). According to these results, copolymers initiated with 1-butanol and 1-octanol were soluble in water at a number average molecular weight lower than approximately 700-1300 Da depending on the HTMC content of the remaining copolymer. One-way ANOVA did not show significant statistical difference in M_n and HTMC content over time between the copolymers except for BU-P6-50H in week 1 which showed significantly lower HTMC content in comparison to other copolymers, and OCT-P10-30H which showed significantly lower M_n from week 4 in comparison to OCT-P18-30H and BU-P18-30H.

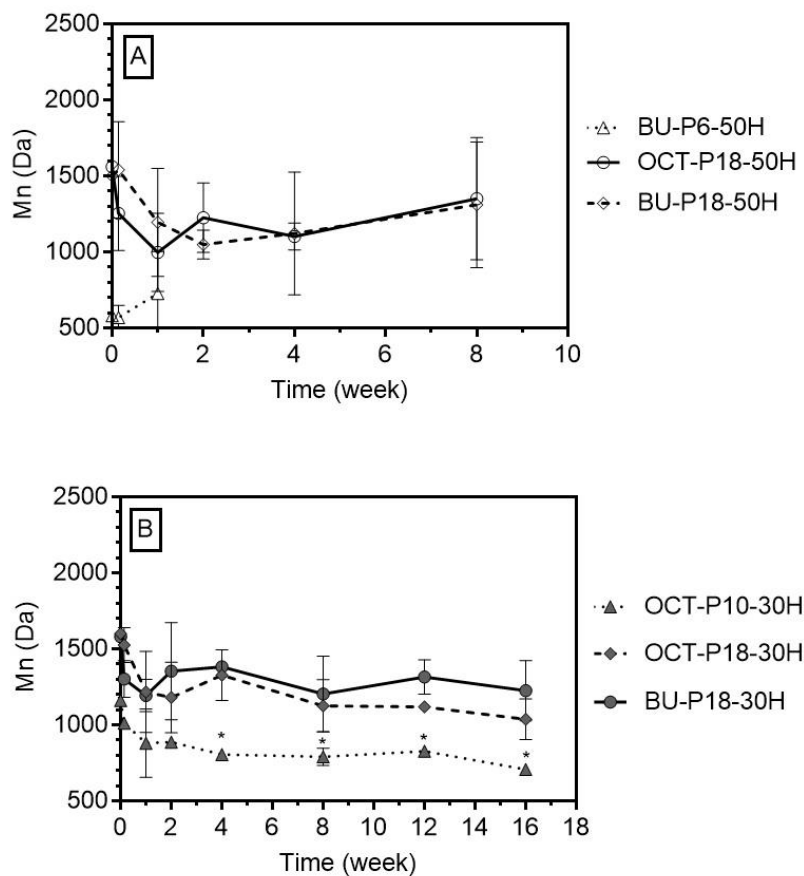


Figure 5.12. Change in M_n of the samples in PBS (pH 7.4) at 37 °C under horizontal agitation of 300 rpm. The PBS was changed every other day. A: 50% HTMC, B: 30% HTMC. Statistical difference of OCT-P10-30H with OCT-P18-30H and BU-P18-30H overtime (*), $p < 0.05$, one-way ANOVA, $n=3$.

The degradation mechanism of the HTMC homopolymer has been studied by Dr. Fei Chen of the Amsden group. According to this study as water diffuses into the polymer bulk, the HTMC units are cleaved quickly. The degradation occurs through intramolecular nucleophilic attack of the carbon monoxide anion formed from the pendant hydroxyl groups of the repeating units or the hydroxyl end group in water on the carbonate bond.^{176,180} Upon cleavage of HTMC units, the polymer chain length decreases gradually until oligomers become short enough to dissolve in the surrounding aqueous phase. Therefore, the degradation of P(TMC-co-HTMC) would be expected to depend on the rate of diffusion of water into the copolymer bulk. As water diffuses into the copolymer, HTMC units cleave, gradually producing oligomers. If the resulting oligomer is soluble in water, the copolymer bulk will lose mass. Thus, the degradation rate of the P(TMC-co-HTMC) would be expected to depend on the initial HTMC content, the hydrophilicity of the initiator, the arrangement of the HTMC units and the initial molecular weight. Increasing the copolymer hydrophilicity by incorporating a higher HTMC content and/or using a more hydrophilic initiator would be expected to facilitate water diffusion into the polymer bulk. Comparing the degradation of the P18 copolymers that possessed different initial HTMC content revealed that the presence of a greater number of HTMC units (50 mol% vs 30 mol%) providing more hydrophilic/degradable units along the backbone led to initially quick cleavage of the chains as the HTMC content dropped significantly to approximately 20 mol% within a week (Figure 5.11.A), and showing 55-70 wt% mass loss depending on the initiator used (Figure 5.10). Afterwards the changes in mass loss, HTMC% and M_n of the remained copolymers with 50 mol% initial HTMC content showed almost the same trend as the copolymers with 30 mol% initial HTMC content. At 50 mol% initial HTMC

content, copolymers initiated with more hydrophilic initiator, BU-P18-50H, showed significantly higher mass loss for approximately 20 wt% in week 1 in comparison to OCT-P18-50H which was followed at fairly constant difference over time (Figure 5.10). The effect of the hydrophilicity of the initiator was not observed in the mass loss of the copolymers with 30 mol% initial HTMC content. According to the close HTMC content and M_n of the remained P18 copolymers at later time points, it can be concluded that the HTMC content is the main factor increasing the hydrophilicity of the resulting copolymer which in combination with the hydrophilic initiator led to higher mass loss. As the HTMC content decreased to approximately 20 mol%, the number of hydrophilic/degradable units of the resulting cleaved chains decreased and the effect of the initiator hydrophilicity is obscured.

If the HTMC units are distributed randomly along the backbone, cleaving the HTMC units would lead to low molecular weight oligomers that are mostly composed of TMC repeating units. The water solubility of the resulting cleaved oligomers would depend on their molecular weight which is determined by the initial HTMC content and the initial molecular weight of the copolymer. At high HTMC content of 50 mol%, significantly higher mass loss was observed for the copolymer with lower initial molecular weight (BU-P6-50H) in comparison to BU-P18-50H and OCT-P18-50H. However, this effect of initial molecular weight on the degradation was not observed in the series of the copolymers with 30 mol% initial HTMC content due to the limited water solubility of PTMC.

An important consideration for the potential application of these copolymers as a growth factor delivery device is the change in pH of the degradation medium by the generation of

degradation products. One of the degradation products of the copolymers is carbon dioxide, which in water is converted to carbonic acid. Therefore, the pH of the PBS solution was monitored with time during degradation for copolymers initially containing 30 and 50 mol% HTMC, initiated with 1-octanol or 1-butanol (Figure 5.13). For the more rapidly degrading copolymers with 50 mol% HTMC content and during the first days of the degradation study, the pH dropped to 6.1 then returned to a neutral pH within 2 weeks. The decrease in pH corresponds to the period of most rapid mass loss (Figure 5.10) and decrease in HTMC content of the copolymer (Figure 5.11), and therefore is attributed to the formation of high amounts of carbonic acid in water. It is notable, however, that the pH of the PBS degradation medium was only mildly acidic. The pH of the medium surrounding the more slowly degrading copolymers with 30 mol% HTMC content always remained close to neutral, a result of the reduced amount of carbon dioxide generated with time.

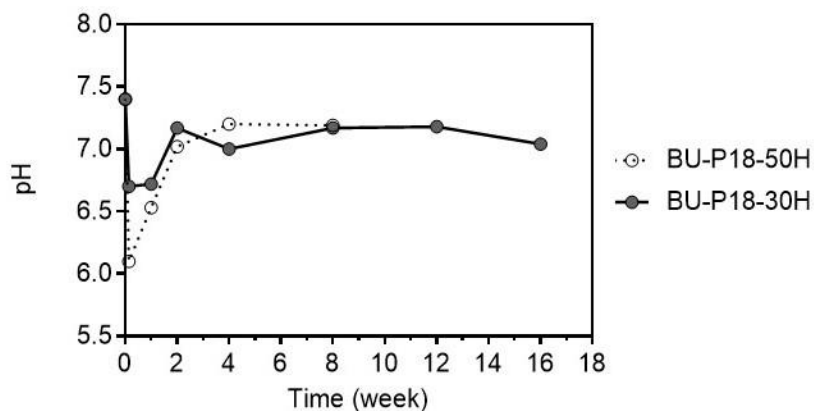


Figure 5.13. pH of degradation medium during in vitro degradation in PBS.

5.5.4 Copolymer Viscosity

Due to the moderate *in vitro* degradation rate of the 1000-2000 Da copolymers containing 30 mol%, these copolymers were chosen for further examination as a growth factor delivery vehicle. As such, it was necessary to assess whether the copolymers would be injectable. Previous studies showed that liquid polymers can be readily injected by hand through standard gauge needles at a viscosity less than about 100 Pa·s.^{221,237} The viscosity of the copolymer is related to its T_g , which can be adjusted by choice of initiator, by the number of HTMC repeating units, and the molecular weight (Table 5.2). All the copolymers showed Newtonian flow behavior with average viscosities ranging from 45-362 Pa·s at 25 °C and 15-93 Pa·s at 37 °C (Table 5.3). The viscosity was higher for the copolymers with higher molecular weight, and there was no significant effect of the initiator on viscosity. All three copolymers would be expected to be injectable at 37 °C, which was confirmed by manual injection through an 18 ½ gauge needle at 37 °C.

Table 5.3. viscosity measurements at 25 °C and 37 °C

Sample	25 °C (Pa·s)	37 °C (Pa·s)
OCT-P10-30H	45 ± 4.8	15 ± 1.8
OCT-P18-30H	362 ± 5.6	92 ± 2.3
BU-P18-30H	346 ± 17.2	98 ± 4.7

5.6 Conclusion

In this chapter, it was demonstrated that distributing HTMC units randomly along the backbone of an TMC-HTMC copolymer yielded a hydrolytically degradable copolymer. A comparison of copolymers of different molecular weights and HTMC content prepared with different initiators showed that the HTMC content was the most influential parameter affecting degradation. A high HTMC content of 50 mol% caused rapid mass loss reaching 60-95 wt% within 2 weeks depending on the initial molecular weight of the copolymer, and a slightly acidic pH during the first days of degradation. In contrast, a lower HTMC content of 30 mol% showed gradual mass loss over time, reaching 47-55 wt% within 16 weeks, while the solution pH always remained close to neutral. The initial molecular weight also affected the degradation rate as the copolymers with lower initial molecular weight degraded faster as a result of the more likely generation of water-soluble degradation products, particularly for copolymers with higher HTMC content. From these results, the copolymers containing 30 mol% HTMC were chosen for further study as the drug delivery vehicle. These copolymers had viscosities less than 100 Pa·s at 37 °C and were manually injectable. In the next chapters, *in vivo* degradation mechanism and tissue response of these compounds as well as the protein release will be presented.

Chapter 6

***In vivo* degradation and tissue response to low molecular weight poly(trimethylene carbonate-co-5-hydroxyl trimethylene carbonate) (P(TMC-co-HTMC))**

6.1 Abstract

The purpose of this study was to determine the *in vivo* degradation mechanism of, and assess the tissue response to, 1000-2000 Da P(TMC-co-HTMC)s initiated with 1-octanol or 1-butanol at a 30 mol% HTMC content after subcutaneous injection in rats. The change in molecular weight and change in copolymer composition were monitored and evaluated as a function of implantation time over 22 weeks. The tissue response was assessed histologically using Masson's trichrome staining and immunohistochemically by staining for CD68 positive cells. The *in vivo* degradation study revealed rapid degradation of the HTMC units followed by gradual elimination of the short chains produced via HTMC cleavage. The lower molecular weight copolymer degraded significantly faster due to the fewer backbone cleavage events required to produce short, water-soluble oligomers. The tissue response to the implanted copolymers was comparable to that of a MONOCRYL suture, indicating that the copolymer can be considered biocompatible. These findings suggest that these copolymer compositions are promising candidates for use as an injectable drug delivery vehicle.

6.2 Introduction

Inflammation is the natural response to the implantation of a biomaterial. The severity and duration of the implantation depends on the implantation technique, the extent of the injury caused by the implantation process, the blood-material interaction, provisional matrix formation, the extent of cell necrosis following implantation, the degradation rate of the biomaterial, the toxicity of the implanted biomaterial and its degradation products, as well as the physical properties and the shape of the implant.^{100,101} One advantage of the use of a liquid injectable delivery formulation in protein therapeutic angiogenesis is the minimally-invasive implantation through injection and the lack of mechanical irritation of the surrounding tissue which can result in a thick fibrous encapsulation layer,^{243,244} and may subsequently delay drug absorption into the tissue. The liquid injectable delivery formulation should be biocompatible providing stable healing without significant ongoing inflammation or irritation.^{100,101,205,206}

In this chapter, the influence of the poly(trimethylene carbonate-co-5-hydroxyl trimethylene carbonate) (P(TMC-co-HTMC)) molecular weight, initiator and viscosity on its *in vivo* degradation rate and the tissue response to the copolymer were studied. To achieve this objective, P(TMC-co-HTMC) was prepared through the co-polymerization of 5-benzyloxy trimethylene carbonate (BTMC) with trimethylene carbonate (TMC) via ring-opening solution polymerization using hydrogen chloride solution in diethyl ether (HCl·Et₂O) as a catalyst. Following copolymerization, the BTMC repeating units were debenzylated to yield a P(TMC-co-HTMC) copolymer with hydroxyl pendant groups along the backbone.^{177,230} Based on the results achieved in Chapter 5, an HTMC mol% of

30 and a molecular range of 1000-2000 Da were chosen due to the moderate *in vitro* degradation rate of these copolymers. It was reasoned that the chosen copolymer composition would also show a moderate *in vivo* degradation rate which would allow for effective growth factor delivery. The change in molecular weight and copolymer composition were monitored and evaluated as a function of implantation time. The tissue response to P(TMC-co-HTMC)s was assessed histologically using Masson's trichrome staining and immunohistochemically by staining for CD68 positive (CD68⁺) cells and compared to the tissue response to the implantation of a clinically used suture, MONOCRYL, which is considered to be biocompatible with a standard degradation time of 13-17 weeks.^{245,246}

6.3 Materials

1,3-trimethylene carbonate (TMC) was obtained from Leapchem, Hangzhou, China. 5-benzyloxy trimethylene carbonate (BTMC) was purchased from Obiter research LLC, USA. 1 M hydrogen chloride solution in diethyl ether (HCl·Et₂O), palladium on carbon (Pd/C), palladium hydroxide on carbon (Pd(OH)₂/C), 1-octanol, 1-butanol, celite, sodium citrate, Tween 20, bovine serum albumin (≥98% purity) (BSA) and deuterated dimethyl sulfoxide (DMSO-d₆) were purchased from Sigma-Aldrich Ltd, Canada. Phosphate buffered saline (PBS) powder, tris hydrochloride (TBS), PermOUNT™ mounting medium, anhydrous potassium carbonate (K₂CO₃), formaldehyde, tetrahydrofuran (THF), methanol (MeOH) and dichloromethane (DCM) were purchased from Thermo Fisher Scientific, Canada. Hydrogen gas (H₂) (99.99% purity) was purchased from Linde Ltd, Canada. Water used was of type 1 purity, obtained from a Millipore Milli-Q Plus ultrapure water filtration

system. THF and methanol were dried over activated 3 Å molecular sieves. All other materials were used as received.

Wistar rats were received from Charles River Laboratories, Canada. Tramadol was purchased from Chiron Compounding Pharmacy Inc, Canada. Primary antibody (antirat-CD68 antibody [ED1] ab31630), the secondary antibody (goat anti-mouse IgG H&L (Alexa Fluor® 488 (ab150113) and fluoroshield mounting medium with 4',6-diamidino-2-phenylindole (DAPI) (ab104139) were purchased from abcam, Canada. Masson's trichrome (25088) was purchased from Polysciences Inc, Canada. MONOCRYL* Plus suture 3-0 was purchased from Ethicon, USA.

6.4 Methods

6.4.1 Synthesis and characterization of P(TMC-co-HTMC)

P(TMC-co-HTMC) initiated with 1-octanol or 1-butanol at an HTMC/TMC molar ratio of 30/70 (30 mol% HTMC) and molecular weight range of 1000-2000 Da were prepared and characterized as described in sections 5.4.1.2, 5.4.2 and 5.4.3.

6.4.2 *In vivo* biocompatibility and biodegradation

The following animal study was performed in accordance with the guidelines of the Canadian Council on Animal Care code of ethics governing animal experiment (protocol #Amsden 2015-1627). The study involved subcutaneous injection of the copolymers into the dorsal tissue of male Wistar rats weighing approximately 300 g. Prior to injection, the

copolymer vials were decontaminated by exposure to germicidal UV light in a biosafety cabinet (BSC) for 30 min. Then 1 mL sterile syringes were filled with copolymer using an autoclaved metal spatula while in the BSC, and packed in autoclave bags to be transported to the operating room. Prior to injection, the syringes were heated to 37-40 °C to facilitate injection. The rats were anesthetized with 1 % isoflurane in oxygen for few minutes to achieve a level of surgical anesthesia as indicated by a lack of tail and corneal reflexes. Once anesthetized, the rats were shaved at the site of implantation, the skin was disinfected using 10 % povidone iodine, and washed with saline. To implant the copolymer samples, a small incision was made, and a pocket formed between the skin and the underlying tissue. Then approximately 100 mg of the pre-heated copolymer was injected into the pocket through a 18 ½ gauge needle, and the pocket was closed using suture wound clips. Two implantation sites for each copolymer composition on the dorsal area of each rat were provided. The mass of injection was determined by weighing the syringe plus needle before and after each injection. A small piece of MONOCRYL* Plus 3-0 suture of about 1 cm length was implanted as a control in the same manner. After implantation, tramadol was injected subcutaneously at a dose of 20 mg/kg body weight. The tramadol injection was repeated every 24 h for 3 days. The day following implantation, and every 2 to 3 days afterwards, the animals were observed for signs of unusual behavior including avoidance of other animals, lack of grooming, dull or cloudy eyes, diarrhea, increased respiration, aggression, salivation, listlessness, dehydration, and chattering. After 1, 2, 4, 12 and 22 weeks, two rats were chosen randomly and humanely euthanized by the injection of a lethal dose of Euthanyl at 120 mg/kg body weight. The site of implantation was shaved, and the skin was dissected back. A photograph of the surrounding tissue was taken and the tissue

was visually assessed for signs of inflammation and necrosis. To determine the *in vivo* degradation mechanism, from each rat one injection site of each copolymer composition was opened by a surgical scalpel blade and the remaining copolymer was removed from the site using a spatula. ^1H NMR spectra of the copolymers were recorded in DMSO- d_6 at room temperature on a 400 MHz Bruker Avance spectrometer, and M_n and HTMC molar composition were calculated as described in Section 5.4.3.

6.4.3 Histological and immunohistochemistry analysis

The harvested tissue was fixed in 4 wt% paraformaldehyde in PBS immediately after extraction and stored overnight in a refrigerator at 4 °C. Then tissues were transferred to 75 vol% ethanol and stored in a refrigerator at 4 °C until processing. The resulting tissues were dehydrated in graded ethanol (75% and then 100%), cleared in xylene, and then embedded in paraffin. The tissue blocks in paraffin were cut at 10 μm intervals and deparaffinized by immersing in xylene, graded ethanol (100%, 50% and then 25%) and PBS, respectively. Finally, the tissue sections were stained with a Masson's trichrome stain kit according to the supplier's instructions. The stained sections were dehydrated using xylene and ethanol, and coverslipped with PermountTM mounting medium.^{150,247} All images were obtained using a Zeiss AxioCam microscope camera equipped with Axio Vision software (version 4.7.1.0) using a microscope objective of 20X. A total of 5 images were captured per slide. The thickness of the fibrous capsule and the number of the cells per $10^4 \mu\text{m}^2$ distributed in the inflammatory zone at a distance of 100-300 μm from the copolymer-tissue interface was measured from these images using ImageJ software.

For immunohistochemistry (IHC) analyses, the deparaffinized tissue sections were subjected to heat-mediated antigen retrieval in pH 6 citrate buffer bath at 60 °C overnight and then washed in a bath of 1X TBS-0.025% Tween 20 at room temperature. The endogenous peroxidase activity was blocked using 5000 µg/mL BSA in TBS for 30 min at room temperature. The primary antibody (mouse anti rat-CD68 antibody) diluted in 1% BSA solution in 1X TBS at 1:400 dilution was applied on the sections and incubated at 4 °C in a refrigerator overnight. The day after, the slides were washed by immersion in a bath of 1X TBS-0.025% Tween 20 with gentle agitation. The secondary antibody (goat anti mouse IgG Alexafluor488) diluted in 1X TBS at 1:500 dilution was applied on the sections and incubated at room temperature in a dark room for 1 h. Finally, sections were mounted in Fluoroshield mounting medium with DAPI and coverslipped in a dark room. Tissue sections of spleen at a thickness of 10 µm were used on a separate slide as a positive control. Slides were stored in a refrigerator at 4 °C in a closed box with no exposure to light. Each IHC slide included one negative control. For the negative control, the primary antibody was replaced by 1% BSA solution in 1X TBS. This protocol was optimized based on the immunohistochemistry application guide and instructions from Abcam. All images were taken with a Zeiss Axio Imager M1 microscope camera equipped with ZEN blue software using a microscope objective of 40X. A total of 8 images were captured per slide and the number of CD68⁺ cells per 10⁴ µm² distributed in the inflammatory zone at a distance of 100-300 µm from the copolymer-tissue interface was measured using ZEN blue software.

6.4.4 Statistics

The chemical composition and number average molecular weight of the extracted copolymers were measured on duplicate samples. All data are reported as the average \pm the standard deviation about the average. Statistical differences were determined using a one-way ANOVA. Differences were considered significant for p values less than 0.05.

The thickness of the fibrous capsule and the density of the cells for each copolymer composition were averaged for implantation sites from 5 images for histological analysis (N=5) and 8 images for immunohistochemically analysis (N=8) on two different rats (n=2) at each time point. Statistical differences were determined using a two-way ANOVA with a Bonferroni post-hoc test. Differences were considered significant for p values less than 0.05.

6.5 Results and Discussion

6.5.1 Copolymer properties

A series of 1000-2000 Da copolymers initiated with 1-butanol or 1-octanol and having a 30 mol% HTMC content were prepared using HCl·Et₂O. The resulting copolymers were purified and characterized as explained in chapter 5. Table 6.1 shows the physical-chemical properties of the copolymers. The resulting copolymers showed approximately the same physical-chemical properties as the previous series of the copolymers used for the *in vitro* degradation study of the copolymer in Chapter 5, which supports the reproducibility of the copolymerization and purification processes.

Table 6.1. Physical-chemical properties of P(TMC-co-HTMC) copolymers

Sample	Initiator	Mn (Da)	Tg (°C)	HTMC (%)	Viscosity at 37 °C (Pa·s)
OCT-P10-30H	1-octanol	1160	-35	30	15 ± 1.8
OCT-P18-30H	1-octanol	1740	-26	28	92± 2.3
BU-P18-30H	1-butanol	1730	-25	29	98 ± 4.7

6.5.2 Visual observation and *in vivo* biodegradation

The copolymer pre-heated to 40 °C was injected easily through an 18 ½ gauge needle and into the tissue pocket formed in the subcutaneous space. During the period of the study all the animals gained weight and no signs of discomfort or adverse response such as sores and redness were observed around the injection sites. A photograph of the surrounding tissue was taken after euthanization and exposure of the injection site, and the tissue around the injection site was visually assessed. Figure 6.1 shows representative images of the copolymer samples within the subcutaneous tissue before explanting from the tissue. The injected copolymers formed a depot at the implantation site which was readily observed visually at each time point.

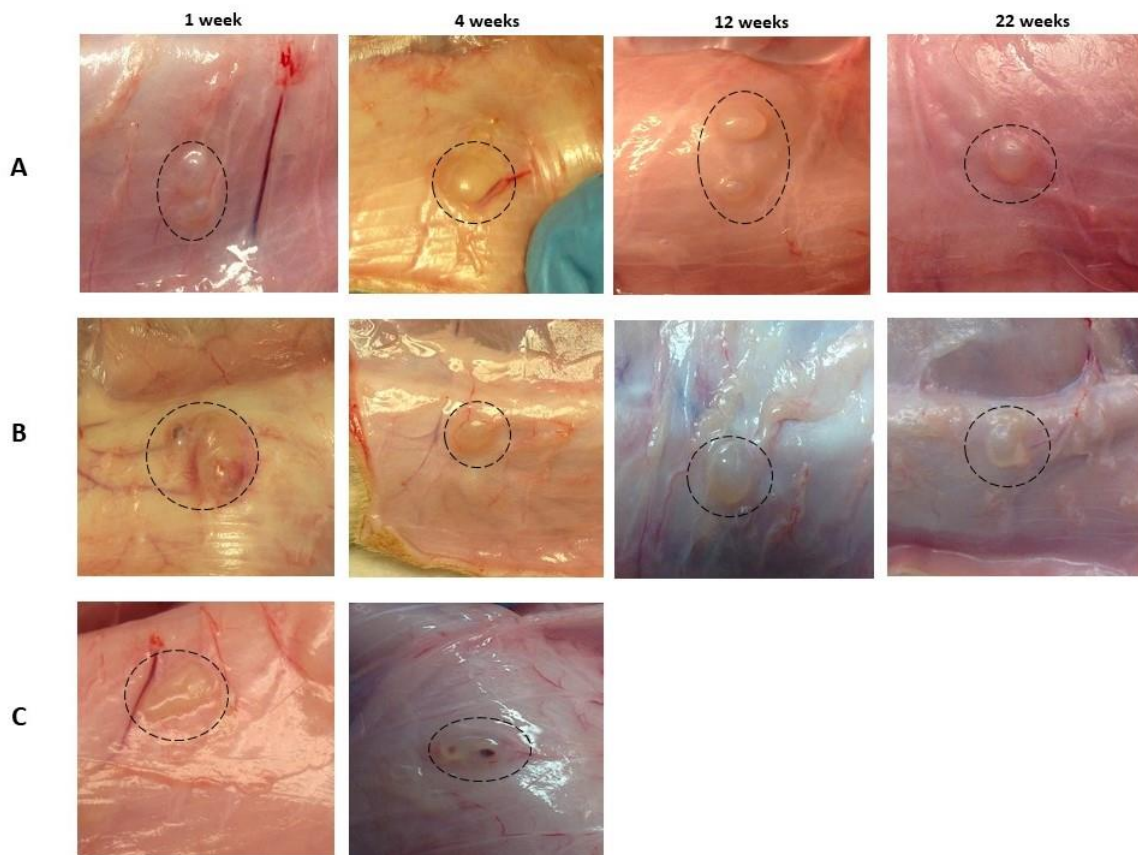


Figure 6.1. Representative photographs of copolymer samples in the subcutaneous tissue before explantation at time points of 1 to 22 weeks. A: BU-P18-30H, B: OCT-P18-30H, C: OCT-P10-30H.

Figure 6.2 shows the change in the number average molecular weight (M_n) and HTMC mol% of the remaining copolymer over the 22 weeks of the *in vivo* study. By week 1, the remaining copolymer samples had lost 55-60% of their initial HTMC content. The HTMC composition of the copolymers then stayed fairly constant with time at approximately 10 mol% except for BU-P18-30H, which showed a significant decrease in HTMC molar % of 5 ± 0.6 by week 22 (p value < 0.05). For the copolymer compositions with an initial M_n of approximately 1700 Da, a 20-40% decrease in M_n was observed over the first week. The M_n then stayed constant up to week 12. By week 22, the M_n had not changed significantly for OCT-P18-30H samples; however, a significant increase was observed in the M_n of the

BU-P18-30H samples (p value < 0.05). In contrast, the M_n remained constant for OCT-P10-30H until week 4, after which the cohesive depot had disappeared.

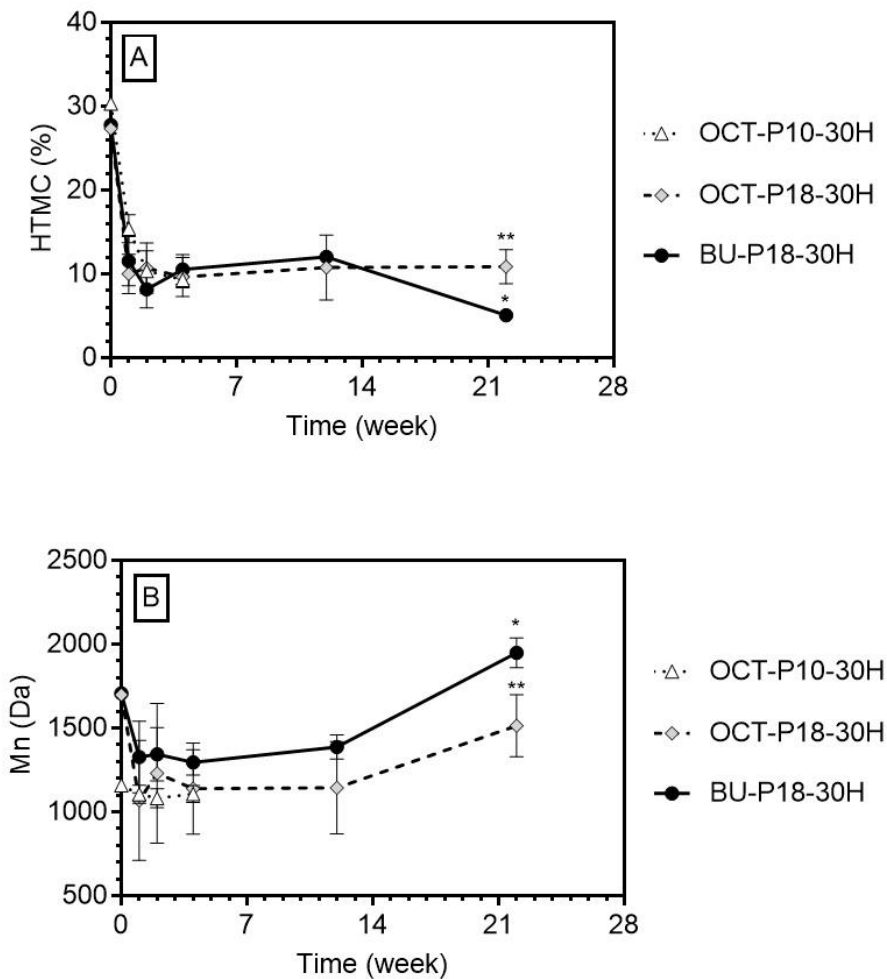


Figure 6.2. Evolution of A: HTMC mole% and B: M_n (Da) during *in vivo* degradation. Each data point represents the average, and the error bars are the standard deviation about the average. Statistical difference between week 22 with previous time points (*), statistical difference between OCT-P18-30H with B-P18-30H at the same time point (**), $p < 0.05$, One-way ANOVA, $n=2$.

According to these results, HTMC units along the backbone were rapidly lost from the copolymer within a week in the body, resulting in the production of lower molecular weight chains containing principally TMC. A statistical comparison of these *in vivo* results with

the *in vitro* degradation results in section 5.5.3 using two-way ANOVA revealed no significant difference in the M_n and HTMC content of the remained copolymers under *in vitro* and *in vivo* condition at the same time points up to week 12. Figure 6.3 shows the representative comparison of M_n and HTMC content corresponding to BU-PA8-30H under *in vivo* and *in vitro* conditions. Representative images for other copolymers are given in Appendix C, Figure C.1 and C.2.

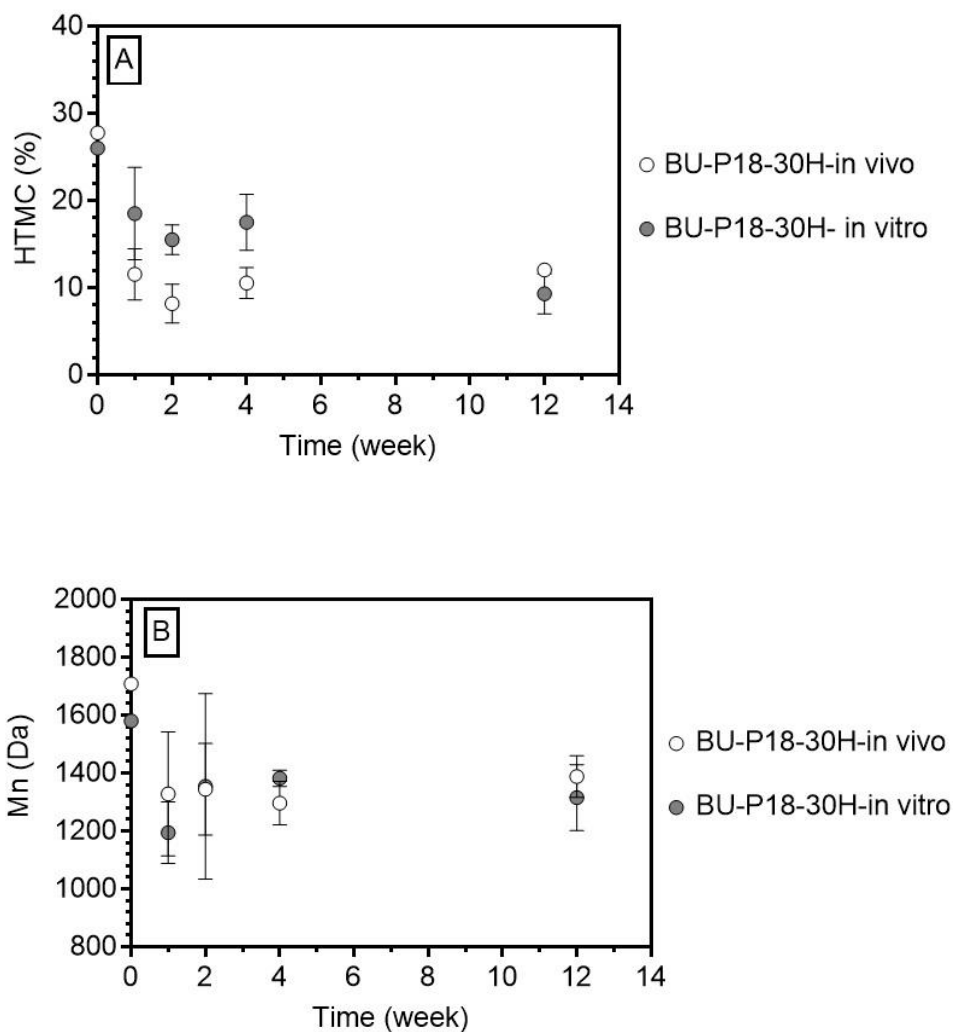


Figure 6.3. *In vivo* versus *in vitro* degradation changes of BU-P18-30H in : A) HTMC mole% and) M_n (Da). Each data point represents the average, and the error bars are the standard deviation about the average.

An extra time point of week 22 was analyzed under the *in vivo* condition. The results of this time point suggest that the hydrophilicity of the initiator influences the copolymer degradation *in vivo* at the later time points as the remaining BU-P18-3OH possessed a significantly higher M_n and lower HTMC mol% in comparison to the OCT-P18-3OH samples. The OCT-P18-3OH and BU-P18-3OH were still observed at the site of injection at 22 weeks. In contrast, the lower molecular weight OCT-P10-3OH had disappeared, indicating it had a faster degradation rate. This faster degradation was due to the fewer backbone cleavage events required to produce short chains that were soluble in the aqueous medium surrounding the samples.

6.5.3 Histological and immunohistochemistry analysis

Harvested tissue sections were stained with Masson's trichrome to determine the host tissue response to the copolymers. Masson's trichrome stains collagen blue, cytoplasm and muscle fiber red and nuclei black. Figures 6.4 and 6.5 show representative photomicrographs of the stained tissue sections at different time points. All the injected copolymers initially formed cohesive depots, but with some small copolymer droplets in the tissue surrounding the injection site that were observed up to week 4. By week 12 the suture and OCT-P10-3OH had disappeared; however, OCT-P18-3OH and BU-P18-3OH could still be found in the tissue at week 22.

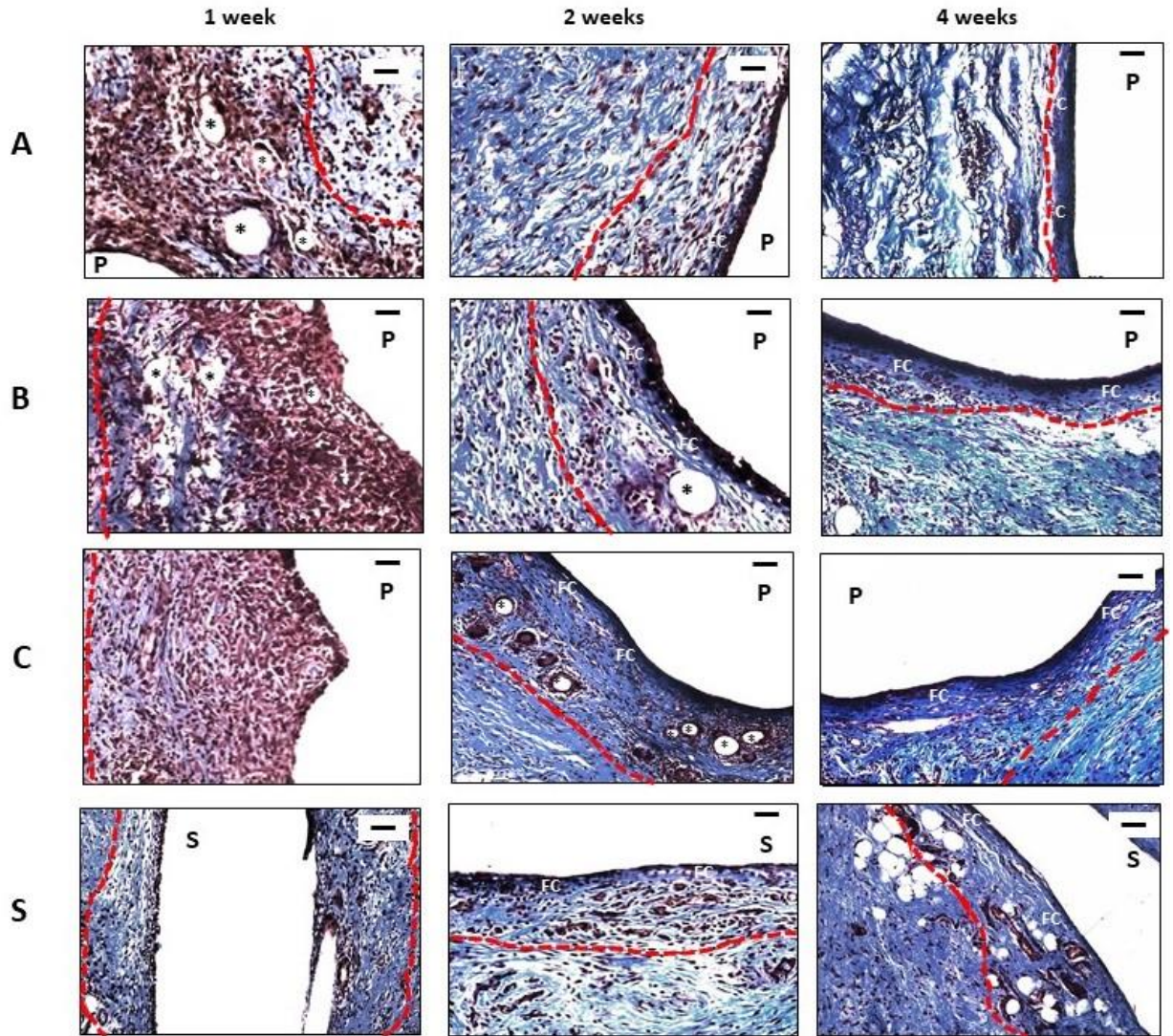


Figure 6.4. Representative photomicrographs of tissue sections (muscle side) of copolymer samples stained with Masson's trichrome at time points of 1, 2 and 4 weeks. A: BU-P18-3H, B: OCT-P18-30H, C: OCT-P10-30H, S: Suture, copolymer (P), suture (S), fibrous capsule (FC), copolymer particle (*). Scale bar: 50 μm , 20X. The dashed line represents the inflammatory zone.

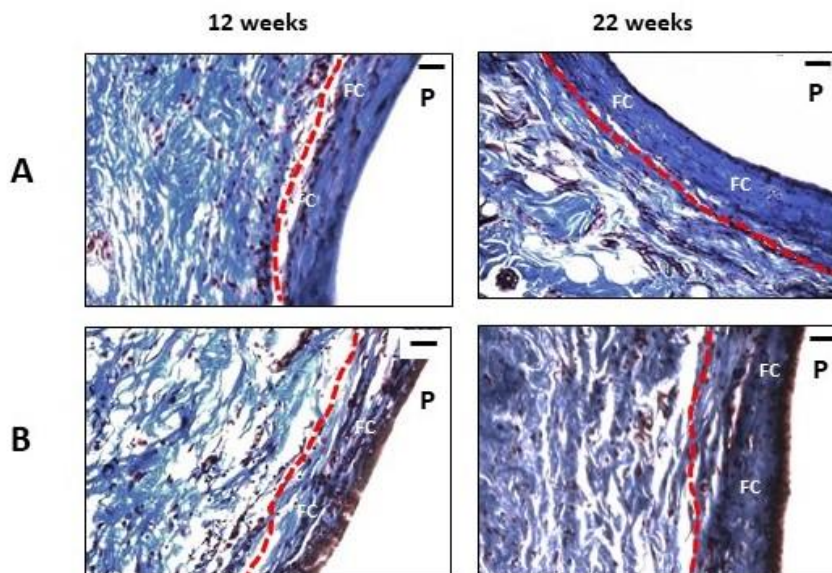


Figure 6.5. Representative photomicrographs of tissue sections (muscle side) of copolymer samples stained with Masson's trichrome at time points of 12 and 22 weeks. A: BU-P18-3H, B: OCT-P18-30H, copolymer (P), suture (S), fibrous capsule (FC). Scale bar: 50 μm , 20X. The dashed line represents the inflammatory zone.

The thickness of the fibrous capsule and the number of the cells present in the inflammatory zone, 0-300 μm from the copolymer-tissue interface, were measured using Image J (Figure 6.6 and 6.7, respectively). The number of cells per area and the thickness of the fibrous capsule around the copolymer droplets were also analyzed. By week 2 a fibrous capsule layer had formed around the injected copolymers and the suture with a range of average thickness of 24-53 μm . The capsule surrounding the OCT-P10-30H samples was significantly thicker than that around the other copolymers. The thickness of the fibrous capsule did not change significantly at week 4 for both the suture and the OCT-P10-30H. The higher molecular weight copolymer samples, OCT-P18-30H and BU-P18-30H, showed a significant gradual increase in the thickness of the fibrous capsule over time from week 2 to 12 which stabilized by week 22. There was no significant difference in capsule

thickness between the copolymers themselves and between the suture and the copolymers from week 4 to 22.

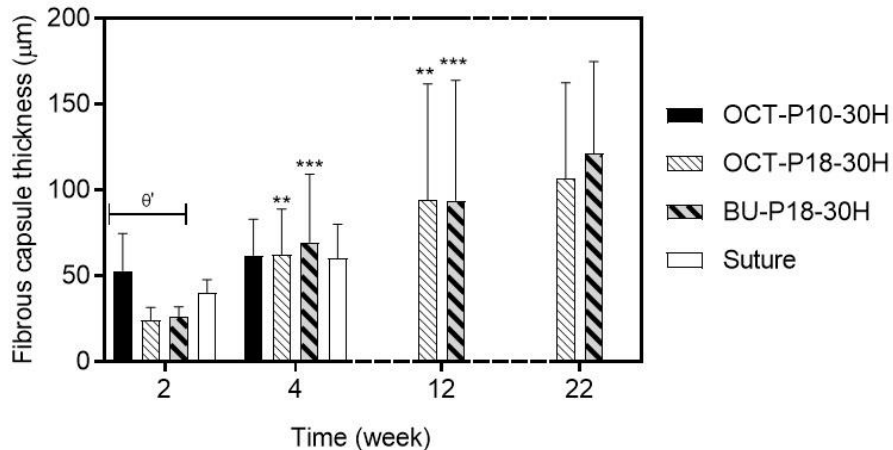


Figure 6.6. Thickness of the fibrous capsule formed around the implants after 2, 4, 12, and 22 weeks of subcutaneous injection in Wistar rats. Tissue sections were chosen randomly, and the error bars indicate the standard deviation of 5 images of each sample (N=5) on two different rats (n=2). Statistical difference with the previous time point for OCT-P18-30H (**), and BU-P18-30H (***), $p < 0.01$. Statistical difference between OCT-P10-30H with other copolymers at the same time point (θ'), $p < 0.05$. Two-way ANOVA with Bonferroni post-hoc test.

As shown in Figure 6.7, there were several layers of infiltrated cells at week 1, which are likely fibroblasts, neutrophils and macrophages,^{100,101,205,206} with no evidence of fibrous capsule formation. Cells distributed at the inflammatory zone with the range of average thickness of 175-200 μm which was significantly thicker than the inflammatory zone around the tissue-suture interface with the thickness of $70 \pm 33 \mu\text{m}$. All three copolymers had a significantly greater density of cells (range of average cell density = 80-88 cells/ $10^4 \mu\text{m}^2$) present at the tissue-copolymer interface than was present at the tissue-suture interface (average cell density = 42 ± 12 cells/ $10^4 \mu\text{m}^2$). There was no significant difference in cell density at the tissue-copolymer interface between the copolymers at week 1. By week 2, the thickness of the inflammatory zone surrounding the tissue-copolymer interface

decreased significantly to 86-100 μm , which was similar in range to that around the suture. By week 2 and 4, the number of cells at the tissue-copolymer interface and within the surrounding inflammatory zone significantly decreased compared to the previous weeks. Also, no significant difference in the cell density in the inflammatory zone was observed between copolymers themselves and between the copolymers and the suture at week 4 (range of average cell density (46-57 cells/ $10^4 \mu\text{m}^2$)). By week 12, the cell density in the inflammatory zone around the copolymers that remained, OCT-P18-30H and BU-P18-30H, decreased significantly in comparison to week 4. The cell density in the inflammatory zone around these copolymers had stabilized by week 22. No significant difference was observed in the cell density in the inflammatory zone between the copolymers themselves or between the copolymers and the suture from week 4 to week 22.

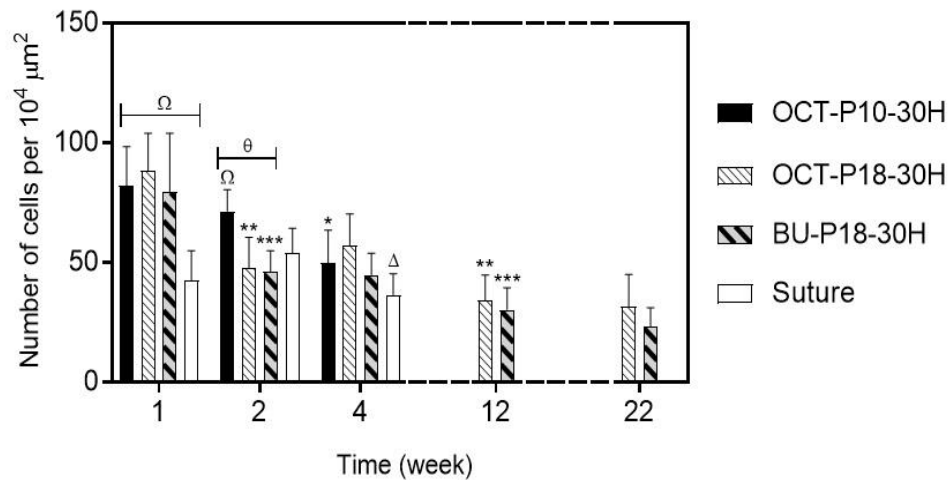


Figure 6.7. Number of cells at the copolymer-tissue interface and the surrounding fibrous capsule per $10^4 \mu\text{m}^2$ after 1 to 22 weeks of subcutaneous injection in Wistar rats. Tissue sections were chosen randomly, and the error bars indicate the standard deviation of 5 images of each sample (N=5) on two different rats (n=2). Statistical difference with the previous time point for OCT-P10-30H (*), OCT-P18-30H (**), BU-P18-30H (***) and suture (Δ), statistical difference between OCT-P10-30H with other copolymers at the same time point (θ), statistical difference between suture with copolymers at the same time point (Ω), $p < 0.01$, Two-way ANOVA with Bonferroni post-hoc test.

Macrophages are cells produced by the differentiation of monocytes within tissue. They are responsible for phagocytosing the cellular debris, invading pathogens and foreign materials in the tissue. Macrophages also secrete chemotactic signals to other cell types participating in the wound healing process. The continued presence of macrophages at the tissue-copolymer interface is a sign of chronic inflammation.^{100,101,205,206} To quantify the number of macrophages at the tissue-copolymer interface, the tissue sections were immunostained with the pan-macrophage marker CD68. CD68 is a glycoprotein that binds to low density lipoprotein, and is highly expressed on monocytes and macrophages.²⁴⁴ Representative images for CD68+ staining in tissue surrounding BU-P18-30H samples as well as the suture control are given in Figure 6.8. Representative images for all the copolymers for each time point are given in Appendix C, Figure C.3.

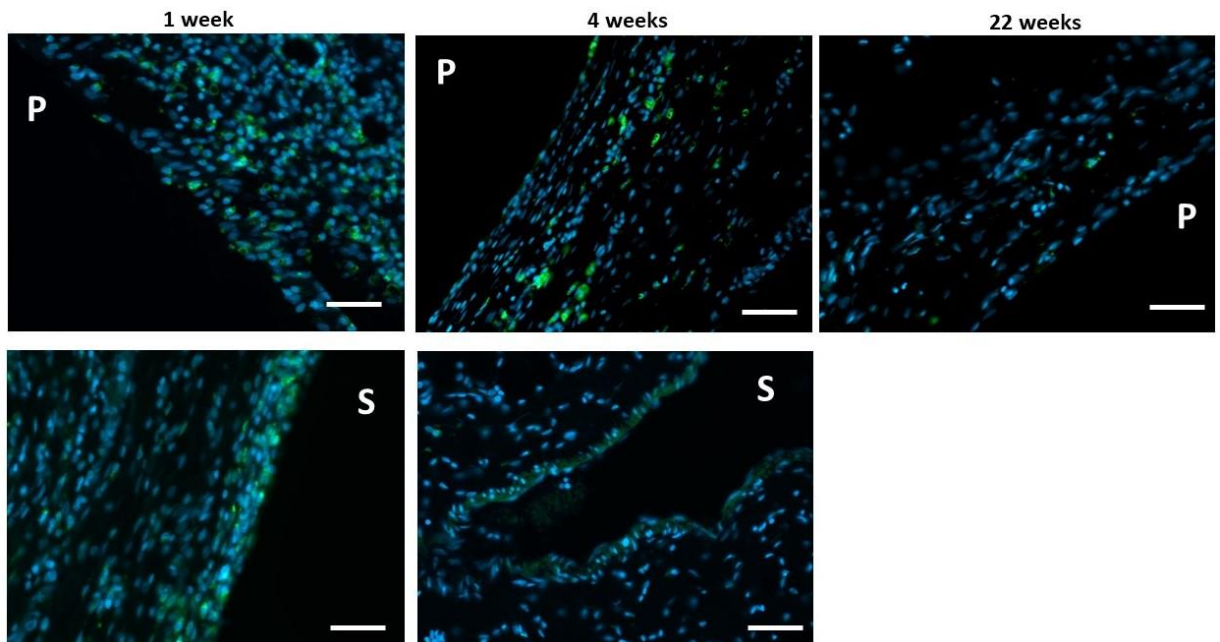


Figure 6.8. Representative photomicrographs of CD68+ cells in tissue (muscle side) surrounding BU-P18-30H and the suture control stained with the pan-macrophage marker CD68 at time points of 1, 4 and 22 weeks. Copolymer (P), suture (S), green color: CD68, blue color: DAPI. Scale bar: 50 μ m, 40X.

From the analysis of the Masson's trichrome images of the inflammatory zone thickness, the region of interest was taken as 0-300 μm from the copolymer/suture-tissue interface. The number of monocytes/macrophages (CD68^+ cells) within this selected area was counted and reported as the number of CD68^+ cells/ $10^4 \mu\text{m}^2$ (Figure 6.9). CD68^+ cells around the copolymer droplets in the tissue within the same region of interest were also included in the counting.

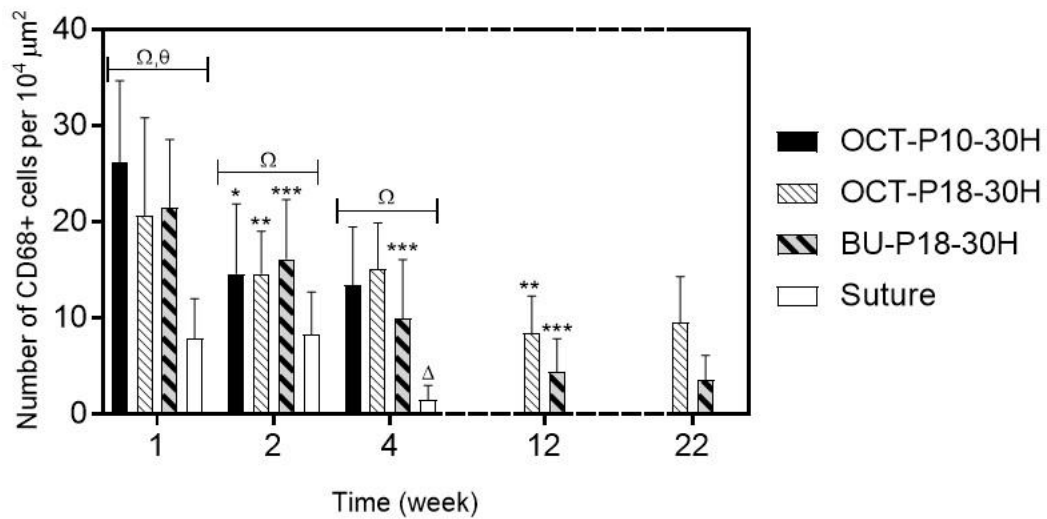


Figure 6.9. Number of CD68^+ cells at the copolymer-tissue interface and the surrounding fibrous capsule per $10^4 \mu\text{m}^2$ after 1 to 22 weeks of subcutaneous injection in Wistar rats. Tissue sections were chosen randomly, and the error bars indicate the standard deviation of 8 images of each sample ($N=8$) on two different rats ($n=2$). Statistical difference with the previous time point for OCT-P10-30H (*), OCT-P18-30H (**), BU-P18-30H (***) and suture (Δ), statistical difference between OCT-P10-30H with other copolymers at the same time point (θ), statistical difference between suture with copolymers at the same time point (Ω), $p < 0.01$, Two-way ANOVA with Bonferroni post-hoc test.

By week 1, there was a significantly greater density of CD68^+ cells present within the inflammatory zone around the implanted copolymers than within the inflammatory zone around the suture. Also, a significantly higher CD68^+ cell density was observed around the OCT-P10-30H copolymer than in the inflammatory zone around the other copolymers.

By weeks 2 and 4, the CD68⁺ cell density at the tissue-copolymer and tissue-suture interfaces as well as within the surrounding inflammatory zone significantly decreased compared to the previous weeks. Furthermore, the CD68⁺ cell density was significantly higher around the copolymers than in the inflammatory zone around the suture. By week 12, the CD68⁺ cell density decreased significantly for the remained copolymers, OCT-P18-30H and BU-P18-30H in comparison to week 4 which stabilized fairly by week 22. Not a significant difference was observed between copolymers from week 2 to week 22.

The purpose of implanting a delivery vehicle containing growth factors is to achieve a locally sustained release of a controlled dose of the growth factor while preserving its bioactivity. Therefore, as with any other foreign material implant, the delivery vehicle should be biocompatible and implanted via a minimally invasive technique while providing stable healing without significant ongoing inflammation or irritation.^{100,101,205,206} Also, it should be considered that the inflammatory response and foreign body reaction caused by the delivery vehicle may affect the movement of the growth factor from the vehicle into the tissue and thus alter the subsequent angiogenesis process.^{243,244}

All the P(TMC-co-HTMC) copolymers exhibited almost the same tissue response. A slightly higher total cell density, higher CD68⁺ cells density and a thicker fibrous capsule was observed around the lower molecular weight OCT-P10-30H in week 1 and 2. This result can be related to its faster degradation and subsequent release of a greater amount of degradation products with time in comparison to the other copolymers. The faster degradation resulted in a more intense but briefer inflammatory response to the implantation of the OCT-P10-30H as compared to the OCT-P18-30H and BU-P18-30H.

At the later time point of 12 weeks, the Monocryl suture and OCT-P10-30H completely disappeared while OCT-P18-30H and BU-P18-30H samples still remained in the tissue surrounded by fewer macrophages and a thicker fibrous capsule in comparison to week 4. The inflammatory response stabilized by week 22 around these copolymers. The tissue surrounding the P(TMC-co-HTMC) copolymers exhibited a higher total cell density at week 1 than was found for the suture; however, no significant difference was observed in the later time points. Also, a significantly higher CD68⁺ cell density was observed in the tissue surrounding all the copolymers than around the suture at different time points. A higher total cell density in week 1 and higher CD68⁺ cell density over time around the copolymers than around the suture may be due to differences in the implantation method. The suture was placed with forceps into the pocket formed between the skin and the underlying tissue. In contrast, the copolymer samples were injected into the pocket through a syringe. Therefore, while injecting the copolymer, the movement of the needle within the pocket formed in the tissue and its contact with the tissue may have caused greater trauma and subsequently a more severe acute inflammatory response. In addition to the difference in the implantation method, other parameters can influence the tissue response including the surface chemistry, mechanical strength and the degradation products of the implant. These parameters determine the composition of the adsorbed layer of proteins and modulate the macrophage activity around the implant.^{100,101,207,208} MONOCRYL suture is a solid filament composed of 25% ϵ -caprolactone and 75% glycolic acid repeating units²⁴⁵ while the copolymer is a viscous liquid and is composed of TMC and HTMC repeating units. Degradation of the suture leads to the release of glycolic acid¹¹⁵ as well as short oligomers mainly composed of ϵ -caprolactone,^{248,249} which are different than the glycerol,

CO₂, and the short oligomers mainly composed of TMC resulting from the degradation of P(TMC-co-HTMC).^{250,180} Therefore, the difference in the degradation products and the protein adsorption to the surface of the copolymer than the suture may cause different inflammatory response which should be studied further.

6.6 Conclusion

This study of the *in vivo* degradation and the tissue response of the injectable P(TMC-co-HTMC) revealed quick degradation of the HTMC units followed by gradual elimination of the short chains produced via HTMC cleavage. Using a lower molecular weight copolymer, *e.g.* OCT-P10-30H, accelerated the degradation rate significantly due to the fewer backbone cleavage events required to produce water-soluble short chains. P(TMC-co-HTMC)s at the molecular range of 1000-2000 Da initiated with either 1-octanol or 1-butanol exhibited the same inflammatory response, which subsided in the later weeks of the study. The observed tissue response was comparable with the tissue response of a commercial and clinically used MONOCRYL suture. However, a longer term *in vivo* study should be completed to investigate the actual degradation time of the higher molecular weight copolymers (OCT-P18-30H and BU-P18-30H). These findings suggest that these copolymer compositions are potential candidates to be used as an injectable delivery formulation depending on the desirable degradation time.

Chapter 7

Protein release from low molecular weight poly(trimethylene carbonate-co-5-hydroxy trimethylene carbonate) (P(TMC-co-HTMC)): the effect of copolymer composition, degradation rate and the protein particle composition

7.1 Abstract

In this chapter, the potential of poly(trimethylene carbonate-co-5-hydroxy trimethylene carbonate) (P(TMC-co-HTMC)) to act as a delivery vehicle for proteins was studied *in vitro*. In this regard, copolymers initiated with 1-octanol or 1-butanol at an HTMC/TMC molar ratio of 30/70 and molecular weight range of 1000-2000 Da were prepared, and the influence of copolymer composition, degradation rate and the protein particle composition on the *in vitro* release of lysozyme, bovine serum albumin (BSA) and VEGF was studied. Finally, the bioactivity of the released vascular endothelial growth factor (VEGF) was assessed using a telomerase-immortalized human aortic endothelial cells (TeloHAEC) proliferation assay. Protein particles were prepared by lyophilization of the different proteins with trehalose in buffer solution individually. The resulting lyophilized powder was sieved and incorporated into the copolymer by simple mixing. A sustained prolonged release of lysozyme of 9-17 weeks was obtained, depending on the copolymer composition and loading capacity, but BSA exhibited a rapid and almost complete release within 4 days. VEGF was also released quickly, with 70-90 % released within 9 days, depending on the salt concentration incorporated into the lyophilized protein powder. However, decreasing the salt content provided longer release time up to 9 weeks. The released VEGF showed

greater than 80% bioactivity throughout the release period. It was determined that the rate of protein release was controlled by the solubility of the lyophilized protein in the aqueous environment within the copolymer, the concentration of the salt included in the lyophilized powder, and the flexibility of the copolymer chains to form superhydrated regions upon water diffusion into the polymer bulk and subsequently dissolution of the protein particles. This study introduced P(TMC-co-HTMC) as a potential vehicle to deliver acid sensitive proteins without loss of their bioactivity for short or long-term delivery approaches depending on the protein physical properties.

7.2 Introduction

Peripheral arterial disease (PAD) is a chronic condition caused by the formation and hardening of fatty plaque (atherosclerosis) within arteries and arterioles, resulting in narrowing or blocking of the vessels carrying blood to the limbs.¹⁻³ This condition affects 8.5 million Americans aged over 40 years, and the number of patients is expected to dramatically increase as the population ages and the number of individuals suffering from obesity, diabetes, smoking and hypertension increases.⁴⁻⁷ Current treatments including pharmacological therapy and controlling the risk factors,² percutaneous transluminal angioplasty (PTA)^{10,11} and bypass surgery¹² have decreased the mortality rates; however, 10-40 % of patients with PAD still require amputation.^{2,3} Amputation itself causes 5-10% mortality for below-the-knee amputations and 15-20% for above-the-knee amputations after bypass surgery. Additionally, 30% of survivors will die within 2 years, and the other 30% will require a second amputation. Finally, full restoration of mobility with no amputation is achieved in less than 50% of patients.^{2,3}

The discovery of angiogenic growth factors represented a potential treatment approach, named therapeutic angiogenesis. In this approach new capillaries are induced to grow from the pre-existing blood vessels around the arterial blockage to carry blood to the deprived tissue, bypassing the site of occlusion.^{19,20} In the natural angiogenesis process, multiple growth factors are involved in forming new and stable blood vessels.^{7,81,251} The body is intrinsically able to produce endogenous angiogenic growth factors and subsequently induce new blood vessels at the site of ischemia.²⁸ However, this natural response occurs very slowly, and it cannot compensate for the lost blood flow completely.¹³

One approach to achieve therapeutic angiogenesis is through the sustained release of exogenous angiogenic growth factors directly to the ischemic site via a minimally invasive, biocompatible, and biodegradable delivery vehicle. Ideally, the delivery vehicle provides a sustained release of individual or combinations of growth factors at an effective local dose and duration with a minimal initial burst effect while the bioactivity of the growth factor is preserved.¹⁴⁻¹⁶ Of the growth factors involved in angiogenesis, those of the VEGF family are of high importance. VEGF-A is the most common and most biologically active isoform of the VEGF family that is secreted into the extracellular environment.⁷ VEGF-A will be referred to as VEGF in this chapter. VEGF stimulates the proliferation and migration of endothelial cells (ECs), which is an essential rate limiting step in physiological angiogenesis.^{252,72}

Many different kinds of injectable delivery vehicles have been utilized to achieve effective angiogenic growth factor delivery, such as microspheres,^{18,108,109,126} hydrogels,^{74,75} and viscous liquid polymers.^{63,149,150,160,164} A viscous liquid injectable delivery vehicle has

some advantages over the other injectable formulations for this application such as simple loading of the growth factors into the vehicle by mixing,^{63,149,150} a less complicated manufacturing process with the absence of water and organic solvents,^{102,105} and a longer release duration than achieved with hydrogels.⁷⁴

In this chapter, the potential of a viscous liquid formulation based on low molecular weight poly(trimethylene carbonate-co-5-hydroxy trimethylene carbonate) (P(TMC-co-HTMC)) is examined. The influence of P(TMC-co-HTMC) molecular weight and viscosity, degradation rate and the protein particle composition on the *in vitro* release, and the bioactivity of the released protein will be determined. To achieve this objective, P(TMC-co-HTMC) was prepared through the co-polymerization of 5-benzyloxy trimethylene carbonate (BTMC) with trimethylene carbonate (TMC) via ring-opening solution polymerization using hydrogen chloride solution in diethyl ether (HCl·Et₂O) as a catalyst. Following copolymerization, the BTMC repeating units were debenzylated to yield P(TMC-co-HTMC) copolymer with hydroxyl pendant groups along the backbone.^{177,230} Based on the results achieved in chapters 5 and 6, an HTMC content of 30 mol% and a molecular weight range of 1000-2000 Da were chosen. These copolymers exhibited a moderate *in vitro* and *in vivo* degradation rate that was long enough to provide the necessary release period of 3-4 weeks for the sustained local release of the bioactive growth factors while not lasting so long as to cause prolonged inflammation at the injection site.¹³ To determine the factors influencing protein release, the model protein drugs lysozyme and bovine serum albumin (BSA) were studied. Finally, a formulation composition of VEGF, BSA and trehalose was chosen and the VEGF release rate and bioactivity of the released VEGF were assessed.

7.3 Materials

1,3-trimethylene carbonate (TMC) was obtained from Leapchem, Hangzhou, China. 5-benzyloxy trimethylene carbonate (BTMC) was purchased from Obiter research LLC, USA. 1 M hydrogen chloride solution in diethyl ether (HCl·Et₂O), palladium on carbon (Pd/C), palladium hydroxide on carbon (Pd(OH)₂/C), 1-octanol, 1-butanol, celite, Tween 20, sodium azide, bovine serum albumin (≥ 98% purity) (BSA), lysozyme from egg white (L7651, ≥ 98% purity), and deuterated dimethyl sulfoxide (DMSO-d₆) were purchased from Sigma-Aldrich Ltd, Canada. Phosphate buffered saline (PBS) powder, anhydrous potassium carbonate (K₂CO₃), D-(+)-trehalose dihydrate (≥ 99% purity), potassium phosphate monobasic (KH₂PO₄), sodium phosphate dibasic heptahydrate (Na₂HPO₄·7H₂O), HEPES, tetrahydrofuran (THF), methanol (MeOH) and dichloromethane (DCM) were purchased from Thermo Fisher Scientific, Canada. Hydrogen gas (H₂) (99.99% purity) was purchased from Linde Ltd, Canada. A bicinichoninic acid (BCA) protein assay kit was purchased from Thermo Scientific, Canada. Recombinant human vascular endothelial growth factor (VEGF-A, 100-20) and a human VEGF-A standard ABTS ELISA development kit (900-K10) were purchased from Peprotech Inc, Canada. Telomerase-immortalized human aortic endothelial cells (TeloHAEC, ATCC[®] CRL-4502[™]) were purchased from ATCC, USA. Basal endothelial cell growth medium (EGM-2) and supplements were purchased from Lonza, Switzerland. The cell proliferation reagent WST-1 (05 015 944 001) was purchased from Roche, USA. All other materials were used as received. Water used was of type 1 purity, obtained from a Millipore Milli-Q Plus ultrapure water filtration system. THF and MeOH were dried over activated 3 Å molecular sieves.

7.4 Method

7.4.1 Synthesis and characterization of P(TMC-co-HTMC)

P(TMC-co-HTMC) initiated with 1-octanol or 1-butanol at an HTMC/TMC molar ratio of 30/70 (30 mol% HTMC) and molecular weight range of 1000-2000 Da were prepared and characterized as described in sections 5.4.1.2, 5.4.2 and 5.4.3.

7.4.2 Preparation of solid protein particles

7.4.2.1 Lysozyme and BSA particles

A series of formulations consisting of the model protein drugs lysozyme and BSA were prepared to determine the influence of different factors on protein release. Lysozyme particles were prepared by dissolving lysozyme and trehalose in pH 7.4 PBS at a lysozyme: trehalose weight ratio of 98:2. Trehalose was added to maintain protein stability. Previous studies have shown that addition of trehalose even at 2 wt% of the total particle weight had a marked impact on the protein stability during both lyophilization and following release.²⁵³ The solution was prepared at 5 wt% at room temperature, then frozen in liquid nitrogen, and lyophilized on a Modulyo D lyophilizer (Thermosavant, USA) at -50 °C and a vacuum of 100 mbar. The dry powder was then sieved through a #325 Tyler sieve to yield < 45 µm diameter particles. The resulting protein particles composed of lysozyme and trehalose will be referred to as L98/T2. BSA/trehalose particles were also prepared using the same method in PBS or phosphate buffer without saline (PB). The resulting protein particles composed of BSA and trehalose will be referred to as BSA98/T2 prepared in PBS

and BSA98/T2-PB prepared in PB without saline. Table 7.1 shows the final composition of the protein particles.

Table 7.1. Composition of protein particles prepared in PBS or PB buffer

Protein particle	Buffer	Lysozyme (wt%)	BSA (wt %)	Trehalose (wt%)	Salt (wt %)
L98/T2	PBS	82.5	...	1.684	15.84
BSA98/T2	PBS	...	82.5	1.684	15.84
BSA98/T2-PB	PB	...	96.2	1.974	1.83

7.4.2.2 VEGF particles

VEGF containing particles were prepared by dissolving trehalose and BSA in pH 7.4 PBS or phosphate buffer without saline (PB) at a BSA: trehalose weight ratio of 97.8:2. This BSA/trehalose solution was prepared at 5 wt% at room temperature, and then filtered through a 0.2 µm sterile filter in a biological safety cabinet (BSC). A VEGF solution was prepared at 1 mg/mL using sterile autoclaved Milli-Q water, and then added to the sterile BSA/trehalose solution. This solution was frozen in liquid nitrogen and lyophilized in a sterile jar on a Modulyo D lyophilizer (Thermosavant, USA) at -50 °C and 100 mbar vacuum. The resulting powder was sieved through a sterile #325 Tyler sieve in a biological safety cabinet to yield < 45 µm particles. The final dry weight ratio of VEGF/BSA/T was 0.2/97.8/2. The resulting VEGF particles will be referred as VEGF/BSA/T prepared in PBS, and VEGF/BSA/T-PB prepared in PB without saline. Table 7.2 shows the final composition of the VEGF particles.

Table 7.2. Composition of VEGF particles prepared in PBS or PB buffer

VEGF particle	Buffer	BSA (wt %)	Trehalose (wt%)	VEGF (wt%)	Salt (wt %)
VEGF/BSA/T	PBS	82.3	1.684	0.1683	15.84
VEGF/BSA/T-PB	PB	96	1.974	0.196	1.83

7.4.3 *In vitro* release study

The lyophilized particles were loaded into the copolymer pre-heated to 37 °C to obtain 0.5, 1 and 2 wt% particle loadings. The resulting copolymer-protein particle suspension was injected into the bottom of a 1 mL glass vial to fill the bottom of the vial to a height of approximately 2-3 mm using a 1 mL syringe with an 18 ½ gauge needle. The exact weight of mixture in each vial was recorded. The glass vial was then filled with pH 7.4 PBS containing 0.02% (v/v) Tween 20 and 0.02% (w/v) sodium azide at a ratio of 100 mg copolymer in 1 mL of PBS. Tween 20 was included to prevent nonspecific adsorption of protein to the glass vial and sodium azide was included as an antimicrobial.¹⁷¹ The vials were capped and agitated in a thermomixer at 37 °C with horizontal shaking at 300 rpm. The PBS was replaced at each time point with fresh buffer, and the removed buffer was frozen in liquid nitrogen, and stored at -80 °C for subsequent analysis. As a control, copolymer only samples were used. For the VEGF release study, copolymer containing only BSA98/T2 was used as the control. To measure the bioactivity of the released VEGF the release medium was 1% BSA and 1% antibiotics in pH 7.4 PBS at 37 °C.⁶³ All release experiments were performed in triplicate, and protein assays were run in triplicate for each sample at each time point. The lysozyme concentration and BSA concentration in the

release medium were measured using the BCA protein assay kit according to the supplier's protocol. The VEGF concentration in the release medium was measured using a human VEGF-A standard ABTS ELISA development kit according to the supplier's protocols. The color development was measured using an EnSpire 2300 microplate reader (PerkinElmer).

7.4.4 Cell culture

TeloHAECs were cultured in EGM-2 supplemented with 0.04% (v/v) hydrocortisone, 0.1% (v/v) gentamicin amphotericin B (GA-1000), 2% (v/v) fetal bovine serum (FBS), 0.1% (v/v) ascorbic acid, 0.1% (v/v) heparin, 0.4% (v/v) human fibroblast growth factor-B, 0.1% (v/v) VEGF, 0.1% (v/v) insulin growth factor-1, and 0.1% (v/v) human epidermal growth factor under standard conditions at 37 °C in incubator until they reached approximately 80% confluence.

7.4.5 Bioactivity assay

The bioactivity of the released VEGF was assessed by determination of its ability to stimulate the proliferation of TeloHAECs as compared to the proliferation obtained with the same concentration of as-received VEGF. After passage 10-30, TeloHAECs were trypsinized and rinsed twice using Hanks' balanced salt solution (HBSS) buffer. Cells were re-suspended in growth factor free EGM-2 containing 0.04% (v/v) hydrocortisone, 0.1% (v/v) GA-1000, 0.5% (v/v) FBS, 0.1% (v/v) ascorbic acid, 0.1% (v/v) heparin at a concentration of 30,000 cells/mL. 100 µL of this cell suspension was added to each well

of a 96-well plate, and the plate was incubated at 37 °C for 1 h. The released medium from each sampled vial at the selected time point was diluted to a VEGF concentration of 5 ng/mL using growth factor free basal media, and 100 µL of the resulted dilute release medium was added to a given well. The final concentration of the cells and VEGF in each well were 3000 cells/well and 2.5 ng/mL, respectively. The bioactivity assay was run in triplicate for each time point.

As a control of the bioactivity assay, the standard calibration curve of the as-received VEGF was prepared. For this purpose, VEGF standard solutions with concentrations of 0 to 40 ng/mL were prepared in the same growth factor free basal media using as-received VEGF. Then, 100 µL of the standard solution at different concentrations was added to the 100 µL of the cell suspension in each well, in triplicate. The bioactivity assay was run in triplicate for each concentration. The standard solutions were aliquoted, frozen in liquid nitrogen and stored at -80 °C until needed.

The bioactivity assay was run by measuring the metabolic activity of the cells after 48 h incubation at 37 °C using a WST-1 assay kit. For this purpose, 20 µL of WST-1 reagent was added to each well and incubated at 37 °C for 2 h. An absorbance measurement at 450/690 nm was taken using a Molecular Devices SpectraMax 190 with Softmax Pro 5 as the software. The bioactivity was calculated as a fraction of the activity expressed by the cells incubated with the release medium divided by the activity that would be expressed by cells exposed to an equivalent concentration of as-received VEGF, as determined from the standards.

7.4.6 Statistics

All data are reported as the average \pm the standard deviation about the average. Statistical differences in the release kinetics were determined using a two-way ANOVA with a Bonferroni post-hoc test. Differences were considered significant for p values less than 0.01.

7.5 Results and Discussion

7.5.1 Release of model proteins

To determine the factors influencing the protein release, the model proteins lysozyme and BSA were studied as proteins with different physical properties including isoelectric point, water solubility and molecular weight. Other than the protein physical properties, the effect of copolymer physical properties (molecular weight, T_g and viscosity) and copolymer degradation rate as well as protein loading capacity were studied. Due to the low viscosity of the copolymers, the protein particles were easily mixed into the copolymer at 37 °C using a spatula. Table 7.3 shows the physical-chemical properties of the copolymers used in this study. The resulting copolymers showed approximately the same physical-chemical properties as the previous series of the copolymers used in Chapters 5 and 6, which supports the reproducibility of the copolymerization and purification processes.

Table 7.3. Physical-chemical properties of P(TMC-co-HTMC)

Copolymer	Initiator	M _n (Da)	T _g (°C)	HTMC (%)	Viscosity (Pa·s, 37 °C)
OCT-P10-30H	1-octanol	1180	-35	30	15 ± 1.8
OCT-P18-30H	1-octanol	1740	-26	28	92 ± 2.3
BU-P18-30H	1-butanol	1730	-25	28.5	98 ± 4.7

To determine the effect of these parameters, the lysozyme and BSA were co-lyophilized individually with trehalose as a cryoprotectant and lyoprotectant in pH 7.4 PBS.^{39,40} The resulting protein particles were ground and sieved to less than 45 μm, and then loaded at different loading capacities into 1000-2000 Da P(TMC-co-HTMC)s with an HTMC content of 30 mol% initiated with either 1-octanol or 1-butanol. To simplify the examination of the influence of various formulation parameters, the initial release studies were performed by injecting approximately 100 mg of the copolymer formulation incorporating the protein particles into a 1 mL glass vial with a 0.4 cm internal diameter. The copolymer formed a cylinder with release available from only one surface. Release was thus unidirectional from a surface area of approximately 0.12 cm².

To gain an understanding of those formulation parameters influential to protein release, initial experiments were conducted using lysozyme and BSA as model protein drugs. Lysozyme has a molecular weight of 14 kDa,²⁵⁴ an isoelectric point of 11,²⁵⁵ and a water solubility of 18 mg/mL in pH 7 1.5 %w/v NaCl solution at 25 °C.²⁵⁶ In contrast BSA has a molecular weight of 66.5 kDa²⁵⁷, an isoelectric point of 4.7–4.9^{257–259} and a water solubility of 448 mg/mL at 25 °C, in pH 7.4, 0.9 %w/v NaCl solution.²⁵⁹ Formulation parameters examined in the model proteins included the copolymer physical properties and

degradation rate, the total mass loading of protein particles in the copolymers and the effect of protein properties included the water solubility and net charge.

Figure 7.1 shows the release of lysozyme from P(TMC-co-HTMC)s containing 1 wt% of L98/T2 particles. An initial burst release of 1.3 % of the lysozyme was observed after 1 hour of incubation due to dissolution of surface resident particles. The initial burst release continued to the range of the average release of 4-8 % in the first 24 h. No significant difference in *in vitro* release between the copolymers was observed over the first 4 days. Following the burst phase, a two-phase release profile was observed for all the copolymers, with an initially faster release period followed by a longer and slower release period till lysozyme was completely released. The duration and fraction of lysozyme released during the first phase was copolymer dependent. OCT-P10-30H, having the lower molecular weight of 1180 Da, released approximately 75 % of the incorporated lysozyme over a period of 1.5 weeks. The release rate during the first phase was significantly slower from the higher molecular weight OCT-P18-30H and BU-P18-30H, reaching respectively 46 % and 66 % release by approximately 4 weeks. The lysozyme release during the second phase was dependent on the fraction of lysozyme remaining in the copolymer following the first release phase, with the release from OCT-P10-30H being slowest and release from the OCT-P18-30H being highest. Lysozyme was completely released from these copolymers by 17 weeks.

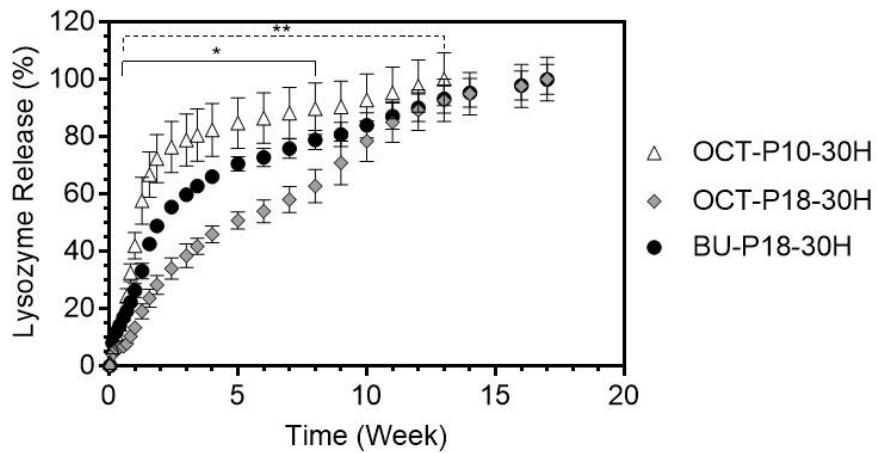


Figure 7.1. Influence of P(TMC-co-HTMC) initiator and molecular weight on lysozyme release. The particle loading for each case was 1 wt%. Statistical difference of OCT-P18-30H with BU-P18-30H at each time point (*), statistical difference of OCT-P10-30H with OCT-P18-30H and BU-P18-30H at each time point (**), $p < 0.01$, $n=3$.

Figure 7.2 shows the effect of the loading capacity, 1 wt% vs 2 wt%, on the release of lysozyme from BU-P18-30H. Using a 2 wt% loading, the release started with a minimal burst release of approximately 1 % within the first hour of the study continued to 11 % in the first 24 h. In comparison to the lower loading capacity of 1 wt%, no significant difference was observed in the first 2 days. Finally, a complete release was achieved at week 8. In contrast to the 1 wt% loading formulation, a continuous sustained release was observed with the 2 wt% loading.

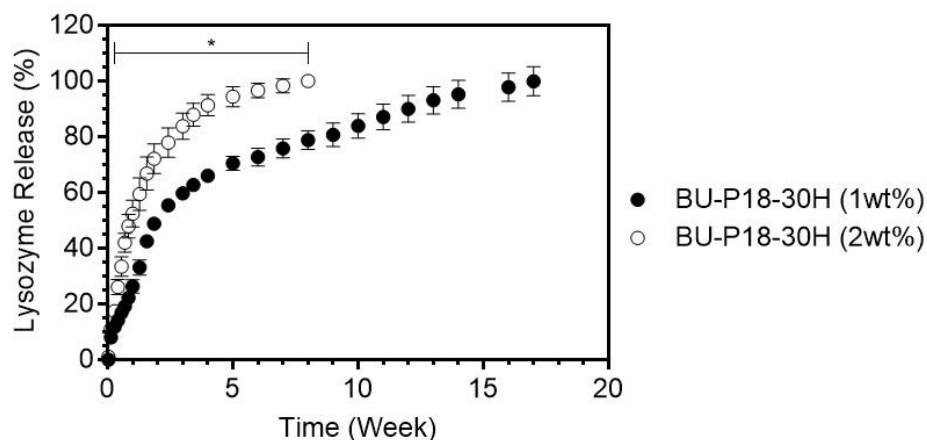


Figure 7.2. Influence of particle loading on lysozyme release incorporated in L98/T2 particles from BU-P18-30H. Statistical difference of 1 wt% loading with 2 wt% loading at each time point (*), $p < 0.01$.

Figure 7.3 shows the release of BSA from BU-P18-30H containing different amounts of BSA98/T2 particles of varying total salt content. BU-P18-30H was chosen based on the release profile of lysozyme as BU-P18-30H demonstrated a sustained release of the lysozyme for 70-100 % release within 5 weeks depending on the loading capacity. An initial low burst release of 0.6-2 % of BSA was observed during the first hour due to dissolution of surface resident particles, followed by a rapid release of approximately 30-40 % within 24 h. No significant difference was observed in the BSA release by increasing the particle loading (Figure 7.3.A) or the salt content (Figure 7.3.B). All formulations exhibited a continuous sustained release, reaching 80 % release within 3 days with complete release within 7 days.

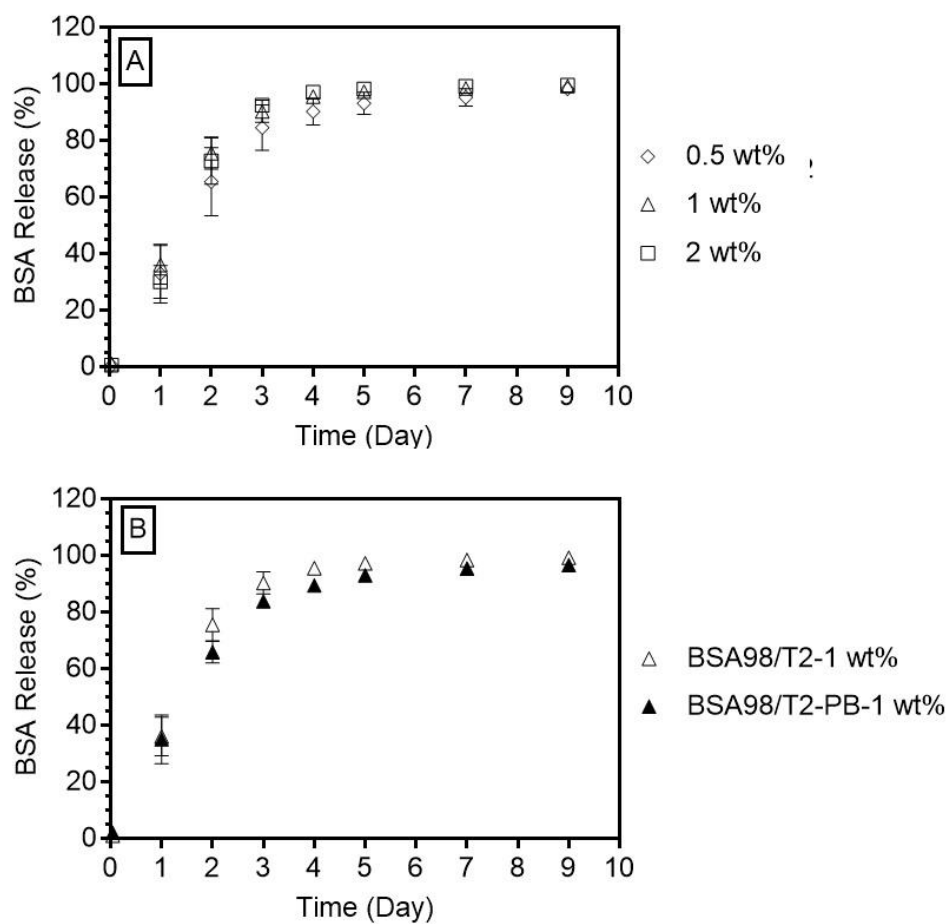


Figure 7.3. *In vitro* release profiles of BSA incorporated in BSA98/T2 particles from BU-P18-30H copolymer. A) influence of particle loading on release of BSA incorporated into the particles prepared in PBS buffer (BSA98/T2 particles), and B) influence of salt content on BSA release incorporated into the BSA98/T2 particles prepared in PBS (BSA98/T2) or PB buffer (BSA98/T2-PB), n = 3.

Comparing the release of BSA from BU-P18-30H to the release of lysozyme under the same particle formulation and particle loading conditions revealed that lysozyme released significantly more slowly than BSA (Figure 7.4). Over the first three days BSA and lysozyme had release rates of $365 \pm 50 \mu\text{g/day}$ and $46 \pm 26 \mu\text{g/day}$, respectively.

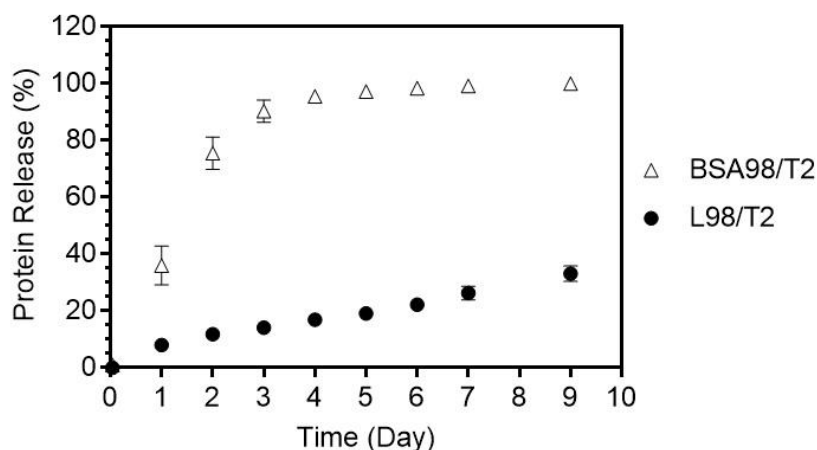


Figure 7.4. *In vitro* release profiles of BSA and lysozyme incorporated in protein particles containing the same concentration of salt and protein from BU-P18-30H copolymer showing the influence of protein physical properties. The particle loading for each case was 1 wt%, n = 3.

Using this type of formulation, different mechanisms may affect the release rate, including the degradation rate of the copolymer, the hydration extent of the copolymer, and protein transport either by diffusion or convection within the hydrated copolymer. According to previous studies on the release of protein particles from liquid viscous hydrolysable polymers, the release process can be explained as follows.¹⁷¹ Upon contact with the release medium, particles resident at the surface, and those particles in contact with them, dissolve and diffuse into the release media, generating the burst effect. The burst effect is low when low particle loadings are used.²⁶⁰ Water from the surrounding medium also dissolves into, and diffuses through, the copolymer matrix until it encounters a copolymer-enclosed drug particle. At the particle/copolymer interface, the water dissolves a portion of the particle to form a saturated solution. An activity gradient is generated between the saturated solution and the surrounding aqueous medium. The activity gradient draws water into the copolymer to generate an osmotic pressure equal to the osmotic pressure of the saturated solution at the particle/copolymer interface. As a result of the low molecular weight of the

copolymer, water is forced into the copolymer region surrounding the capsules, generating superhydrated regions, wherein the water concentration is higher than that obtained from fully hydrating the copolymer in the absence of the encapsulated particle^{261,262} The water forced into the surrounding copolymer forms what have been termed “zones of excess hydration”.⁴³ These zones eventually overlap to form a continuous pathway extending to the surface. The dissolved solutes are transported through this superhydrated region to the surface. At the same time, the copolymer is degrading. The degradation of the copolymer increases the rate at which water can penetrate the copolymer, increasing the water content of the superhydrated regions as well as reduces the distance over which a dissolved solute must transport in order to be released.

As seen in Figure 7.1, the release of lysozyme increased as the molecular weight of the copolymer decreased. According to the physical properties of OCT-P10-30H ($T_g = -35$ °C, viscosity = 15 ± 1.8 Pa·s) as well as its *in vitro* degradation study in Chapter 5, the increase in release rate of lysozyme from OCT-P10-30H is attributed to the higher flexibility of the copolymer chains to form superhydrated regions as well as an increase in the contribution of copolymer degradation, lower M_n of the remained fraction of OCT-P10-30H in water over time in comparison to other copolymers, on lysozyme release. The super-saturation of the copolymer phase by water not only depends on the osmotic activity of the entrapped particles but it is also determined by the relaxation ability of the copolymer chains to resist the swelling pressure, as reflected by copolymer T_g . At lower molecular weight, copolymer chains are more flexible, and copolymer is less viscous. Therefore, it takes a shorter time for more flexible chains to adapt themselves to the swelling pressure, thus facilitating the formation of the superhydrated regions.^{63,171,261} These effects cause the zone of excess

hydration to form faster as the copolymer molecular weight decreases. The use of a more hydrophilic initiator such as 1-butanol vs 1-octanol caused a significant increase in the release rate of lysozyme from the copolymers with same molecular weight of approximately 1700 Da, which is likely due to the an increase in water content of the copolymer during lysozyme release.^{15,63,171} The initial faster release period observed for all copolymers is likely a diffusion-controlled release phase, while the second slower release period is likely a copolymer degradation-controlled release phase.

The difference in release between lysozyme and BSA was considered to be due to the difference in protein solubility in the aqueous medium within the copolymer matrix. Once water contacts the protein/trehalose/buffer salt particles, it dissolves the incorporated salt and trehalose generating a concentrated salt and trehalose region around the protein particles in the superhydrated regions. BSA has a significantly higher solubility in equivalent NaCl solutions, and so dissolves faster and to a higher concentration in the superhydrated regions and subsequently releases faster than lysozyme.

7.5.2 *In vitro* VEGF release

Van Belle and coworkers showed that 25-50 ng/mL of VEGF induced maximum endothelial cell proliferation and migration over a 48 hour period.²⁶³ Further, previous studies have revealed that 3-4 weeks of sustained and local delivery of bioactive growth factors into the hypoxic tissue is necessary to form a stable vascular network and provide effective blood flow.^{13,14,35} Using these results as a basis, our target for VEGF release was approximately 25-50 ng/day released for a period of 3-4 weeks as a first approximation of

a therapeutically relevant dose. Based on previous studies, to achieve this dosing requires diluting VEGF within the solid particles such that the VEGF is a very small fraction of the total solids present.⁶³ According to these previous results, a particles composition of 97.8 wt% BSA, 2 wt% trehalose and 0.2 wt% VEGF was chosen. To determine the effect of salt content on VEGF release from VEGF/BSA/T particles, the particles were prepared at the mentioned ratio using two different buffer solutions: PBS (VEGF/BSA/T particles) or PB without saline (VEGF/BSA/T-PB particles). Finally, VEGF particles were distributed into BU-P18-30H at 1 and 2 wt% loading and the release was studied using 7.4 pH PBS as the release medium at 37 °C.

The VEGF was released from the VEGF/BSA/T particles contained NaCl with an initial low burst release of ~ 0.8-1.1 % after 1 h due to the dissolution of surface resident particles. However, VEGF was subsequently released quickly reaching between 46-58 % within 24 h depending on the particle loading, and 90 % release within 9 days (Figure 7.5). The VEGF release rate decreased in the later days of the study reaching complete release in 7 weeks. As was seen with BSA release, there was little effect of the initial particle loading on the VEGF release kinetics. Doubling the loading resulted in approximately 10 % higher release at day 1; however, there were no significant differences in the later days.

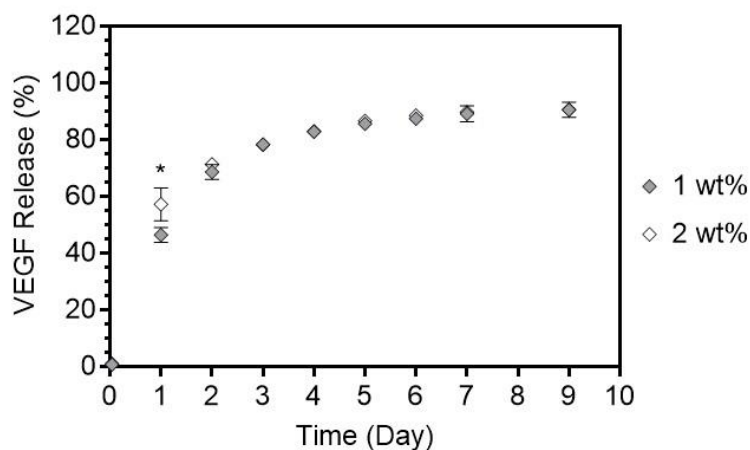


Figure 7.5. Release of VEGF from BU-P18-30. The VEGF was incorporated into VEGF/BSA/T particles prepared in PBS. Statistical difference of 1 wt% loading with 2 wt% loading at each time point (*), $p < 0.01$, $n = 3$.

Comparing the VEGF release with the BSA and lysozyme release from BU-P18-30H (Figure 7.6) revealed that VEGF was released at a similar rate as BSA but significantly faster than lysozyme. The presence of BSA as the main component in the VEGF/BSA/T protein particles (containing 97.8 wt% BSA) likely determined the release behavior of VEGF. A possible explanation for the similarity in the release profile of BSA and VEGF is that the VEGF becomes electrostatically complexed to BSA and the two molecules diffuse together to be released. BSA has an isoelectric point of 4.7–4.9^{257–259} while VEGF has an isoelectric point of 8.5–8.9.⁸² Therefore at the pH conditions within the environment of the dissolving protein particles, BSA and VEGF would carry an opposite net charge. Support for this explanation comes from recent studies describing heteroprotein complexation between BSA and lysozyme.^{264,265}

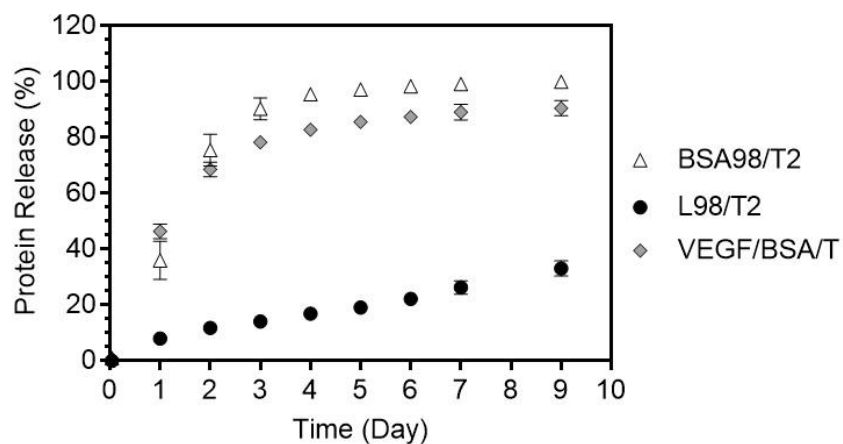


Figure 7.6. Influence of the physical properties of the protein on the release rate from BU-P18-30H. The particle loading for each case was 1 wt%, n = 3.

Comparing the VEGF release from the VEGF/BSA/T-PB particles prepared in PB buffer to VEGF/BSA/T particles prepared in PBS at 1 wt% loading showed a significantly lower release rate of approximately 13 wt% difference in day 1 increasing to approximately 15-20 wt% difference up to day 17. VEGF was released for a longer time from VEGF/BSA/T-PB reaching 90 wt% release after 5 weeks and the complete release after 9 weeks (Figure 7.7).

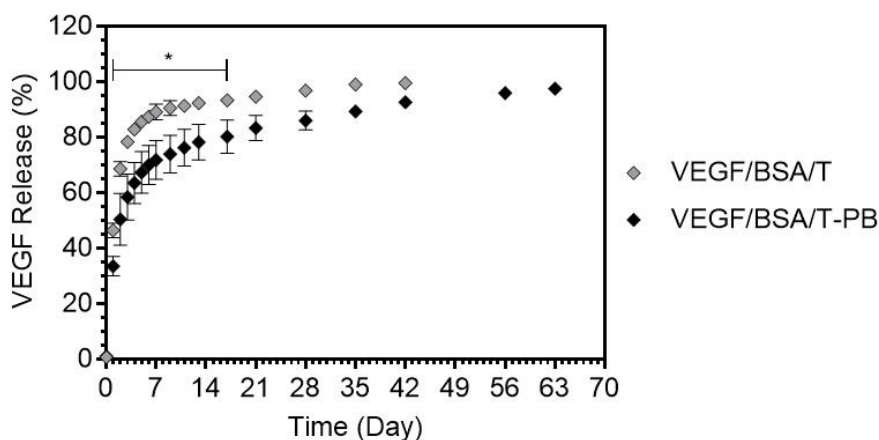


Figure 7.7. Influence of the particle salt content on VEGF release rate from BU-P18-30H. The particle loading for each case was 1 wt%. Statistical difference of Formulation A with Formulation B at each time point (*), $p < 0.01$, $n = 3$.

The previous studies on osmotically driven release mechanism showed that, as the concentration of the osmotically active excipients such as trehalose or salt in the protein particles increases, the protein release rate increases.^{149,171} Release of VEGF from the VEGF/BSA/T-PB particles prepared in PB, which has approximately 9 times lower salt concentration than PBS, revealed that the rate of VEGF release was strongly influenced by the salt content in the incorporated particles, suggesting that release was also affected by the osmotic activity of the solution formed within the copolymer by the dissolved particles. The lower osmotic pressure produced by the VEGF/BSA/T-PB particles reduced the extent of water penetration into the copolymer which subsequently retarded the dissolution and release of the VEGF, leading to a slower release rate.

7.5.3 Bioactivity assay

The bioactivity of VEGF in the release media was assessed using an *in vitro* assay based on the proliferation of TeloHAECs. The bioactivity of the released VEGF from Formulations A and B was calculated relative to the proliferation of TeloHAECs grown in the presence of the same concentration of as-received VEGF. Greater than 80% bioactivity was obtained for the released VEGF throughout the release study (Figure 7.8). The bioactivity of the VEGF after lyophilization was also determined, with bioactivities of $94\% \pm 0.6$ and $117\% \pm 3.5$ for VEGF/BSA/T and VEGF/BSA/T-PB particles, respectively.

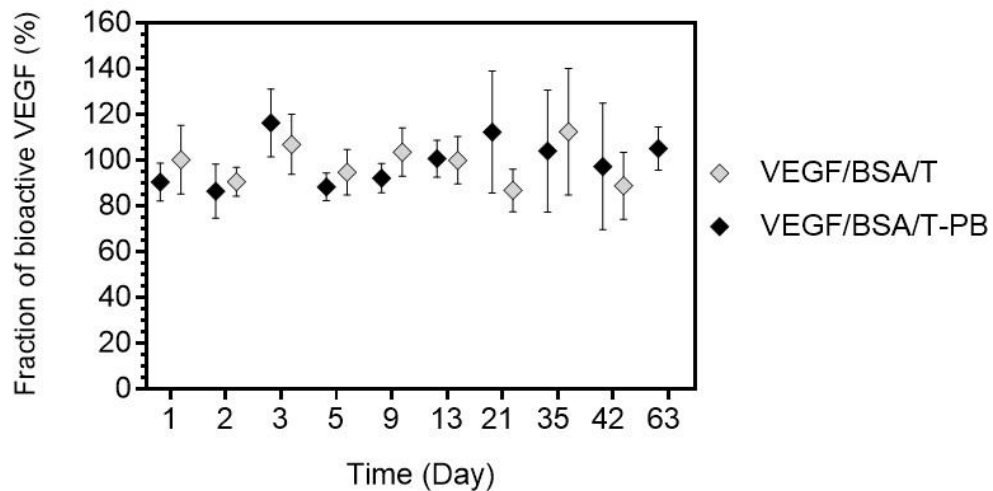


Figure 7.8. Fraction of bioactive VEGF in the release media relative to the same concentration of as-received growth factors. Each point represents the average of the released protein from three samples with 3 replicates per sample.

Protecting growth factor bioactivity is one of the most important parameters that should be considered when designing a growth factor delivery device. According to the preparation steps of the protein particles in this study, several sources of the stress may have affected the bioactivity of the VEGF, including shear strain caused by agitation, filtration, sieving

and grounding, as well as temperature and pH fluctuation during freezing, lyophilization, thawing, and protein release.^{79,86-90} In this study, VEGF was lyophilized with trehalose, which acts as a cryoprotectant and lyoprotectant to maintain the protein stability.^{90,96,97} Trehalose has a high glass transition temperature, which reduces the motion of the protein molecules during the drying stage by forming highly viscous glassy matrices that stabilize the protein molecules and maintains their native conformation.^{93,95,98} Also, the presence of the buffer salts in the lyophilizing solution controls the solution pH before freezing.^{83,95} Studies on the bioactivity of the growth factors released from other formulations such as PLGA microspheres revealed that the acidic degradation products resulting in a decrease in pH of the surrounding aqueous solution and within the polymer,¹¹⁴⁻¹¹⁷ significantly caused the growth factor denaturation^{119,107} and inhibit cell viability.¹²⁰ In contrast to PLGA, the study on the degradation mechanism of P(TMC-co-HTMC) revealed that copolymer degradation leads to release of non acidic products including glycerol, CO₂, and the short oligomers mainly composed of TMC.^{172,180} Also, as mentioned in Chapter 5, the pH of the medium surrounding the copolymers with 30 mol% HTMC content always remained close to neutral. Therefore, the high bioactivity of the released VEGF can also be attributed to the lack of acidic products formed from the degradation of the P(TMC-co-HTMC).

7.6 Conclusion

A formulation utilizing viscous, liquid injectable P(TMC-co-HTMC) with a 30 mol% HTMC and a molecular weight range of 1000-2000 Da provided sustained protein release. In this formulation, particles of lysozyme, BSA and VEGF were co-lyophilized with

trehalose and salt and incorporated into the copolymer by simple mixing. The rate of protein release was determined by the solubility of the lyophilized protein in the aqueous environment within the copolymer, the concentration of the salt included in the lyophilized powder, and the flexibility of the copolymer chains to form superhydrated regions upon water diffusion into the polymer bulk. The target release rate of VEGF was a sustained release at the rate of 25-50 ng/day. However, our study showed VEGF release of 60-80 % within the first 3 days depending on the salt content of the particles. These rates correspond to an average rate of 767 ± 45 ng/day and 638 ± 64 ng/day in day 1 and 374 ± 42 ng/day and 194 ± 28 ng/day in day 2 for VEGF/BSA/T and VEGF/BSA/T-PB, respectively. Therefore, it is necessary to optimize the formulation to provide a release rate closer to the target rate. Notably, VEGF released from this formulation maintained a high bioactivity, a result due principally to the lack of acidic products formed from the degradation of the P(TMC-co-HTMC). Thus, P(TMC-co-BTMC) has potential as a vehicle to deliver acid sensitive proteins without loss of their bioactivity.

Chapter 8

Conclusion and Recommendations

8.1 Conclusion

Injectable and hydrolysable polymeric delivery systems based on modified low molecular weight conjugated PTMC, ester or anhydride-linked PTMC, and low molecular weight poly(trimethylene carbonate-co-5-hydroxy trimethylene carbonate), P(TMC-co-HTMC), were successfully synthesized and characterized. Based on the *in vitro* degradation of the conjugated PTMC, the conjugation approach using anhydride or ester bond is not an efficient approach providing the desired degradation time and/or neutral release medium needed for preserving the bioactivity of the released growth factors. Preparing P(TMC-co-HTMC) using different catalysts revealed that HCl·Et₂O and Sn(oct)₂ are both able to provide a random comonomer distribution; however, HCl·Et₂O is more favored for biological applications due to the lower toxicity burden. *In vitro* and *in vivo* degradation of the resulting random copolymers prepared using HCl·Et₂O was tailored by adjusting the initial HTMC content, initial molecular weight and the choice of initiator. During *in vitro* degradation, the pH of the medium surrounding the copolymer always remained near neutral. The *in vivo* and *in vitro* degradation mechanism is based on the degradation of HTMC units followed by gradual elimination/dissolution of the short polymeric chains mostly composed of TMC. The tissue response to the subcutaneously injected copolymers at the molecular weight range of 1000-2000 Da with 30 mol% initial HTMC content subsided with time but was still ongoing after 22 weeks. The observed tissue response was comparable with the tissue response of a commercial and clinically used MONOCRYL

suture indicating that the copolymer can be considered biocompatible. Rate of protein release (lysozyme, BSA and VEGF) under *in vitro* conditions from the same copolymers as used for the *in vivo* degradation study is controlled by the solubility of the lyophilized protein in the aqueous environment within the copolymer, the concentration of the salt included in the lyophilized powder, and the flexibility of the copolymer chains to form superhydrated regions upon water diffusion into the polymer bulk and subsequently dissolution of the protein particles. The released VEGF showed greater than 80% bioactivity throughout the release period. This delivery formulation can serve as a potential biocompatible vehicle to deliver acid sensitive proteins without loss of their bioactivity for short or long-term delivery approaches depending on the protein physical properties.

8.2 Recommendations

- *In vitro* degradation study of copolymers at different molecular weight and HTMC content in the medium containing cholesterol esterase and lipase is needed to be studied. This result should be compared with the *in vitro* degradation of PTMC homopolymer at the same molecular weight in the presence of the same enzyme as well as with the degradation of the analog copolymers in PBS to determine the effect of HTMC units on the enzymatic hydrolysis.
- It is necessary to study the *in vitro* degradation of the copolymer with or without protein particles using the same copolymer batch to determine the effect of forming superhydrated regions in copolymer bulk on copolymer degradation.

- A longer-term *in vivo* degradation study of the 1700 Da copolymers until the copolymers are completely resorbed still needs to be done.
- Optimizing the protein particle composition to achieve the target release rate of 25-50 ng/day is still needs to be done. In this case using VEGF/BSA/T-PB formulation at lower loading capacity and lower VEGF content is suggested.

References

1. Choi, D.; Hwang, K. C.; Lee, K. Y.; Kim, Y. H. Ischemic heart diseases: Current treatments and future. *Journal of Controlled Release* (2009), 140 (3), 194-202.
2. Norgren, L.; Hiatt W.R.; Dormandy, J. A.; Nehler M. R.; Harris K. A. Inter-society consensus for the management of peripheral arterial disease (TASC II). *Journal of Vascular Surgery* (2007), 45 (1), S5–S67.
3. Zhan, L. X.; Branco, B. C.; Armstrong, D. G.; Sr, J. L. M. The society for vascular surgery lower extremity threatened limb classification system based on wound , ischemia , and foot infection (WIFI) correlates with risk of major amputation and time to wound healing. *Journal of Vascular Surgery* (2011), 61, 939–944.
4. Allison, M.A.; Ho, E.; Denenberg, J.O.; Langer, R.D. et. al. Ethnic-specific prevalence of peripheral arterial disease in the united states. *American Journal of Preventive Medicine* (2007), 32 (4), 328–333
5. Roger, V. L. et al. Heart disease and stroke statistics-2011 update a report from the american heart association. *Circulation* (2011), 123 (4), e18–e209.
6. Go, A. S. et al. Heart disease and stroke statistics - 2014 Update: A report from the american heart association. *Circulation* (2014), 129 (3), e28-e292.
7. Germani, A.; Di Campli, C.; Pompilio, G.; Biglioli, P.; Capogrossi, M. C. Regenerative therapy in peripheral artery disease. *Cardiovascular Therapeutics* (2009), 27 (4), 289–304.
8. Hirsch, A. T.; Criqui, M.H.; Treat-Jacobson D. et al. Hirsch, A. T. et al. Peripheral Arterial Disease Detection, Awareness, and Treatment in Primary Care. *Journal of American Medicine Association* (2001), 286(11), 1317-1324.
9. McDermott, M.M.; Liu, K. et al. McDermott, M. M. et al. Leg symptoms in peripheral arterial disease: associated clinical characteristics and functional impairment. *Journal of American Medicine Association* (2001), 286(13), 1599-1606.
10. Arain, S. A.; White, C. J. Endovascular therapy for critical limb ischemia. *Vascular Medicine* (2008), 13, 267–279.
11. Bosiers, M.; Hart, J. P.; Deloose, K.; Verbist, J. Endovascular therapy as the primary approach for limb salvage in patients with critical limb ischemia : experience with 443 infrapopliteal procedures. *Vascular* (2006), 14 (2), 63–69.
12. Bradbury, A. Bypass versus angioplasty in severe ischaemia of the leg (BASIL): multicentre , randomised controlled trial. *Lancet* (2005), 366 (9501), 1925-1934
13. Lee, K. Y.; Peters, M. C.; Mooney, D. J. Comparison of vascular endothelial growth factor and basic fibroblast growth factor on angiogenesis in SCID mice. *Journal of Controlled Release* (2003), 87 (1-3), 49-56.

14. Silva, E.A.; Mooney D. J. Spatiotemporal control of vascular endothelial growth factor delivery from injectable hydrogels enhances angiogenesis. *Journal of Thrombosis and Haemostasis* (2007), 5 (3), 590–598.
15. Chapanian, R.; Amsden, B. G. Combined and sequential delivery of bioactive VEGF165 and HGF from poly(trimethylene carbonate) based photo-cross-linked elastomers. *Journal of Controlled Release* (2010), 143, 53–63.
16. Amsden, B. Delivery approaches for angiogenic growth factors in the treatment of ischemic conditions. *Expert Opinion in Drug Delivery* (2011), 8(7), 873–890.
17. Semenza, G. L. Vasculogenesis, angiogenesis, and arteriogenesis: mechanisms of blood vessel formation and remodeling. *Journal of Cellular Biochemistry* (2007), 102, 840–847.
18. Amsden, B. G. Delivery approaches for angiogenic growth factors in the treatment of ischemic conditions. *Expert Opinion in Drug Delivery* (2011), 8(7), 873–890.
19. Heil, M.; Eitenmüller, I.; Schmitz-Rixen, T.; Schaper W. Arteriogenesis versus angiogenesis: similarities and differences. *Journal of Cellular and Molecular Medicine* (2006), 10(1), 45-55.
20. Djonov, V.; Makanya, A. N. (2005). New insights into intussusceptive angiogenesis. In: Clauss M.; Breier G. Eds. *Mechanisms of Angiogenesis*; Switzerland: Springer, 17-33.
21. Abramson, D.; Dobrin, P., Eds. (1984). In: *Blood vessels and lymphatics in organ systems*; Orlando, Florida: Academic press inc, 771.
22. Shima, D.T.; Adamis, A.P.; Ferrara, N.; Yeo, K.T. et. al. Hypoxic induction of endothelial cell growth factors in retinal cells: identification and characterization of vascular endothelial growth factor (VEGF) as the Mitogen. *Molecular Medicine* (1995), 1 (2), 182–193.
23. Fukumura, D.; Xu, L.; Chen, Y.; Gohongi, T. et. al. Advances in brief hypoxia and acidosis independently up-regulate vascular endothelial growth factor transcription in brain tumors in vivo. *American Association for Cancer Research* (2001), 61(16), 6020–6024.
24. Kinnaird, T.; Stabile, E.; Burnett, M.S., Epstein S.E. Bone marrow-derived cells for enhancing collateral development. *Circulation Research* (2004), 354–364.
25. Lamalice, L.; Le Boeuf, F.; Huot, J. Endothelial cell migration during angiogenesis. *Circulation Research* (2007), 100 (6), 782-794.
26. Gerhardt, H.; Betsholtz, C. (2005). How do endothelial cells orientate? In: Clauss M.; Breier G. Eds. *Mechanisms of Angiogenesis*; Switzerland: Springer, 3–15.
27. Carmeliet, P.; Collen, D.; Vessel, B. Genetic Analysis of Blood Vessel: role of Endothelial versus smooth muscle cells. *Trends in cardiovascular medicine* (1997), 7 (8), 271–281.
28. Papetti, M.; Herman, I. M. Mechanisms of normal and tumor-derived angiogenesis. *American Journal of Physiology-Cell Physiology* (2002), 282 (5), 947–970.
29. Buschmann, I.; Schaper, W. The pathophysiology of the collateral circulation (arteriogenesis). *The Journal of Pathology* (2001), 190 (3), 338–342.

30. Heilmann, C.; Beyersdorf, F.; Lutter, G. Collateral growth: cells arrive at the construction site. *Cardiovascular Surgery* (2002), 10 (6), 570-578.
31. Stress, S. et al. Selectively Upregulates. 94, 885–891 (1994).
32. Lee, C. W.; Stabile, E.; Kinnaird, T.; Shou, M. et. al. Temporal patterns of gene expression after acute hindlimb ischemia in mice insights into the genomic program for collateral vessel development. *Journal of American College of Cardiology* (2001), 43 (3), 474–482.
33. Heil, M.; Ziegelhoeffer, T.; Pipp, F.; Kostin, S. et. al. Blood monocyte concentration is critical for enhancement of collateral artery growth. *American Journal of Physiology-Hearth and Circulatory Physiology* (2002), 283, H2411–H2419.
34. Lawall, H.; Bramlage, P.; Amann, B. Treatment of peripheral arterial disease using stem and progenitor cell therapy. *Journal of Vascular Surgery* (2011), 445-453.
35. Cao, L.; Mooney, D. J. Spatiotemporal control over growth factor signaling for therapeutic neovascularization. *Advanced Drug Delivery Reviews* (2007), 59, 1340-1350.
36. Losordo, D. W.; Dimmeler, S. Review : Clinical cardiology : new frontiers therapeutic angiogenesis and vasculogenesis for ischemic disease Part II : cell-based therapies. *Circulation* (2004), 109 (22), 2692–2697.
37. Losordo, D. W. & Dimmeler, S. Clinical cardiology: new frontiers therapeutic angiogenesis and vasculogenesis for ischemic disease Part II : cell-Based therapies. *Circulation* (2004), 109 (22), 2692–2697.
38. Bhang, S.H.; Cho, S.W.; Lim, J. M.; Kan J. M. Locally delivered growth factor enhances the angiogenic efficacy of adipose-derived stromal cells transplanted to ischemic limbs. *Stem Cells Journal* (2009), 27 (8), 1976-1986.
39. Nakagami, H.; Morishita, R.; Maeda, K.; Kikuchi, Y.; Ogihara, T. Adipose tissue-derived stromal cells as a novel option for regenerative cell therapy. *Journal of Atherosclerosis and Thrombosis* (2005), 13 (2), 77–81
40. Lua, D.; Chena, B.; Liang, Z.; Denga, W. et al. Comparison of bone marrow mesenchymal stem cells with bone marrow-derived mononuclear cells for treatment of diabetic critical limb ischemia and foot ulcer : A double-blind , randomized , controlled trial. *Diabetes Research an. Clinical Practice* (2011), 92, 26–36.
41. Finney, M. R.; Greco, N. J.; Haynesworth, S. E.; Martin, J. M. et al. Direct comparison of umbilical cord blood versus bone marrow–derived endothelial precursor cells in mediating neovascularization in response to vascular ischemia. *American Society for Blood and Marrow Transplantation* (2006), 593, 585–593.
42. Rafii, S.; Lyden, D. Therapeutic stem and progenitor cell transplantation for organ vascularization and regeneration. *Nature Medicine* (2003), 9 (6), 37–42.
43. Urbich, C.; Aicher, A.; Heeschen, C.; Dernbach, E. et al. Soluble factors released by endothelial progenitor cells promote migration of endothelial cells and cardiac resident progenitor cells. *Journal of Molecular and Cellular Cardiology* (2005), 39, 733–742.
44. Belkin, M.; Acsády, G. Peripheral blood-derived autologous stem cell therapy for the

treatment of patients with late-stage peripheral artery disease results of the short- and long-term follow-up. *Cytotherapy* (2013), 15, 1245–1252.

45. Weem, S. M. O. P.; Teraa, M.; Borst, G. J. De. Bone marrow derived Cell Therapy in critical limb ischemia : A meta-analysis of randomized placebo controlled trials. *European Journal of Vascular and Endovascular Surgery* (2015), 50, 775–783.
46. Zhang, M.; Methot, D.; Poppa1, V.; Fujio, Y.; Walsh, K.; Murry, C.E. Cardiomyocyte grafting for cardiac repair: graft cell death and anti-death strategies. *Journal of Molecular and Cellular Cardiology* (2001), 33, 907–921.
47. Giacca, M.; Zacchigna, S. VEGF gene therapy : therapeutic angiogenesis in the clinic and beyond. *Gene Therapy* (2012), 19, 622–629.
49. Svensson, E.; Marshall, D.J.; Woodard, K.; Lin, H. et al. Efficient and stable transduction of cardiomyocytes after intramyocardial injection or intracoronary perfusion with recombinant adeno-associated virus vectors. *Circulation* (1999), 99 (2), 201-205.
50. Monahan, P. E.; Samulski, R. J. AAV vectors : is clinical success on the horizon? *Gene Therapy* (2000), 7, 24–30.
51. Boden, J.; Lassance-Soares, R. B.; Wang, H.; Wei, Y. et al. Vascular regeneration in ischemic hindlimb by adeno-associated. *Journal of the American Heart Association* (2016), 5 (6), 1-17.
52. Cooke, J. P.; Losordo, D. W. Modulating the vascular response to limb ischemia Angiogenic and cell therapies. *Circulation Research* (2015), 116, 1561–1579.
53. Fowkes, G. R.; Price, J. F. Act, T. Gene therapy for critical limb ischaemia : the TAMARIS trial. *The Lancet* (2011), 377 (9781), 1894–1896.
54. Cross, M.; Dexter, T. M. Growth factors in development, transformation, and tumorigenesis review. *Cell* (1991), 64, 271–280.
55. Lee, K.; Silva, E. A.; Mooney, D. J. Growth factor delivery-based tissue engineering: general approaches and a review of recent developments. *Journal of the Royal Society Interface* (2011), 8, 153–170.
56. Daugherty, A. L.; Mrsny, R. J. Local tissue distribution and cellular fate of vascular endothelial growth factor (VEGF) following intramuscular injection. *Journal of Drug Targeting* (2010), 18, 27–35.
57. Epstein, S. E.; Fuchs, S.; Zhou, Y. F.; Baffour, R.; Kornowski, R. Therapeutic interventions for enhancing collateral development by administration of growth factors : basic principles , early results and potential hazards. *Cardovascular Research* (2001), 49 (3), 532–542.
58. Richardson, T. P.; Peters, M. C.; Ennett, A. B.; Mooney, D. J. Polymeric system for dual growth factor delivery. *Nature Biotechnology* (2001), 19, 1029–1034.
59. Cao, R.; Brakenhielmi, E.; Pawliuk, R.; Wariaro, D. et. al. Angiogenic synergism , vascular stability and improvement of hind-limb ischemia by a combination of PDGF-BB and FGF-2. *Nature Medicine* (2003), 9 (5), 604-613.

60. Zhanga, H.; Jia, X.; Hana, F.; Zhang J. Z. et al. Biomaterials dual-delivery of VEGF and PDGF by double-layered electrospun membranes for blood vessel regeneration. *Biomaterials* (2013), 34, 2202–2212.
61. Hao, X.; Silva, E.A.; Månsson-Broberg, A.; Mooney, D.J. et. al. Angiogenic effects of sequential release of VEGF-A 165 and PDGF-BB with alginate hydrogels after myocardial infarction. *Cardiovascular Research* (2007), 75, 178–185.
62. Wu, C. K.; Pettit, A. R.; Toulson, s.; Grøndahl, L. et al. Responses in vivo to purified poly(3-hydroxybutyrate-co-3-hydroxyvalerate) implanted in a murine tibial defect model. *Journal of Biomedical Materials Research-Part A* (2009). 846-854.
63. Babasola, I. O.; Rooney, M.; Amsden, B. G. Corelease of Bioactive VEGF and HGF from Viscous Liquid Poly(5- ethylene ketal ε-caprolactone-co-D,L-lactide). *Molecular Pharmaceutics* (2013), 10, 4552–4559.
64. Nagy, J. A.; Dvorak, A. M.; Dvorak, H. F. VEGF-A(164/165) and PlGF: roles in angiogenesis and arteriogenesis. *Trends in Cardiovascular Medicine* (2003), 13, 169–175.
65. Carmelieti, P.; Moons, L.; Lutunni, A.; Vincentic, V.; et.al. Synergism between vascular endothelial growth factor and placental growth factor contributes to angiogenesis and plasma extravasation in pathological conditions. *Nature Medicine* (2001), 7, 575–583.
66. Lutun, A.; Tjwa, M.; Moons, L.; Wu, Y.; et. al. Revascularization of ischemic tissues by PlGF treatment, and inhibition of tumor angiogenesis, arthritis and atherosclerosis by anti-Flt1. *Nature Medicine* (2002). 8, 831–840.
67. Cheng, D.; Sefton, M. V. Dual Delivery of Placental Growth Factor and Vascular Endothelial Growth Factor from Poly(Hydroxyethyl Methacrylate-Co-Methyl Methacrylate) Microcapsules Containing Doubly Transfected Luciferase-Expressing L929 Cells. *Tissue Engineering: Part A* (2009), 15 (8), 1929-1939.
68. Attanasio, S.; Snell, J. Therapeutic Angiogenesis in the Management of Critical Limb Ischemia Current Concepts and Review. *Cardiology Review* (2009), 17, 115–120.
69. Kim, B.-S.; Chen, J.; Weinstein, T.; Noiri, E.; Goligorsky, M. S. VEGF expression in hypoxia and hyperglycemia: reciprocal effect on branching angiogenesis in epithelial-endothelial co-cultures. *Journal of the American Society of Nephrology* (2002), 13, 2027–2036.
70. Ishida, A.; Murray, J.; Saito, Y.; Canthou, C.; et al. Expression of vascular endothelial growth factor receptors in smooth muscle cells. *Journal of Cellular Physiology* (2001), 188, 359–368.
71. Gille, H.; Kowalski, J.; Li, B.; LeCouter, J.; et al. Analysis of biological effects and signaling properties of Flt-1 (VEGFR-1) and KDR (VEGFR-2). A reassessment using novel receptor-specific vascular endothelial growth factor mutants. *American Society of Biochemistry and Molecular Biology* (2001), 276, 3222–3230.
72. Gerber, H. P.; McMurtrey, A.; Kowalski, J.; Yan, M.; et al. Vascular endothelial growth factor regulates endothelial cell survival through the phosphatidylinositol 3'-kinase/Akt signal transduction pathway. Requirement for Flk-1/KDR activation. *American Society of Biochemistry and Molecular Biology* (1998), 273, 30336–30343.

73. Chen, F.; Zhang, M.; Wu, Z. Biomaterials toward delivery of multiple growth factors in tissue engineering. *Biomaterials* (2010), 31, 6279–6308.
74. Hoare, T. R.; Kohane, D. S. Hydrogels in drug delivery: progress and challenges. *Polymer* (2008), 49, 1993–2007.
75. Vermonden, T.; Censi, R.; Hennink, W. E. Hydrogels for protein delivery. *Chemical Reviews* (2012), 112 (5), 2853–2888.
76. Langer, R. Biomaterials in drug delivery and tissue engineering: one laboratory's experience. *Accounts of Chemical Research* (2000), 33, 94–101.
77. Gu, F.; Amsden, B.; Neufeld, R. Sustained delivery of vascular endothelial growth factor with alginate beads. *Journal of Controlled Release* (2004), 96, 463–472.
78. Suzuki, H.; Ohkuchi, A.; Matsubara, S.; Takei Y. et al. Effect of recombinant placental growth factor 2 on hypertension induced by full-length mouse soluble fms-like tyrosine kinase 1 adenoviral vector in pregnant mice. *Hypertension* (2009), 54, 1129-1135.
79. Hafeli, U. BOOK REVIEW: Controlled Drug Delivery: Challenges and strategies, edited by Kinam Park. *Annals of Biomedical Engineering* 26, 1102 (1998).
80. Croll, S. D.; Ransohoff, R. M.; Cai, N.; Zhang, Q. et al. VEGF-mediated inflammation precedes angiogenesis in adult brain. *Experiment Neurology* (2004), 187, 388-402.
81. Shantsila, E.; Watson, T.; Lip, G. Y. H. Endothelial progenitor cells in cardiovascular disorders. *Journal of the American College of Cardiology* (2007), 49 (7), 741-752.
82. Cleland, J. L.; Duenas, E. T.; Park, A.; Daugherty, A.; et al. Development of poly-(D,L-lactide--coglycolide) microsphere formulations containing recombinant human vascular endothelial growth factor to promote local angiogenesis. *Journal of Controlled Release* (2001), 72, 13–24.
83. Chi, E. Y.; Krishnan, S.; Randolph, T. W.; Carpenter, J. F. Physical stability of proteins in aqueous solution: mechanism and driving forces in nonnative protein aggregation. *Pharmaceutical Research* (2003), 20 (9), 1325-1336.
84. Cromwell, M. E. M.; Hilario, E.; Jacobson, F. Protein aggregation and bioprocessing. *The AAPS Journal* (2006), 8 (3), e572-579.
85. Rosenberg, A. S. Effects of Protein Aggregates : an immunologic perspective. *The AAPS Journal* (2006), 8 (3), 501–507.
86. Wang, W. Instability, stabilization , and formulation of liquid protein pharmaceuticals. *International Journal of Pharmaceutics* (1999), 185, 129–188.
87. Ii, H.; Auné, K. C.; Tanford, C. Thermodynamics of the denaturation of lysozyme by guanidine hydrochloride. II. dependence on denaturant concentration at 25 °C. *Biochemistry* (1969), 8 (11), 4586–4590.
88. Griebenow, K.; Castellanos, I. J.; Cruz, G. Encapsulation-induced aggregation and loss in activity of γ -chymotrypsin and their prevention. *Journal of Controlled Release* (2002), 81 (3), 307–319.

89. Diwan, M.; Park, T. G. Pegylation enhances protein stability during encapsulation in PLGA microspheres. *Journal of Controlled Release* (2001), 73, 233–244.
90. Fu, K.; Griebenow, K.; Hsieh, L.; Klibanov, A. M.; Langer, R. FTIR characterization of the secondary structure of proteins encapsulated within PLGA microspheres. *Journal of Controlled Release* (1999), 58, 357–366.
91. Arakawa, T.; Timasheff, S. N. The Stabilization of proteins by osmolytes. *Journal of Biophysical Society* (1985), 47, 411–414.
92. Timasheff, N. Preferential interactions of proteins with solvent components in aqueous amino acid solutions. *Archives of Biochemistry and Biophysics* (1983), 224 (1), 169–177.
93. Ohtake, S.; Kita, Y.; Arakawa, T. Interactions of formulation excipients with proteins in solution and in the dried state. *Advanced Drug Delivery Review* (2011), 63, 1053–1073.
94. Arakawa, T. Hydration as a major factor in preferential solvent-protein interactions. *Crystal Growth and Design* (2002), 2 (6), 549–551.
95. Kamerzell, T. J.; Esfandiary, R.; Joshi, S. B.; Middaugh, C. R.; Volkin, D. B. Protein – excipient interactions : Mechanisms and biophysical characterization applied to protein formulation development. *Advanced Drug Delivery Review* (2011), 63, 1118–1159.
96. Weert, M. V. D.; Steenbergen M. J. V. ; Cleland, J. L.; Heller, J.; et al. Semisolid , self-catalyzed poly(Ortho Ester)s as controlled-release systems:protein release and protein stability issues. *Journal of Pharmaceutical Sciences* (2002), 91 (4), 1065–1074.
97. Crommelin, D. J. A.; Jiskoot, W. Distinct effects of sucrose and trehalose on protein stability during supercritical fluid drying and freeze-drying. *European Journal of Pharmaceutical Sciences* (2006), 7, 336–345.
98. Yoshioka, S.; Takeda, Y. The effects of additives on the stability of freeze-dried stored at elevated temperature. *International Journal of Pharmaceutics* (1991), 71, 137–146.
99. Ramos, A. N. A.; Raven, N. D. H.; Sharp, R. J.; Bartolluci, S.; et al. Stabilization of enzymes against thermal stress and freeze-drying by mannosylglycerate. *Applied and Environmental Microbiology* (1997), 63 (10), 4020–4025.
100. Anderson, J. M.; Rodriguez, A.; Chang, D. T. Foreign body reaction to biomaterials. *Seminar in Immunology* (2008), 20, 86–100.
101. Anderson, J. M. Biological Response to Biomaterials. *Annual Review of Materials Research* (2001), 31, 81–110.
102. Ramazani, F.; Chen, W.; Nostrum, C. F.; Storm, G.; et al. Strategies for encapsulation of small hydrophilic and amphiphilic drugs in PLGA microspheres: state-of-the-art and challenges. *International Journal of Pharmaceutics* (2016), 499, 358–367.
103. Kenley, R. A.; Lee, M. O.; Mahoney, T. R.; Sanders, L. M. Poly(lactide-co-glycolide) decomposition kinetics in vivo and in vitro. *Macromolecules* (1987), 20, 2398–2403.
104. Athanasiou, K. A.; Niederauer, G. G.; Agrawal, C. M. Biocompatibility and clinical applications of polylactic acid / polyglycolic acid copolymers. *Biomaterials* (1996), 17, 93-

- 102.
105. Cohen, S.; Yoshioka, T.; Lucarelli, M.; Hwang, L.H.; Langer, R. Controlled delivery systems for proteins based on poly(Lactic-Glycolic Acid) microspheres. *Pharmaceutical Research* (1991), 8 (1), 713-720.
106. Wei, G.; Pettway, G. J.; Mccauley, L. K.; Ma, P. X. The release profiles and bioactivity of parathyroid hormone from poly (lactic-co-glycolic acid) microspheres. *Biomaterial* (2004), 25, 345–352.
107. Takahata, H.; Lavelle, E. C.; Coombes, A. G. A.; Davis, S. S. The distribution of protein associated with poly (DL -lactide co-glycolide) microparticles and its degradation in simulated body fluids. *Journal of Controlled Release* (1998), 50, 237–246.
108. Yan, J.; Yang, S.; Sun, H.; Guo, D.; et al. Effects of releasing recombinant human growth and differentiation factor-5 from poly (lactic- co -glycolic acid) microspheres for repair of the rat degenerated intervertebral disc. *Journal of Biomaterials Applications* (2014), 29 (1), 72–80.
109. Ma, G. Microencapsulation of protein drugs for drug delivery : Strategy , preparation , and applications. *Journal of Controlled Release* (2014), 193, 324–340.
110. Rocha, F. G.; Sundbackb, C. A.; Krebs, N. J.; Leach, K. et al. The effect of sustained delivery of vascular endothelial growth factor on angiogenesis in tissue-engineered intestine. *Biomaterials* (2008), 29, 2884–2890.
111. Karam, J.; Muscari, C.; Sindji, L.; Bastiat, G.; et al. Pharmacologically active microcarriers associated with thermosensitive hydrogel as a growth factor releasing biomimetic 3D scaffold for cardiac tissue-engineering. *Journal of Controlled Release* (2014), 192, 82–94.
112. Osswald, C. R.; Kang-Mieler J.J. Controlled and extended release of a model protein from a microsphere-hydrogel drug delivery system. *Annals of Biomedical Engineering* (2015), 43 (11), 2609–2617..
113. Elisseff, J.; McIntosh W.; Fu, K; Blunk, T.; Langer R. Controlled-release of IGF-I and TGF-P 1 in a photopolymerizing hydrogel for cartilage tissue engineering. *Journal of Orthopaedic Research* (2001),19, 1098-1 1104.
114. Fu, K.; Pack, D. W.; Klibanov, A. M.; Langer, R. Visual evidence of acidic environment within degrading poly(lactic-co- glycolic acid) (PLGA) microspheres. *Pharmaceutical Research* (2000), 17 (1), 100-106.
115. Vey, E.; Roger, C.; Meehan, L.; Booth, J.; et al. Degradation mechanism of poly(lactic-co-glycolic) acid block copolymer cast films in phosphate buffer solution. *Polymer Degradation and Stability* (2008), 93, 1869-1876.
116. Fu, K.; Pack, D. W.; Klibanov, A. M.; Langer, R. Visual evidence of acidic environment within degrading poly(lactic-co-glycolic acid) (PLGA) microspheres. *Pharmaceutical Research* (2000) 17, 100–106 (2000).
117. Shenderova, A.; Burke, T.G.; Schwendeman, S. P. Stabilization of hydroxycamptothecin in PLGA microsphere. *Pharmaceutical Research* (1997), 14 (10), 1406-1414.

118. Sokolsky-papkov, M.; Agashi, K.; Olaye, A.; Shakesheff, K.; Domb, A. J. Polymer carriers for drug delivery in tissue engineering. *Advanced Drug Delivery Reviews* (2007), 59, 187–206.
119. Park, T. G.; Lu, W.; Crotts, G. Importance of in vitro experimental conditions on protein release kinetics, stability and polymer degradation in protein encapsulated poly (d,l-lactic acid-co-glycolic acid) microspheres. *Journal of Controlled Release* (1995), 33, 211–222.
120. Sung, H.-J.; Meredith, C.; Johnson, C.; Galis, Z. S. The effect of scaffold degradation rate on three-dimensional cell growth and angiogenesis. *Biomaterials* (2004), 25, 5735–5742.
121. Ekholm, M.; Hietanen, J.; Lindqvist, C.; Rautavuori, J.; Santavirta, S.; Suuronen, R. A histological study of tissue reactions to ϵ -caprolactone-lactide-copolymer in paste form. *Biomaterials* (1999), 20 (14), 1257-1262.
122. Zhu, G.; Mallery, S. R.; Schwendeman, S. P. Stabilization of proteins encapsulated in injectable poly (lactide-co-glycolide). *Nature Biotechnology* (2000), 18, 52-57.
123. Li, L.; Schwendeman, S. P. Mapping neutral microclimate pH in PLGA microspheres. in *Journal of Controlled Release* (2005), 101, 163-173.
124. Ding, A. G.; Schwendeman, S. P. Acidic microclimate pH Distribution in PLGA microspheres monitored by confocal laser scanning microscopy. *Pharmaceutical Research* (2008), 25 (9), 2041-2052.
125. Jiang, W.; Schwendeman, S. P. Stabilization and controlled release of bovine serum albumin encapsulated in poly(D, L-lactide) and poly(ethylene glycol) microsphere blends. *Pharmaceutical Research* (2001), 18 (6), 878-885.
126. King, T. W.; Patrick, C. W. Development and in vitro characterization of vascular endothelial growth factor (VEGF)-loaded poly(DL-lactic-co-glycolic acid)/poly(ethylene glycol) microspheres using a solid encapsulation/single emulsion/solvent extraction technique. *Journal of Biomedical Material Research* (2000), 51, 383–390.
127. Xin, H. Z.; Wang, C. H.; Tong, Y. W. In vitro characterization of hepatocyte growth factor release from PHBV/PLGA microsphere scaffold. *Journal of Biomedical Material Research -Part A* (2009), 411-423.
128. Park. H.; Park, K. Biocompatibility issues of implantable drug delivery systems. *Pharmaceutical Research* (1996), 13 (12), 1770-1776.
129. Hiemstra, C.; Zhong, Z.; Steenbergen, M. J. Van; Hennink, W. E.; Feijen, J. Release of model proteins and basic fibroblast growth factor from in situ forming degradable dextran hydrogels. *Journal of Controlled Release* (2007), 122, 71–78.
130. Jun, X.; Hong, S.; Li, J. Hydrolytic degradation and protein release studies of thermogelling polyurethane copolymers consisting of poly [(R) -3-hydroxybutyrate], poly (ethylene glycol), and poly (propylene glycol). *Biomaterials* (2007), 28, 4113–4123.
131. Hiemstra, C.; Zhong, Z.; Van Tomme, S. R.; Steenberger M. J. V. In vitro and in vivo protein delivery from in situ forming poly (ethylene glycol) – poly (lactide) hydrogels. *Journal of Controlled Release* (2007), 119 (3), 320–327.

132. Huynh, D.P.; Nguyen, M. K.; Pi, B.S.; Kim, M. S. et al. Functionalized injectable hydrogels for controlled insulin delivery. *Biomaterials* (2008), 29, 2527–2534.
133. Wang, N. X.; Recum, H. A. Von. Affinity-Based Drug Delivery. *Macromolecular Bioscience* (2011), 11, 321–332.
134. Vulic, K.; Shoichet, M. S. Tunable Growth Factor Delivery from Injectable Hydrogels for Tissue. *Journal of the American Chemical Society* (2012), 134, 882-885.
135. Sivashanmugam, A.; Kumar, R. A.; Priya, M. V.; Nair, S. V.; Jayakumar, R. An overview of injectable polymeric hydrogels for tissue engineering. *European Polymer Journal* (2015), 72, 543–565.
136. Tam, K. C.; Xiong, X. Y.; Tam, K. C.; Gan, L. H. Polymeric nanostructures for drug delivery applications based on pluronic copolymer systems. *Journal of Nanoscience and Nanotechnology* (2006), 6, 1638-2650.
137. Singh, S.; Webster, D. C.; Singh, J.; Thermosensitive polymers : Synthesis , characterization , and delivery of proteins. *International Journal of Pharmaceutics* (2007), 341, 68–77.
138. Garbern, J. C.; Hoffman, A. S.; Stayton, P. S. Injectable pH-and temperature-responsive Poly(N-isopropylacrylamide-co-propylacrylic acid) copolymers for delivery of angiogenic growth factors. *Biomacromolecule* (2010), 11, 1833-1839.
139. Liu, J.; Lin, S.; Li, L.; Liu, E. Release of theophylline from polymer blend hydrogels. *International Journal of Pharmaceutics* (2005), 298, 117–125.
140. Bajpai, A. K.; Shrivastava, J. In vitro enzymatic degradation kinetics of polymeric blends of crosslinked starch and carboxymethyl cellulose. *Polymer International* (2005), 54, 1524–1536.
141. Gupta, D.; Tator, C. H.; Shoichet, M. S. Fast-gelling injectable blend of hyaluronan and methylcellulose for intrathecal , localized delivery to the injured spinal cord. *Biomaterials* (2006), 27, 2370–2379.
142. Schneider, J. P.; Pochan, D. J.; Ozbas, B.; Rajagopal, K.; et al. Responsive hydrogels from the intramolecular folding and self-assembly of a designed peptide. *Journal of American Chemistry Society* (2002), 124, 15030–15037.
143. Geisler, I. M.; Schneider, J. P. Evolution-based design of an injectable hydrogel. *Advanced Functional Materials* (2012), 22, 529–537.
144. Matter, S.; Guvendiren, M.; Lu, H. D.; Burdick, J. A. Shear-thinning hydrogels for biomedical applications. *Soft Matter* (2012), 8, 260-272.
145. Aulisa, L.; Dong, H.; Hartgerink, J. D. Self-Assembly of Multidomain Peptides : Sequence Variation Allows Control over Cross-Linking and Viscoelasticity. *Biomacromolecule* (2009), 10, 2694–2698.
146. Lindsey, S.; Piatt, J. H.; Wortington, P.; Sonmez, C.; et al. Beta Hairpin Peptide Hydrogels as an Injectable Solid Vehicle for Neurotrophic Growth Factor Delivery. *Biomacromolecule* (2015), 16, 2672-2683.

147. Altunbas, A.; Lee, S. J.; Rajasekaran, S. A.; Schneider, J. P.; Pochan, D. J. Encapsulation of curcumin in self-assembling peptide hydrogels as injectable drug delivery vehicles. *Biomaterials* (2011), 32, 5906–5914.
148. Kiick, K. L. Peptide- and protein-mediated assembly of heparinized hydrogels. *Soft Matter* (2008), 4, 29–37.
149. Sharifpoor, S.; Amsden, B. In vitro release of a water-soluble agent from low viscosity biodegradable, injectable oligomers. *European Journal of Pharmaceutics and Biopharmaceutics* (2007), 65, 336–345.
150. Amsden, B. G.; Timbart, L.; Mareck, D.; Chapanian, R.; et. al. VEGF-induced angiogenesis following localized delivery via injectable, low viscosity poly(trimethylene carbonate). *Journal of Controlled Release* (2010), 145, 109-115.
151. Amsden, B. G.; Cheng, Y. Enhanced fraction releasable above percolation threshold from monoliths containing osmotic excipients. *Journal of Controlled Release* (1994), 31, 21–32.
152. Golomb, G.; Fisher, P.; Rahamim, E. The relationship between drug release rate, particle size and swelling of silicon matrices. *Journal of Controlled Release* (1990), 12, 121–132.
153. Gu, F.; Neufeld, R.; Amsden, B. Sustained release of bioactive therapeutic proteins from a biodegradable elastomeric device. *Journal of Controlled Release* (2007), 117, 80-89.
154. Coulson, E.; Winters, L.; Coulson, G. E.; Clarke, K. J. Effect of Osmotic Stress on the Ultrastructure and Viability of the Yeast. *Journal of General Microbiology* (1983), 129, 2023–2034.
155. Gu, F.; Neufeld, R.; Amsden, B. Maintenance of vascular endothelial growth factor and potentially other therapeutic proteins bioactivity during a photo-initiated free radical cross-linking reaction forming biodegradable elastomers. *European Journal Pharmaceutics and . Biopharmaceutics* (2007), 66, 21-27.
156. Gu, F., Neufeld, R.; Amsden, B. Osmotic-driven release kinetics of bioactive therapeutic proteins from a biodegradable elastomer are linear, constant, similar, and adjustable. *Pharmaceutical Research* (2006), 23 (4), 782-789.
157. Chapanian, R.; Amsden, B. G. Osmotically driven protein release from photo-cross-linked elastomers of poly (trimethylene carbonate) and poly (trimethylene carbonate-co- D , L - lactide). *European Journal of Pharmaceutics and Biopharmaceutics* (2010), 74, 172–183.
158. Timbart, L.; Tse, M. Y.; Pang, S. C.; Babasola, O.; Amsden, B. G. Low viscosity poly(trimethylene carbonate) for localized drug delivery: Rheological properties and in vivo degradation. *Macromolecular Bioscience* (2009), 9, 786–794.
159. Sharifpoor, S.; Amsden, B. In vitro release of a water-soluble agent from low viscosity biodegradable, injectable oligomers. *European Journal of Pharmaceutics and Biopharmaceutics* (2007), 65, 336-345.
160. Barr, J. Bioerodible injectable Poly (ortho ester) for tetracycline controlled delivery to periodontal pockets: preliminary trial in humans. *AAPS PharmSci* (2002), 4 (4), 1-7.
161. Gurny, R.; Heller, J.; Barr, J. Control of molecular weight for auto-catalyzed poly (ortho

- ester) Obtained by polycondensation reaction. *International Journal of Polymer Analysis and Characterization* (2002), 7, 145-161.
162. Sokolsky-papkov, M.; Golovanevski, L.; Domb, A. J.; Weiniger, C. F. Prolonged local anesthetic action through slow release from poly(lactic acid-co-castor Oil). *Pharmaceutical Research* (2009), 26 (1), 32–39.
 163. Hatefi, A.; Amsden, B. Biodegradable injectable in situ forming drug delivery systems. *Journal of Controlled Release* (2002), 80, 9–28.
 164. Trimaille, T.; Gurny, R.; Mo, M. Poly (hexyl-substituted lactides): Novel injectable hydrophobic drug delivery systems. *Journal of Biomedical Materials* (2006), 80A (1), 55-65.
 165. Jain, J. P., Modi, S.; Kumar, N. Hydroxy fatty acid based polyanhydride as drug delivery system : Synthesis , characterization , in vitro degradation , drug release , and biocompatibility. *Journal of Biomedical Materisl* (2007), 84A (3), 740-752.
 166. Alexander, H. Biological response of intramedullary bone to poly-L-lactic acid. *Journal of Applied Biomaterail* (1993), 4, 13-27.
 167. Mabey, W.; Mill, T. Critical review of hydrolysis of organic compounds in water under environmental conditions. *Journal of Physical and Chemical Reference Data* (1978), 7 (2), 383-415.
 168. Vey, E.; Roger, C.; Meehan, L.; Booth, J.; et al. Degradation mechanism of poly(lactic-co-glycolic) acid block copolymer cast films in phosphate buffer solution. *Polymer Degradation and Stability* (2008), 93, 1869–1876.
 169. Babasola, O. I.; Amsden, B. G. Surface eroding, liquid injectable polymers based on 5-ethylene ketal ϵ -caprolactone. *Biomacromolecules* (2011), 12 (10), 3423-3431.
 170. Babasola, I. O., Bianco, J. ; Amsden, B. G. In vivo degradation and tissue response to poly(5-ethylene ketal ϵ -caprolactone-co-D,L-lactide). *Biomacromolecules* (2012), 13, 2211-2217.
 171. Babasola, I. O.; Zhang, W.; Amsden, B. G. Osmotic pressure driven protein release from viscous liquid , hydrophobic polymers based on 5-ethylene ketal e -caprolactone : Potential and mechanism. *European Journal of Pharmaceutics and Biopharmaceutics* (2013), 85, 765–772.
 172. Albertsson, A.; Eklund, M. Influence of molecular structure on the degradation mechanism of degradable polymers: in vitro degradation of poly(trimethylene carbonate), poly(trimethylene carbonate-co-caprolactone), and poly(adipic anhydride). *Journal of Applied Polymer Science* (1995), 57, 87–103.
 173. Zhang, Z., Kuijter, R., Bulstra, S. K., Grijpma, D. W.; Feijen, J. The in vivo and in vitro degradation behavior of poly (trimethylene carbonate). *Biomaterials* (2006), 27, 1741–1748.
 174. Vyner, M. C., Li, A.; Amsden, B. G. The effect of poly(trimethylene carbonate) molecular weight on macrophage behavior and enzyme adsorption and conformation. *Biomaterials* (2014), 35, 9041–8.

175. Chapanian, R.; Tse, M. Y.; Pang, S. C.; Amsden, B. G. The role of oxidation and enzymatic hydrolysis on the in vivo degradation of trimethylene carbonate based photocrosslinkable elastomers. *Biomaterials* (2009), 30, 295-306.
176. Acemoglu, M. et al. Novel bioerodible poly(hydroxyalkylene carbonates): A versatile class of polymers for medical and pharmaceutical applications. *Macromolecules* (1995), 28, 3030–3037.
177. Wang, X.-L.; Zhuo, R.-X.; Liu, L.-J.; He, F.; Liu, G. Synthesis and characterization of novel aliphatic polycarbonates. *Journal of Polymer Science- Part A Polymer Chemistry* (2002), 40, 70–75.
178. Zhou, Y.; Zhuo, R. X.; Liu, Z. L. Synthesis and characterization of novel aliphatic poly(carbonate-ester)s with functional pendent groups. *Macromolecular Rapid Communications* (2005), 26, 1309–1314.
179. Feng, J.; Wang, X. L.; He, F.; Zhuo, R. X. Non-catalyst synthesis of functionalized biodegradable polycarbonate. *Macromolecular Rapid Communications* (2007), 28, 754–758.
180. Chen, F.; Huyer, L. D.; Amsden, B. G. Insights into the hydrolytic degradation of poly (1 , 3-glycerol carbonate). doi:10.3389/conf.FBIOE.2016.01.02014
181. Landau, R.; Wahren, J.; Wahren, J. Glycerol production and utilization sites and quantitation in humans : sites and questions. *American Chemical Society* (1996), E1110–E1117.
182. Cherniack, S.; Longobardo, S. Oxygen and carbon dioxide gas stores of the body. *Biophysiological Review* (1970), 50 (2), 196-243.
183. Feng, J.; Zhuo, R. X.; Zhang, X. Z. Construction of functional aliphatic polycarbonates for biomedical applications. *Progress in Polymer Science* (2012), 37, 211–236.
184. Rokicki, G. Aliphatic cyclic carbonates and spiroorthocarbonates as monomers. *Progress in Polymer Science* (2000), 25, 259–342.
185. Storey, R. F.; Sherman, J. W. Kinetics and mechanism of the stannous octoate-catalyzed bulk polymerization of ϵ -caprolactone. *Macromolecules* (2002), 35, 1504-1512.
186. Nachtergaele, A.; Coulembier, O.; Dubois, P.; Helvenstein, M.; et al. Organocatalysis paradigm revisited: Are metal-free catalysts really harmless? *Biomacromolecules* (2015), 16, 507–514.
187. Dobrzynski, P.; Pastusiak, M.; Bero, M. Less toxic acetylacetonates as initiators of trimethylene carbonate and 2 , 2-dimethyltrimethylene carbonate ring. *Journal of Polymer Science: Part A: Polymer Chemistry* (2005), 43, 1913–1922.
188. Darensbourg, D. J.; Ganguly, P.; Billodeaux, D. Ring-opening polymerization of trimethylene carbonate using aluminum(III) and tin(IV) salen chloride catalysts. *Macromolecules* (2005), 38, 5406-5410.
189. Delcroix, D.; Martín-Vaca, B.; Bourissou, D.; Navarro, C. Ring-opening polymerization of trimethylene carbonate catalyzed by methanesulfonic acid: Activated monomer versus

active chain end mechanisms. *Macromolecules* (2010), 43, 8828–8835.

190. Leibfarth, F.; Lohmeijer, B. G. G.; Leibfarth, F.; Pratt, R. C.; et al. Organocatalytic ring opening polymerization of cyclic monomers: mechanistic and synthetic studies. *Biomacromolecules* (2007), 8, 153-160.
191. Coady, D. J.; Fukushima, K.; Horn, H. W.; Rice, J. E.; Hedrick, J. L. Dbu salts as new bifunctional hydrogen bonding catalysts for ring opening polymerizations. *Polymer Preprints* (2011), 52(2), 245-246.
192. Feng, J.; Zhuo, R-X, Zhang, X-Z. Construction of functional aliphatic polycarbonates for biomedical applications. *Progress in Polymer Science* (2012), 37, 211–236
193. Coulembier, O.; Lemaire, V.; Josse, T.; Minoia, A.; et al. Synthesis of poly(l-lactide) and gradient copolymers from a l-lactide/trimethylene carbonate eutectic melt. *Chemical Science* (2012), 3, 723–726.
194. Kim, M. S.; Hyun, H.; Kim, B. S.; Khang, G.; Lee, H. B. Polymeric nano-micelles as drug carrier using polyethylene glycol and polytrimethylene carbonate linear and star-shaped block copolymer. *Current Applied Physics* (2008), 8, 646–650.
195. Hyun, H.; Kim, M.S.; Khang, G.; Lee, H.B. Ring-opening polymerization of trimethylene carbonate by poly(ethylene glycol) in the presence of HCl·Et₂O as a monomer activator. *Journal of Polymer Science: Part A* (2006), 44, 4235-4241.
196. Coady, D. J.; Engler, A. C.; Hedrick, J. L. Organocatalyzed ROP of well-defined biocompatible star-polymer for use as delivery vectors. *Polymer Preprints* (2011), 52 (2), 303–304.
197. Shibasaki, Y.; Sanda, F.; Endo, T. Activated monomer cationic polymerization of 1,3-dioxepan-2-one initiated by water-hydrogen chloride. *Macromolecular Rapid Communications* (1999), 20, 532–535.
198. Coady, D. J.; Fukushima, K.; Horn, H. W.; Rice, J. E.; Hedrick, J. L. Catalytic insights into acid/base conjugates: highly selective bifunctional catalysts for the ring-opening polymerization of lactide. *Chemical Communications* (2011), 47, 3105–3107.
199. Chen, F.; Amsden, B. G. Homopolymerization and copolymerization kinetics of trimethylene carbonate bearing a methoxyethoxy side group. *Journal of Polymer Science, Part A: Polymer Chemistry* (2016), 544–552.
200. Ray, W. C.; Grinstaff, M. W. Polycarbonate and poly(carbonate - ester)s synthesized from biocompatible building blocks of glycerol and lactic acid. *Macromolecule* (2003), 36, 3557–3562.
201. Wang, X. L.; Zhuo, R. X.; Huang, S. W.; Liu, L. J.; He, F. Synthesis, characterization and in vitro cytotoxicity of poly[(5-benzyloxy-trimethylene carbonate)-co-(trimethylene carbonate)]. *Macromolecular Chemistry and Physics* (2002), 203, 985–990.
202. Lai, K.; Ji, L-J.; Long, C-Y.; Li, L.; et al. Synthesis of functionalizable and biodegradable polymers via ring-opening polymerization of 5-benzyloxy-trimethylene carbonate and ϵ -caprolactone. *Journal of Applied Polymer Science* (2011), 123, 2204–2210.

203. He, F.; Jia, H-L.; Liu, G.; Wang, Y-P.; et al. Enzymatic synthesis and characterization of novel biodegradable copolymers of 5-benzyloxy-trimethylene carbonate with 1,4-dioxan-2-one. *Biomacromolecules* (2006), 7, 2269–2273.
204. Wolinsky, J. B.; Ray, W. C.; Colson, Y. L.; Grinstaff, M. W. Poly(carbonate ester)s based on units of 6-hydroxyhexanoic acid and glycerol. *Macromolecules* (2007), 40, 7065-7068.
205. Franz, S., Rammelt, S., Scharnweber, D.; Simon, J. C. Biomaterials immune responses to implants: A review of the implications for the design of immunomodulatory biomaterials. *Biomaterials* (2011), 32, 6692–6709.
206. Harmsen, M. C.; Luyn, M. J. A. V. A. N. Cellular and molecular dynamics in foreign body reaction. *Tissue Engineering* (2006), 12 (7), 1955-1970.
207. Tang, B. L.; Eaton, J. W. Fibrin (ogen) Mediates Acute Inflammatory Responses to Biomaterials. *Journal of Experimental Medicine* (1993), 215 (8), 2147-2156.
208. Thull, R. Physicochemical principles of tissue material interactions. *Biomolecular Engineering* (2002), 19, 43–50.
209. Hunt, J. A.; Strickland, B. F.; Williams, D. F. Effect of biomaterial surface charge on the inflammatory response : Evaluation of cellular infiltration and TNF α production. *Journal of Biomedical Materials Research* (1996), 31, 139–144.
210. Defife, K. M.; Colton, E.; Nakayama, Y.; Matsuda, T.; Anderson, J. M. Spatial regulation and surface chemistry control of monocyte/macrophage adhesion and foreign body giant cell formation by photochemically micropatterned surfaces. *Journal of Biomedical Materials Research: Part A* (199), 45 (2), 148-154.
211. Szaba, F. M.; Smiley, S. T. Roles for thrombin and fibrin (ogen) in cytokine / chemokine production and macrophage adhesion in vivo. *Blood* (2002), 99, 1053–1060.
212. Smiley, S. T.; King, J. A.; Hancock, W. W. Fibrinogen stimulates macrophage chemokine secretion through toll-like receptor 4. *The Journal of Immunology* (2001), 167 (5), 2887-2894.
213. Lishko, V. K.; Podolnikova, N. P.; Yakubenko, V. P.; Yakovlev, S. et. al. Multiple Binding Sites in Fibrinogen for Integrin $\alpha_M\beta_2$ (Mac-1). *The Journal of Biological Chemistry* (2004), 279 (43), 44897–44906.
214. Hu, W.; Eaton, J. W.; Tang, L. Molecular basis of biomaterial-mediated foreign body reactions. *Blood* (2001), 98 (4), 1231–1239.
215. Tang, L.; Eaton, J. W. Natural responses to unnatural materials : A molecular mechanism for foreign body reactions. *Molecular Medicine* (1999), 5, 351–358.
216. Tang, L.; Liu, L.; Elwing, H. B. Complement activation and inflammation triggered by model biomaterial surfaces. *Journal of Biomedical Materials Research* (1998), 41(2), 333-340.
217. Pangburn, M. K.; Pangburn, K. L. W.; Meri, S.; Sharma, A. K. Molecular mechanisms of target recognition in an innate immune system: interactions among factor H, C3b, and target in the alternative pathway of human complement. *The Journal of Immunology* (2000), 164,

4742-4751.

218. Enoch, S.; Leaper, D. J. Basic science of wound healing. *Surgery* (2007), 26 (2), 31-37.
219. Fournier, E., Passirani, C.; Benoit, J. P. Biocompatibility of implantable synthetic polymeric drug carriers : focus on brain biocompatibility. *Biomaterials* (2003), 24, 3311–3331.
220. Ramot, Y.; Haim-Zada, M.; Domb, A. J.; Nyska, A. Biocompatibility and safety of PLA and its copolymers. *Advanced Drug Delivery Reviews* (2016), 107, 153-162.
221. Timbart, L.; Tse, M. Y.; Pang, S. C.; Babasola, O.; Amsden, B. G. Low viscosity poly(trimethylene carbonate) for localized drug delivery: Rheological properties and in vivo degradation. *Macromolecular Bioscience* (2009), 9, 786-794.
222. Amsden, B. G.; Timbart, L.; Mareck, D.; Chapanian, R.; et al. VEGF-induced angiogenesis following localized delivery via injectable, low viscosity poly(trimethylene carbonate). *Journal of Controlled Release* (2010), 145, 109–115.
223. Berleau, L. T. The Carboxyl-terminal domain(111-165) of vascular endothelial growth factor is critical for its mitogenic potency. *J. Biol. Chem.* 271, 7788–7795 (1996).
224. Wang, Y. et al. The self-assembly of biodegradable cationic polymer micelles as vectors for gene transfection. *Biomaterials* (2007), 28, 5358–5368.
225. Carbone, A. L.; Uhrich, K. E. Design and Synthesis of Fast-Degrading Poly (anhydride-esters). *Macromolecular Rapid Communicatios* (2009), 1021–1026.
226. Kim, J.; Dadsetan, M.; Ameenuddin, S.; Windebank, A. J.; et al. In vivo biodegradation and biocompatibility of PEG / sebacic acid-based hydrogels using a cage implant system. *Journal of Biomedical Materials Research* (2010), 191–197.
227. Leong, K. W.; Brott, B. C.; Langer, R. Bioerodible polyanhydrides as drug-carrier matrices. I: Characterization, degradation, and release characteristics. *Journal of Biomedical Materials Research* (1985), 19, 941-955.
228. Crotts, G.; Park, T. G. Protein delivery from poly (lactic-co-glycolic acid) biodegradable microspheres : Release kinetics and stability issues. *Journal of Microencapsulation* (1998), 15 (6), 699-713.
229. Makadia, H. K.; Siegel, S. J. Poly lactic-co-glycolic acid (PLGA) as biodegradable controlled drug delivery carrier. *Polymers* (2011), 3, 1377–1397.
230. Yang, J.; Hao, Q.; Liu, X.; Ba, C.; Cao, A. Novel biodegradable aliphatic poly(butylene succinate-co-cyclic carbonate)s with functional carbonate building blocks. 1. Chemical synthesis and their structural and physical characterization. *Biomacromolecules* (2004), 5, 209–218.
231. Magniont, C.; Escadeillas, G.; Oms-multon, C.; Caro, P. De. The bene fi ts of incorporating glycerol carbonate into an innovative pozzolanic matrix. *Cement and Concrete Research* (2010), 40, 1072–1080.
232. Technology, G. C. Synthesis and characterization of OH-terminated poly(trimethylene carbonate)s by alcohol-initiated ring-opening polymerization in melt bulk without using any

- catalyst. *Polymer Journal* (2004), 36, 28–33..
233. Chesterman, J. P. Reversibly photo-crosslinkable polycarbonate-based polymersomes for drug encapsulation and delivery. (2016). doi 10663653.
 234. Sen, M. Y.; Puskas, J. E. Green polymer chemistry: Telechelic poly(ethylene glycol)s via enzymatic catalysis. *Journal of Polymer Science-Part A: Polymer Chemistry* (2008), 46 (9), 3024-3028.
 235. Sunkara, H. B. (12) United States Patent. 2, (2010).
 236. Coady, D. J.; Fukushima, K.; Horn, H. W.; Rice, J. E.; Hedrick, J. L. Catalytic insight into acid/base conjugates: Highly selective bifunctional catalyst for the ring-opening polymerization of lactide. *Chemistry Communications* (2011), 47, 3105-3107.
 237. Amsden, B.; Hatefi, A.; Knight, D.; Bravo-Grimaldo, E. Development of biodegradable injectable thermoplastic oligomers. *Biomacromolecules* (2004), 5, 637–642.
 238. Li, Y.; Manickam, G.; Ghoshal, A.; Subramaniam, P. More efficient palladium catalyst for hydrogenolysis of benzyl groups. *Synthetic Communications* (2006), 36, 925–928.
 239. Wolinsky, J. B.; Iii, W. C. R.; Colson, Y. L.; Grinstaff, M. W. Poly (carbonate ester)s based on units of 6-hydroxyhexanoic acid and glycerol. *Macromolecules* (2007), 40, 7065–7068.
 240. Darensbourg, D. J.; Choi, W.; Ganguly, P.; Richers, C. P. Biometal derivatives as catalysts for the ring-opening polymerization of trimethylene carbonate. Optimization of the Ca (II) Salen Catalyst System. *Macromolecules* (2006), 39, 4374–4379.
 241. Section, E. Anionic Ring-Opening Polymerization of a Structure with Amine Initiators. *Macromolecules* (1998), 31, 919–923.
 242. Poot, A.; Grijpma, D. W.; Feijen, J. In vitro degradation of trimethylene carbonate based (Co) polymers. *Macromolecular Bioscience* (2002), 2 (9), 411–419.
 243. Matsusue, Y.; Hanafusa, S.; Yamamuro, T.; Shikinami, Y.; Ikada, Y. Tissue reaction of bioabsorbable ultra high strength poly(L-Lactide) rod: A long-term study in rabbits. *Clinical Orthopaedics and Related Researches* (1995), 317, 246-253.
 244. Silva, P. D. A. & Gordon, S. Phagocytosis stimulates alternative glycosylation of macrosialin (mouse CD68), a macrophage-specific endosomal protein. *Biochemical Journal* (1999), 338, 687–694.
 245. Bezwada, R. S. et al. Monocryl suture, a new ultra-pliable absorbable monofilament suture. *Biomaterials* (1995), 16, 1141–1148.
 246. Molea, G.; Schonauer, F.; Bifulco, G.; Angelo, D. D. Comparative study on biocompatibility and absorption times of three absorbable monofilament suture materials (Polydioxanone, Poliglecaprone 25, Glycomer 631). *British Journal of Plastic Surgery* (2000), 53, 137–141.
 247. Babasola, I. O.; Bianco, J.; Amsden, B. G. In vivo degradation and tissue response to poly(5-ethylene ketal ϵ -caprolactone-co-D,L-lactide). *Biomacromolecules* (2012), 13, 2211–2217.
 248. Dash, T. K.; Konkimalla, V. B. Poly- ϵ -caprolactone based formulations for drug delivery

- and tissue engineering : A review. *Journal of Controlled Release* (2012), 158, 15–33.
249. Woodruff, M. A.; Hutmacher, D. W. The return of a forgotten polymer — Polycaprolactone in the 21st century. *Progress in Polymer Science* (2010), 35 (10), 1217–1256.
 250. Albertsson, A.-C.; Eklund, M. Influence of molecular structure on the degradation mechanism of degradable polymers: In vitro degradation of poly(trimethylene carbonate), poly(trimethylene carbonate-co-caprolactone), and pPoly(adipic anhydride). *Journal of Applied Polymer science* (1995), 57 (1), 87-103.
 251. Urbich, C.; Aicher, A.; Heesche, C.; Dernbach, E.; et al. Soluble factors released by endothelial progenitor cells promote migration of endothelial cells and cardiac resident progenitor cells. *Journal of Molecular and Cellular Cardiology* (2005), 39, 733–742.
 252. Gille, H. et al. Analysis of biological effects and signaling properties of Flt-1 (VEGFR-1) and KDR (VEGFR-2): A reassessment using novel receptor-specific vascular endothelial growth factor mutants. *Journal of Biological chemistry* (2001), 276 (5), 3222-3230.
 253. Costantino, H. R.; Firouzabadian, L.; Wu, C.; Carrasquillo, K.; et al. Protein spray freeze drying . 2 . effect of formulation variables on particle size and stability. *Journal of Pharmaceutical Science* (2002), 91 (2), 388–395.
 254. Canfield, R. E. The Amino Acid Sequence of Egg White Lysozyme. *Journal of Biological chemistry* (1963), 238 (8), 2698-2707.
 255. Wetter, L. R.; Deutsch, H.F. Immunological studies on egg white proteins.iv. immunochemical and physical studies on lysozyme. *Journal of Biological Chemistry* (1951), 192, 237-242.
 256. Howard, S. B.; Twigg, P. J.; Baird, J. K.; Meehan, E. J. The solubility of hen egg-white lysozyme. *Journal of Crystal Growth* (1998), 90 (1-2), 94-104.
 257. Righetti, P. G.; Tudor, G. Isoelectric points and molecular weight of proteins:A new table. *Journal of Chromatography A* (1981), 220 (2), 115-194.
 258. Salg, S.; Salgi, U.; Bahad, S. Zeta Potentials and Isoelectric Points of Biomolecules : The Effects of Ion Types and Ionic Strengths. *International Journal of Electrochemical Science* (2012), 7, 12404–12414.
 259. Smith, A. The Osmotic Pressure of Concentrated Protein Solutions : Effect of Concentration and pH in Saline Solutions of Bovine Serum Albumin. *Journal of Colloid and Interface Science* (1980), 79 (2), 548-566.
 260. Siegel, R. A.; Kost, J.; Lange, R. Mechanistic studies of macromolecular drug release from macroporous polymers. I. Experiments and preliminary theory concerning completeness of drug release. *Journal of Controlled Release* (1989), 8, 223–236.
 261. Papadokostaki, K. G.; Amarantos, S. G.; Petropoulos, J. H. Kinetics of release of particulate solutes incorporated in cellulosic polymer matrices as a function of solute solubility and polymer swellability . I . sparingly soluble solutes. *Journal of Applied Polymer Science* (1997), 67, 277–287.
 262. Polymer, S.; Ii, M. Combined experimental and computer simulation study of the kinetics

of solute release from a relaxing swellable polymer matrix. II. Release of osmotically active solute. *Journal of Applied Polymer Science* (2004), 92, 2468-2479.

263. Belle, E. V.; Witzendichler, B.; Chen, D.; Silver, M.; et al. Potentiated Angiogenic Effect of Scatter Factor / Hepatocyte Growth Factor via Induction of Vascular Endothelial Growth Factor The Case for Paracrine Amplification of Angiogenesis. *Circulation* (1998), 97 (4), 381-390.
264. Barreto, M.; Wanderlei, C.; Carvalho, P. De.; Garcia-rojas, E. E. Food Hydrocolloids Heteroprotein complex formation of bovine serum albumin and lysozyme : Structure and thermal stability. *Food Hydrocolloids* (2018), 74, 267–274.
265. Vasylieva, M.; Gromovoy, T. Maldi-tof investigation of lysozyme-albumin interaction. *Chemistry Journal of Moldova* (2014), 9(2), 107-110.

Appendix A

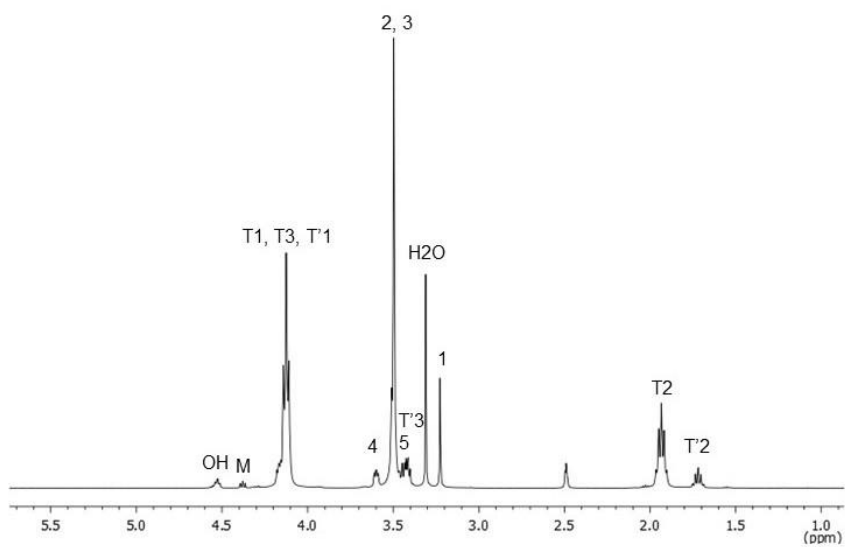


Figure A.1. ¹H NMR spectrum of PTMC initiated with P350 obtained in DMSO-d₆, M/I= 6, Mn=950 Da.

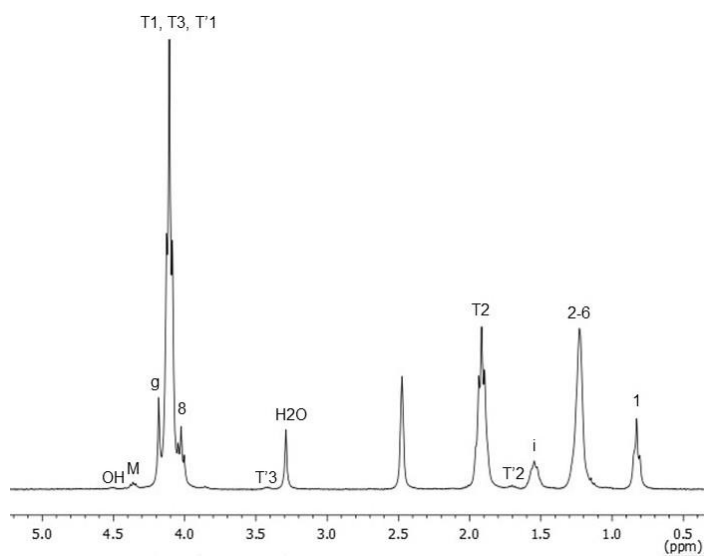


Figure A.2. ¹H NMR spectrum of ester-linked PTMC (OCT-CE-DGC) obtained in DMSO-d₆.

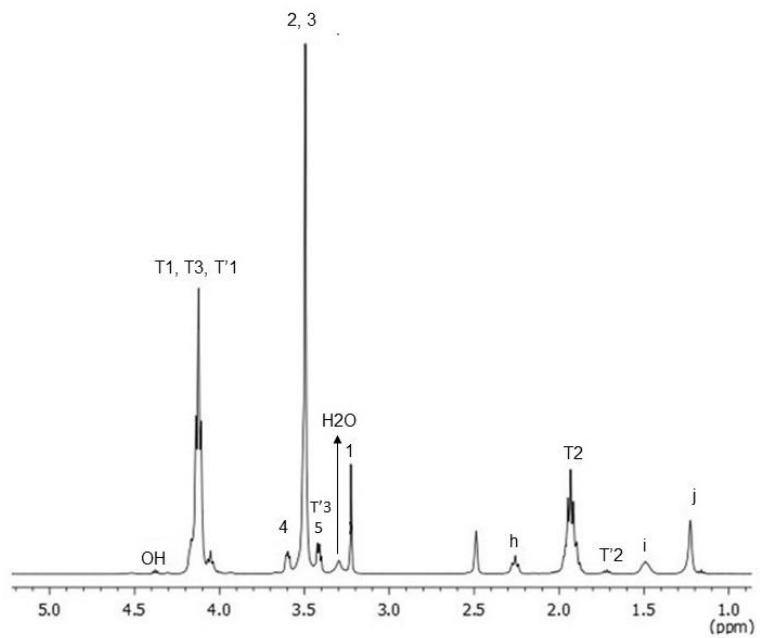


Figure A.3. ¹H NMR spectrum of ester-linked PTMC (P350-CE-SC) obtained in DMSO-d₆, EG/TMC: 1.3.

Appendix B

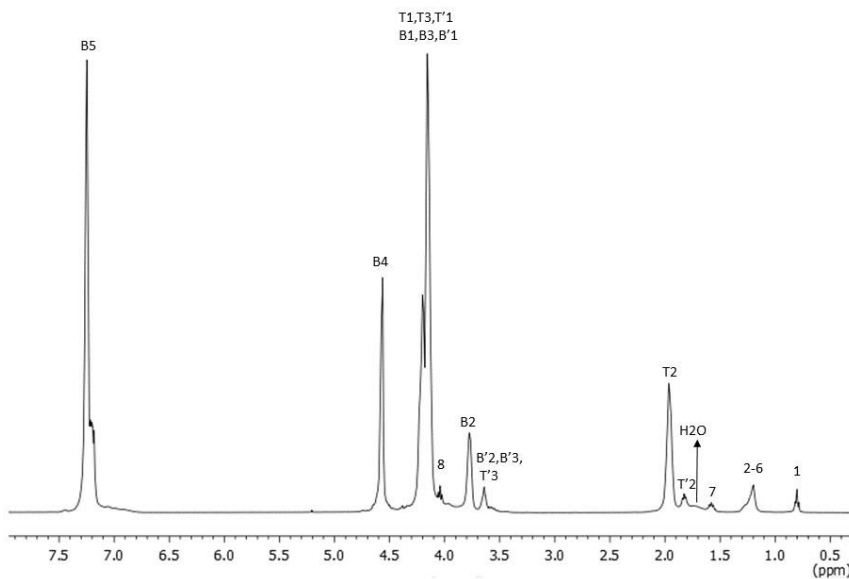


Figure B.1. ^1H NMR spectrum of OCT-P18-50B-DBU obtained in CDCl_3 , $M/I=40$, $M_n=3200$ Da, BTMC: 32.8 %. Labels with prime are corresponding to the copolymer end group.

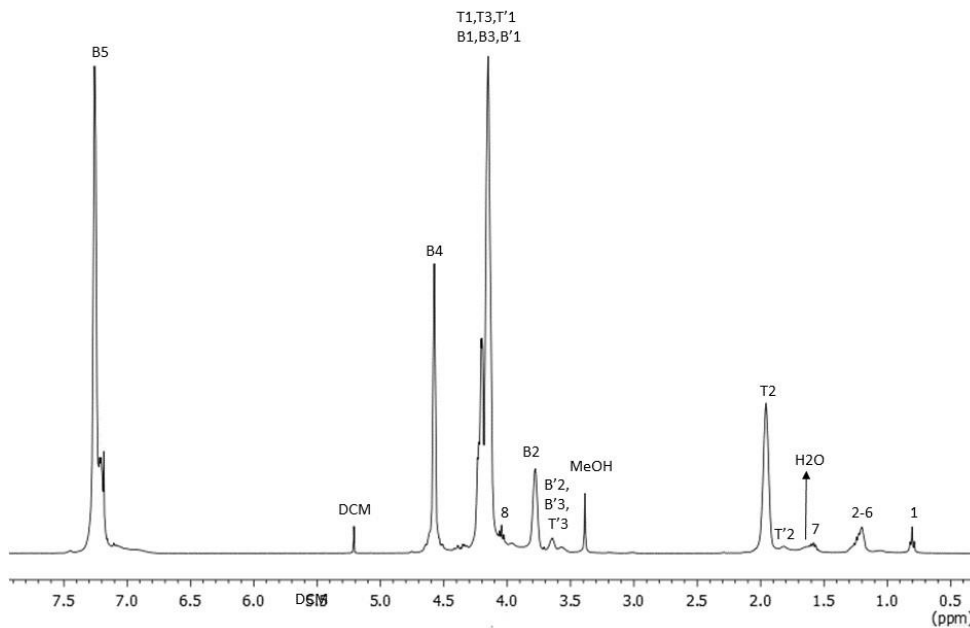


Figure B.2. ^1H NMR spectrum of OCT-P18-50B-Sn obtained in CDCl_3 , $M/I=40$, $M_n=3920$ Da, BTMC:50 %. Labels with prime are corresponding to the copolymer end group.

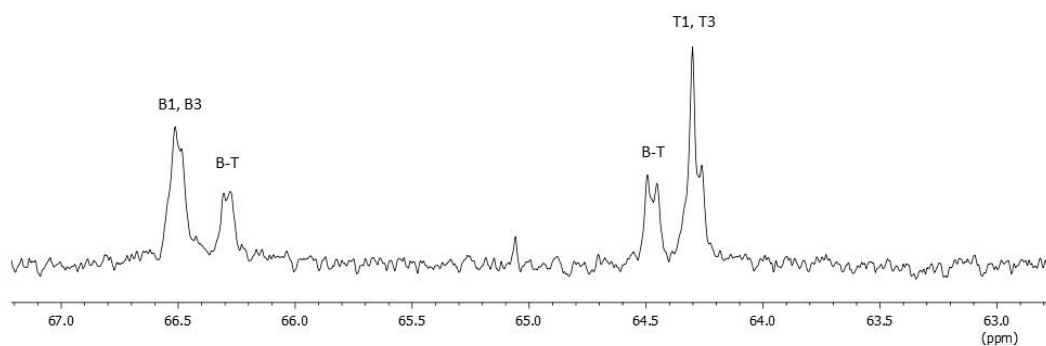


Figure B.3. ^{13}C NMR spectra of A) OCT-P18-50B-DBU obtained in CDCl_3 , $M_n=3200$ Da, BTMC: 32.8 %.

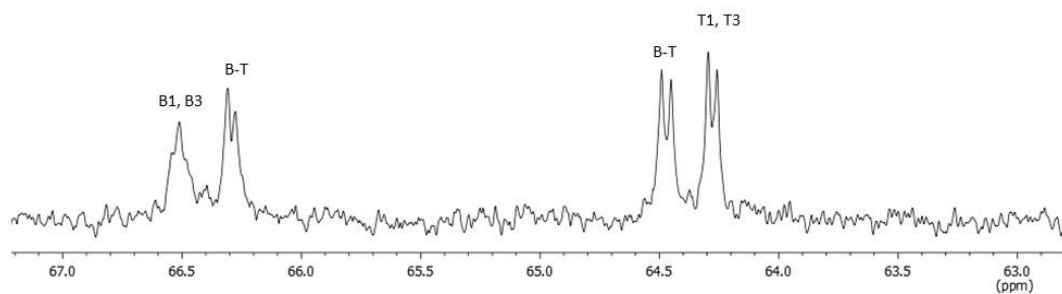


Figure B.4. ^{13}C NMR spectra of A) OCT-P18-50B-Sn obtained in CDCl_3 , $M_n=3920$ Da, BTMC: 50 %.

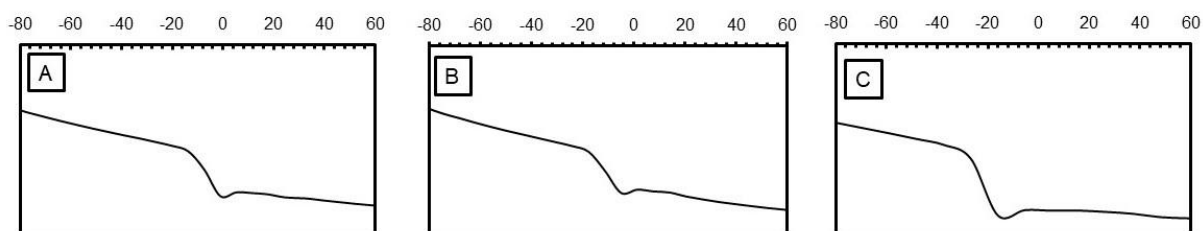


Figure B.5. The glass transition temperature of P(TMC-co-BTMC) from DSC heating thermograph: (A) $\text{Sn}(\text{Oct})_2$, (B) DBU, and (C) $\text{HCl}\cdot\text{Et}_2\text{O}$.

Appendix C

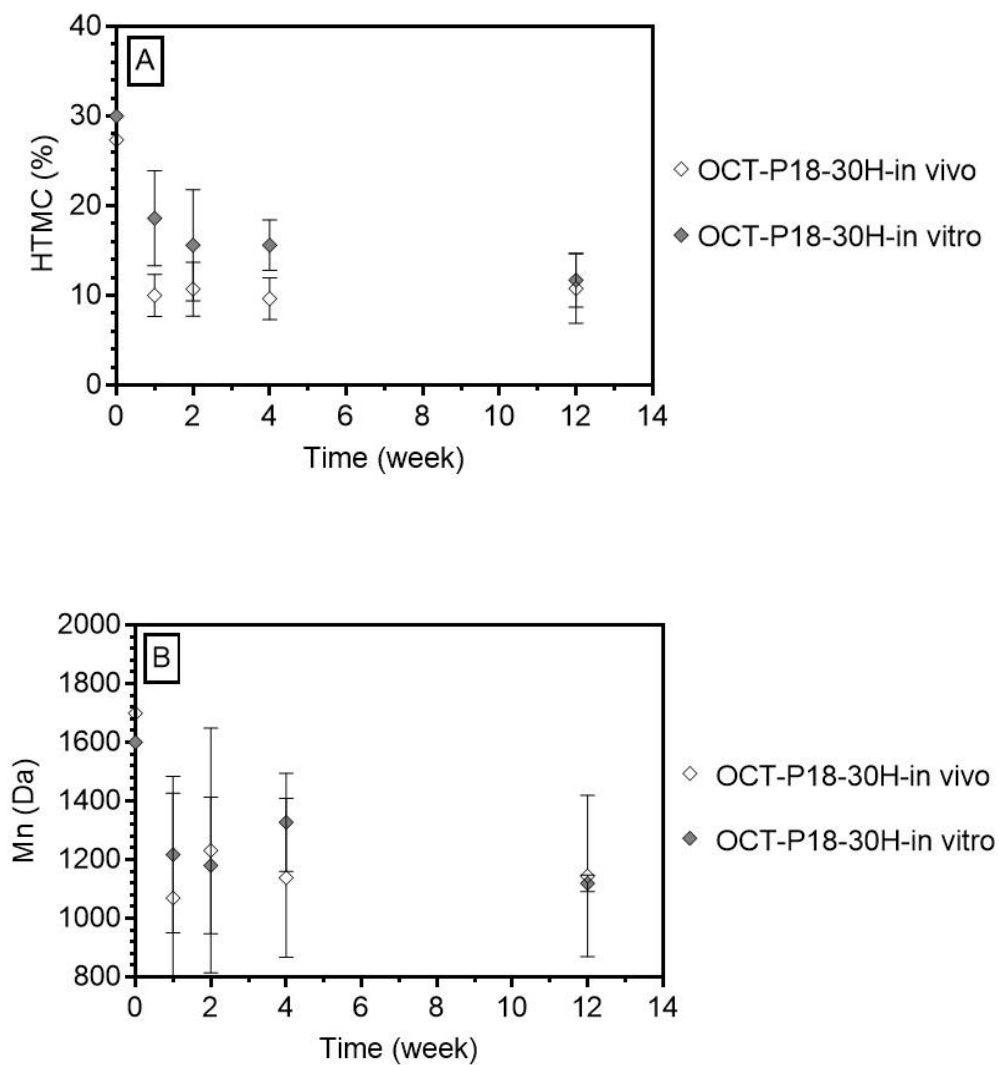


Figure C.1. *In vivo* versus *in vitro* degradation changes of OCT-P18-30H in : A) HTMC mole% and) M_n (Da). Each data point represents the average, and the error bars are the standard deviation about the average.

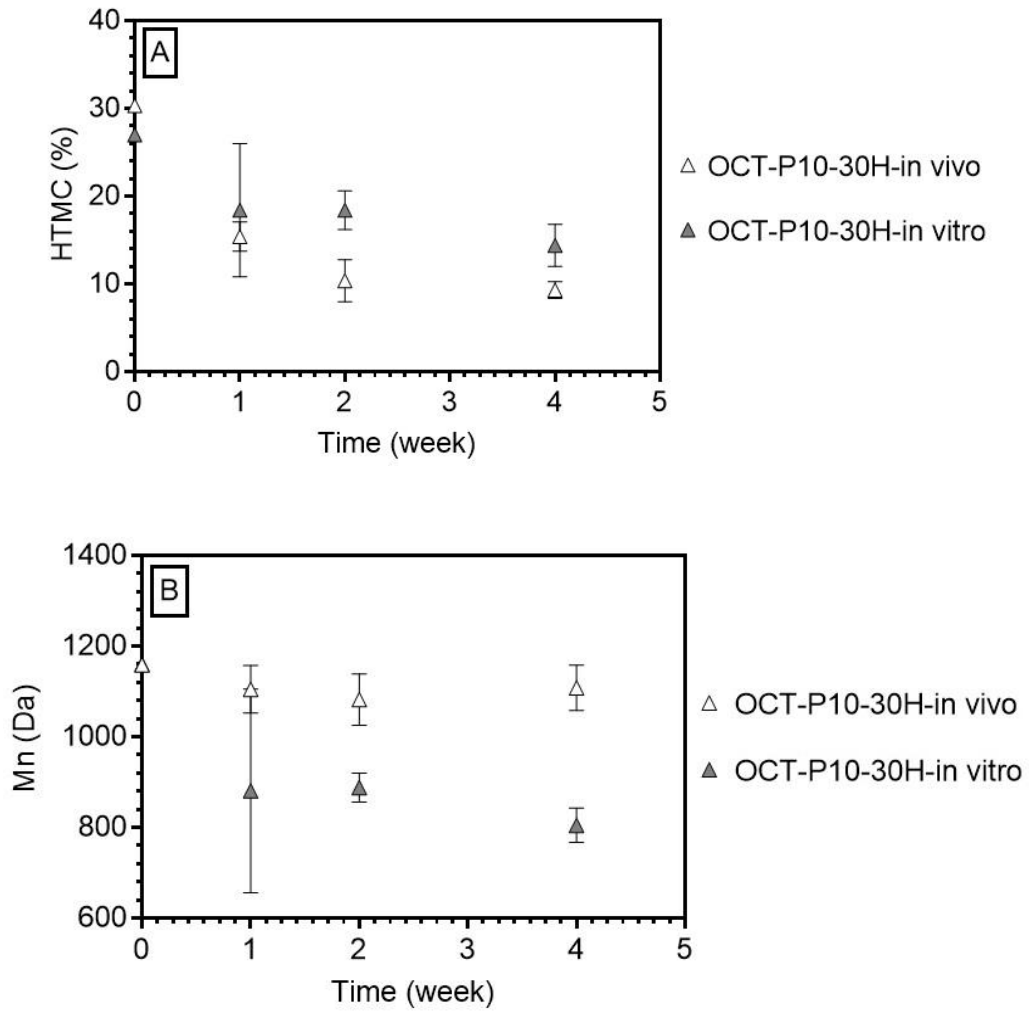


Figure C.2. *In vivo* versus *in vitro* degradation changes of OCT-P10-30H in : A) HTMC mole% and) M_n (Da). Each data point represents the average, and the error bars are the standard deviation about the average.

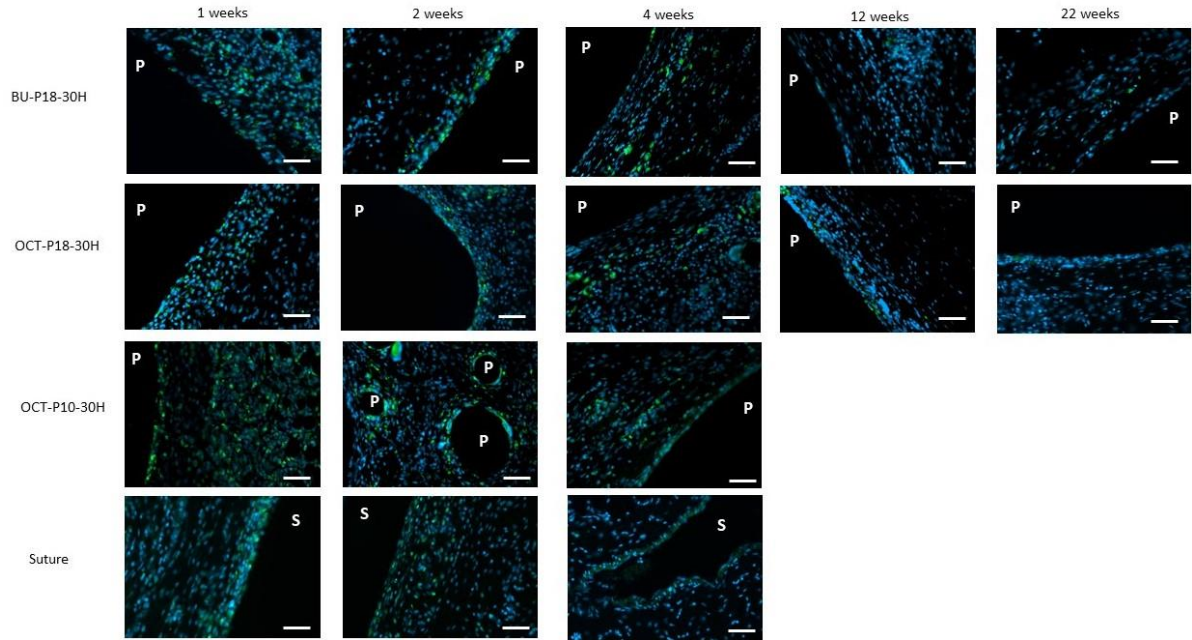


Figure C.3. Photomicrographs of tissue sections (muscle side) of copolymers and suture extracted and stained for CD68. (P): copolymer, (S): suture, green color: FITC, blue color: DAPI, Scale bar: 50 μ m, 40X.